# Chapter 13
# Hydrogen and Fuel Cell Systems

## 13.1 Introduction

The *hydrogen economy* emerged as a potential response to two major problems that mankind faces today, namely, its dependence on fossil fuels and the high level of pollution associated with the fossil fuel combustion process. Indeed, the exploitable and proved fossil fuel reserves are limited. As a consequence of population growth and industrial development of the Asiatic continent (with countries like China and India counting over one billion people each), the rate of fossil fuel exploitation increases constantly together with their costs and the associated pollution levels.

The necessity to shift to an alternative energy–based economy is obvious. Such an economy is based on renewable energy sources such as solar (which includes biomass energy), hydro, wind, tides and currents, ocean thermal, and geothermal. It was mentioned in Chapter 9 that energies are available temporally, incidentally, or locally. For example, solar energy is available during the day; wind energy is available with more intensity in some seasons or days and is not present in others; geothermal energy can be found only in certain locations on the globe. Therefore, with alternative energies there is, most of the times, a mismatch between availability and demand. Moreover, these energies are difficult to store and transport.

The idea of a hydrogen economy was introduced at a scientific conference held in March 1974 in Miami, Florida, titled "The Hydrogen Economy Miami Energy (THEME) Conference," at which the International Association for Hydrogen Energy (IAHE) was established. Today, after 37 years of information dissemination and advances in hydrogen economy technologies, the world's most developed countries (the United States, Japan, and countries in the European Union) and many other countries invest extensively in shifting toward a hydrogen-based economy.

This chapter discusses hydrogen fuel and fuel cell systems. The issues regarding production, storage, and distribution of hydrogen are discussed, along with hydrogen utilization for power generation with fuel cells. The primary focus is on renewable-based hydrogen production through solar, wind, hydro, geothermal, biomass, and other options, and the opportunities and challenges are discussed with several case studies, examples, and applications from various systems.

İ. Dinçer and C. Zamfirescu, *Sustainable Energy Systems and Applications*,
DOI 10.1007/978-0-387-95861-3_13, 

Hydrogen production methods from fossil fuels are also discussed and compared with renewable energy-based technologies. Efficiency evaluation, environmental impact, and sustainability assessment are also discussed.

## 13.2 Hydrogen

Hydrogen is the simplest chemical element with atomic number $Z = 1$, and it is the most abundant chemical element in the universe. As a consequence of its simplicity, hydrogen can lose valence electrons easily, and therefore it is very reactive. Thus, hydrogen cannot be found as an individual element on earth, but rather is embedded in other materials. Water is the most abundant resource of hydrogen on earth; also, hydrogen is part of most fossil fuels and biomass. In nature, hydrogen can also be found in the form of hydrogen sulfide ($H_2S$), which is abundant in some springs, geothermal sites, and the seas. Regarding its properties, hydrogen has a high caloric value, the lowest molecular weight, the highest thermal conductivity among all gases, and the lowest viscosity. Table 13.1 summarizes the main thermophysical properties of hydrogen.

The heating value of hydrogen is much higher than that of conventional fuels if taken as per unit of weight. However, hydrogen cannot be kept in a condensed phase with current technology. Mostly, hydrogen is stored in the form of compressed gas or as cryogenic liquid. In any of these storage conditions, the heating value of hydrogen per unit of volume is the lowest of all the conventional fuels. Nevertheless, the efficiency of power generation systems fueled with hydrogen is much higher than that obtained with conventional fuel, and this fact compensates for the low storage density problem of hydrogen. Furthermore, hydrogen combustion is completely clean, producing only water vapor in the exhaust gas. Heat recovery can be applied intensively to hydrogen combustion to obtain liquid water, which can be recycled to produce hydrogen again via various methods for extracting hydrogen from water, including electrolysis and thermochemical splitting. Therefore, hydrogen can be viewed as an energy storage medium or energy carrier. The major problem with hydrogen as a fuel is the difficulty of storing it in its pure form and the enormous costs of a hydrogen infrastructure, which must be put in place in order to implement a hydrogen energy–based economy. It is arguably believed that the storage and distribution problem is well balanced by the benefits brought by the hydrogen economy.

**Table 13.1** Thermophysical properties of hydrogen

| Property | MP | BP | $T_c$ | $P_c$ | Flammability | IT | AFT | Flame velocity | LHV |
|---|---|---|---|---|---|---|---|---|---|
| Value | 14.01 K | 20.3 K | 32.97 | 12.9 bar | 4.1–75% | 850 K | 2,400 K | 2.75 m/s | 120 MJ/kg |

*MP* melting point; *BP* normal boiling point; *IT* ignition temperature; *AFT* adiabatic flame temperature

## 13.3 Hydrogen Economy

Utilization of any kind of energy resources leads unavoidably to some environmental impact. Increasing the efficiency throughout the whole chain from energy supply to end use is a way to alleviate concerns regarding emissions and their negative environmental impact. Higher efficiency means less resource utilization and associated pollution.

Using hydrogen as an energy carrier can help in reducing environmental damage and in achieving sustainability. If hydrogen is produced from clean and renewable energy sources, the environmental impact is reduced because fossil fuel resources are not consumed and hydrogen combustion emissions do not contribute to global warming or generate substantial waste. At the hydrogen utilization phase, the associated processes (e.g., combustion) are more efficient than with traditional fuels. For example, fuel cell technologies can provide more efficient, effective, and environmentally benign and sustainable alternatives to conventional energy technologies, particularly fossil fuel–driven ones. Hydrogen energy systems are a key component of sustainable development for four main reasons:

- They are compatible with renewable energy sources and carriers for future energy security, economic growth, and sustainable development.
- The variety of hydrogen and fuel cell technologies provide a flexible array of options for their use in various applications with reduced environmental impact and increased efficiency.
- Hydrogen cannot be depleted since the basic source is water. In contrast, fossil fuel and uranium resources are diminished by extraction and consumption.
- These technologies favor system decentralization and local and individual solutions that are somewhat independent of the national network, thus enhancing the flexibility of the system and providing economic and environmental benefits to small isolated populations.

Even if hydrogen is produced from fossil fuel sources, which normally cause a burden on the environment, it is almost certain that hydrogen technologies can provide a cleaner and more sustainable energy system than increased controls on conventional energy systems because hydrogen

- can be extracted from widely available materials such as water, natural gas (NG), petroleum, coal, and biomass; in addition, if sustainable energy sources are used for its production (e.g., renewable energy, nuclear energy, energy recovered from waste heat) its fabrication process becomes low-polluting;
- can be used in stationary and mobile applications without damaging emissions, especially by using fuel cells;
- can be made available everywhere, can substitute for oil and gas, and can be burned without changing the climate.

Hydrogen is only a secondary energy source (a “storage carrier”) and must be produced from a primary energy source. For physical reasons, there will

always be losses from these conversion processes, and therefore in any case the costs of hydrogen must be higher than the costs of the energy used to produce hydrogen. This simple physical reason complicates the decision about priorities and time scales for the introduction of hydrogen. It is the same simple methodology leading to a higher $CO_2$-mitigation effect while using the input energy carrier for the production of hydrogen directly.

The scientific and technical challenges for a hydrogen economy are as follows:

- Reduction of the cost of hydrogen production to a level comparable to the energy cost of petroleum
- Development of a $CO_2$-free route for the mass production of sustainable hydrogen at a competitive cost
- Development of a safe and efficient national infrastructure for hydrogen delivery and distribution
- Development of viable hydrogen storage systems for both vehicular and stationary applications
- Dramatic reduction in costs and significant improvement in the durability of fuel cell systems

The advantages of hydrogen versus fossil fuels are as follows:

- Liquid hydrogen is the best transportation fuel when compared to liquid fuels, such as gasoline, jet fuel, and alcohols, and gaseous hydrogen is the best gaseous transportation fuel.
- While hydrogen can be converted to useful energy forms (thermal, mechanical, and electrical) at the user end generally through five different processes, fossil fuels can be converted generally only through one process: flame combustion. Thus, hydrogen is the most versatile fuel.
- Hydrogen has the highest utilization efficiency when it comes to conversion to useful energy forms (thermal, mechanical, and electrical) at the user end. Roughly, hydrogen is 30% to 40% more efficient than fossil fuels. Thus, hydrogen saves primary energy resources. It could also be termed as the most energy conserving fuel.
- When fire hazards and toxicity are taken into account, hydrogen is the safest fuel.

## 13.4 Hydrogen Production Methods

Hydrogen can be extracted from a large variety of material resources such as water, fossil hydrocarbons, biomass, hydrogen sulfide, boron hydrides, and others. In order to extract and separate hydrogen from such material resources, one needs energy.

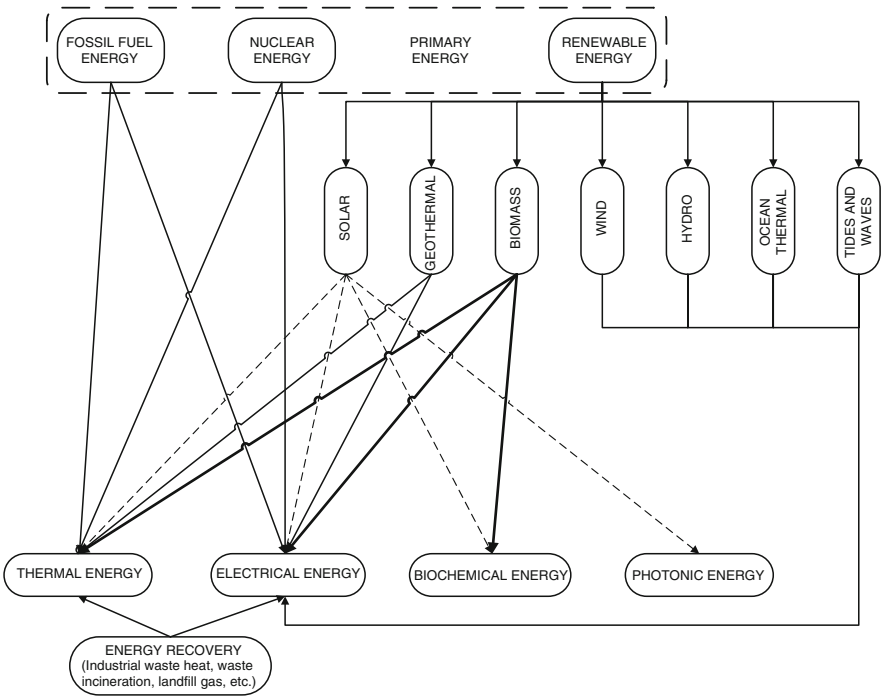


**Fig. 13.1** Paths of generation of basic forms of energy from primary energy

The forms of energy that can drive a hydrogen production process can be classified into four categories: thermal, electrical, photonic, and biochemical. These kinds of energy can be obtained from primary energy (fossil, nuclear, and renewable) or from recovered energy through various paths, as suggested in Fig. 13.1. Electrical and thermal energy can be derived from fossil fuels, renewable energies (like solar, wind, geothermal, tidal, wave, ocean thermal, hydro, and biomass), nuclear energy, or recovered energy like industrial waste heat, municipal waste incineration, landfill gas, and others. Photonic energy comprises solar radiation only and it is, therefore, renewable. Biochemical energy is that stored in organic matter (in the form of carbohydrates, glucose, and sugars), and it can be manipulated by certain microorganisms that can extract hydrogen from various substrates. In Table 13.2, the main hydrogen production methods are described and the material and energy resources specific to each are listed.

Currently, 18% of hydrogen production globally sources from coal, 30% from petroleum, 40% from natural gas, and 12% from other sources of which an important share is represented by water electrolysis (Das and Veziroglu 2008). The sales have increased by 5% to 6% per annum in recent years, with the most $H_2$ use in the fertilizer industry (50%) and the petroleum industry (37%).

**Table 13.2** General hydrogen production methods

| Method | Description | Material resources | Energy supply |
|---|---|---|---|
| Water electrolysis | Water decomposition into oxygen and hydrogen by passing a direct current that drives electrochemical reactions | Water | Electrical |
| High-temperature steam electrolysis | Steam decomposition by using direct current assisted by thermal energy to drive electrochemical reactions to split water molecule | Steam | Electrical + thermal |
| Photoelectrochemical water splitting | Uses electric and photonic energy to electrolyze water and generate $H_2$ and $O_2$ | Water | Photonic + electric |
| Photocatalysis | Uses photonic energy and catalysts to decompose water molecule | Water | Photonic |
| Biophotolysis | Uses a reversible reducible cofactor and photometabolically active microbes to generate hydrogen from water; viz. photosynthesis | Water | Photonic + biochemical |
| Anaerobic digestion (anaerobic fermentation) | Uses biological energy manipulated by microbes to extract hydrogen from biodegradable materials in the absence of oxygen | Biomass | Biochemical |
| Thermolysis | Uses thermal energy to decompose water molecule at very high temperature (~2,500°C) | Water | Thermal |
| Thermochemical water splitting | Thermally driven chemical reactions performed in a loop with the overall result of water splitting | Water | Thermal |
| Thermocatalytic cracking | Uses thermal energy to break the carbon– hydrogen bonds of hydrocarbons and eventually generate hydrogen | Fossil fuels | Thermal |
| Gasification | Converts solid carbonaceous materials (fossil or biofuels, wastes, etc.) into carbon monoxide and hydrogen by reacting them with $O_2$ and/or steam | Water + fossil fuels + biomass | Thermal |
| Reforming | Reacts carbon-based liquid or gaseous fuels with steam at high temperature to produce carbon dioxide and hydrogen | Water + fossil or biofuels | Thermal |

### 13.4.1 Electricity-Driven Hydrogen Production Methods

#### 13.4.1.1 Water Electrolysis

Electrolysis of water is a basic method to produce hydrogen through redox reactions in water by using a direct current. The overall reaction is water decomposition: $H_2O \rightarrow H_2 + 0.5O_2$. Therefore, water electrolysis is an electrically driven method to generate hydrogen, even though electrolysis can be assisted by some additional thermal energy, as is discussed in this section. The typical process involves a liquid electrolyte, such as an aqueous solution containing sulfate anions $SO_4^{2-}$; also, there are available solid polymer electrolytes in the form of proton conducting membranes, such as NAFION (a brand name of Du Pont de Nemours) or other kinds, or oxygen ions conduction membranes. The electrical circuit is closed by external conductors that are connected to the direct current electricity source. The contact between the external conductors and the electrolyte is made through electrodes that normally are plated with precious metals, such as platinum, that have the role of accelerating the electrochemical reactions.

The electrode connected to the negative polarity of the direct current source is called the "anode," which is where the water oxidation reaction takes place, releasing oxygen as follows:

$$2H_2O(l) \rightarrow O_2(g) + 4H^+(aq) + 4e^- \quad \text{at } E^0_{ox} = -1.23\,V. \tag{13.1}$$

The electrode connected to the positive polarity of the source is called the "cathode," which is where the proton reduction reaction occurs, releasing hydrogen as follows:

$$4H^+(aq) + 4e^- \rightarrow 2H_2(g) \quad \text{at } E^0_{red} = 0.0\,V. \tag{13.2}$$

The potentials $E^0_{ox}$ and $E^0_{red}$ are called standard potentials because they correspond to operation at 25°C and standard pressure in pure water. Figure 13.2 presents the conceptual design of an electrolytic cell for water electrolysis. In the electrolytic bath, an ionic medium is maintained by adding some salts or other chemicals that maintain an appropriate pH that helps the transport of ions through it. Within the electrolyte some combination of hydroxyl and protons may occur, and the reverse, water ionization forming hydroxyl and protons according to $H_2O \rightarrow H^+ + OH^-$ without affecting the overall water splitting reaction.

The Gibbs free energy of the water decomposition equation can be calculated with $\Delta G = \Delta H - T\Delta S$, where $\Delta H = H_{prod} - H_{react}$ is the total molar enthalpy difference between products and reactants, thus $\Delta H = h_{H_2} + 0.5h_{O_2} - h_{H_2O}$, where $h$ is the specific molar enthalpy of chemicals and includes the formation enthalpy and the thermomechanical enthalpy; one can assume ideal gas behavior of hydrogen and oxygen and thus their enthalpy as a function of temperature only; moreover, the enthalpy of liquids (like water liquid) is practically independent

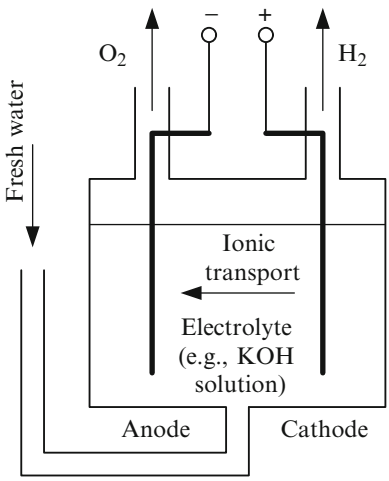


**Fig. 13.2** Simplified design of an electrolysis cell

of pressure; if water is present in the form of steam, then again, the ideal gas law applies. The reaction's entropy is calculated similarly, with the only difference being that the entropy is a function of both temperature and pressure: $s(T,P) = s^0(T) - R\ln(P/P^0)$, where $R$ is the universal gas constant and $s^0(T)$ is the entropy at standard pressure $P^0$.

The Faraday constant relates the Gibbs energy of the reaction with the (ideal/minimum) electric potential that must be applied to the electrodes in order to dissociate the water molecule. The Faraday constant is defined by

$$F = eN_{\mathrm{A}} = -\frac{\Delta G}{n\Delta E_{\mathrm{EL}}} = 96485.3\,\mathrm{C/mol}, \tag{13.3}$$

where $e = 1.602 \times 10^{-19}\,\mathrm{C}$ is the electron's charge, $N_{\mathrm{A}} = 6.022 \times 10^{23}\,\mathrm{mol}^{-1}$ is the Avogadro number, $n$ is the number of moles of electrons per mol of decomposed water, and $\Delta E_{\mathrm{EL}} = E_{\mathrm{red}} - E_{\mathrm{ox}}$ is the difference of potential between the electrodes. The above equation can be solved for $\Delta E_{\mathrm{EL}}$:

$$\Delta E_{\mathrm{EL}} = -\frac{\Delta G(T,P)}{nF} = \left[-\frac{\Delta H(T)}{nF}\right] - \left[-T\frac{\Delta S(T,P)}{nF}\right], \tag{13.4}$$

which by rearranging it further becomes

$$\Delta E_{\mathrm{TOT}} = \Delta E_{\mathrm{EL}} + \Delta E_{\mathrm{TH}}, \tag{13.5}$$

where

$$\Delta E_{\mathrm{TOT}} = -\frac{\Delta H(T,P)}{nF} \tag{13.6}$$

is the total equivalent electric potential difference that must be applied to the electrolytic cell and

$$\Delta E_{\mathrm{TH}} = -\frac{T\Delta S(T,P)}{nF} \tag{13.7}$$

is the equivalent potential difference that must be applied to the cell in order to generate the thermal energy $Q_{\mathrm{TH}}$ needed to drive the reaction. Note that the portion of energy $Q_{\mathrm{TH}}$ can be given either in the form of heat, accounting for $Q_{\mathrm{TH}} = -T\Delta S(T,P)$, or as electricity that is converted through the joule effect into heat, by applying a difference of potential at the electrodes as indicated by Eq. (13.7). The total energy needed to drive the reaction $\Delta H(T,P)$ can be given totally through electricity by applying the difference of potential $\Delta E_{\mathrm{TOT}}$ to the electrodes, or partially as electricity through $\Delta E_{\mathrm{EL}}$ corresponding to energy $\Delta G(T,P)$ transmitted to the reaction and $Q_{\mathrm{TH}}$ as the thermal counterpart.

There are three possibilities to conduct the electrolysis for splitting the $H_2O$ molecule:

- Cold electrolysis of liquid water at or close to the ambient temperature: in this case, the minimal potential difference between the electrodes is given by Eq. (13.5) calculated for standard conditions, $\Delta E_{\mathrm{TOT}}(T_0,P_0)$; alkaline and proton exchange membrane (PEM) electrolyzer cells can be used.
- High-pressure electrolysis; in this case, the electric potential difference is calculated with $\Delta E_{\mathrm{TOT}}(T,P)$. Here, $(T,P)>(T_0,P_0)$. The high-pressure electrolysis is attractive because it facilitates hydrogen and oxygen compression and storage. In order to increase the efficiency of the process, both temperature and pressure must be increased; moreover, the water is given in pressurized liquid form. It is thermodynamically efficient to pressurize water rather than to compress hydrogen and oxygen products. However, there is a design trade-off in the sense that too high an operating pressure leads to reduced efficiency and higher cost.
- High-temperature steam electrolysis (HTSE) in solid oxide electrolysis cells (SOECs): in this case, water is converted to steam with the expense of thermal energy. Moreover, the electrochemical bath is heated, directly (through steam) or indirectly (through heat transfer) so that the electric energy needed by the process is only $\Delta E_{\mathrm{EL}}(T,P_0)$. The remaining energy is supplied thermally as $Q_{\mathrm{TH}}$.

When the efficiency of electricity generation (which is normally $\eta_{\mathrm{E}} = 20$–$30\%$) is accounted for, the electrolysis energy efficiency assuming no losses becomes

$$\eta_{\mathrm{EL}} = \frac{\Delta H}{(\Delta H/\eta_{\mathrm{E}})} = \eta_{\mathrm{E}}, \tag{13.8}$$

where $\Delta E_{\mathrm{TOT}}/\eta_{\mathrm{E}}$ represents the heat input needed to generate the total electricity to drive the electrolysis; in that case that the process is driven only electrically. If HTSE is considered, then

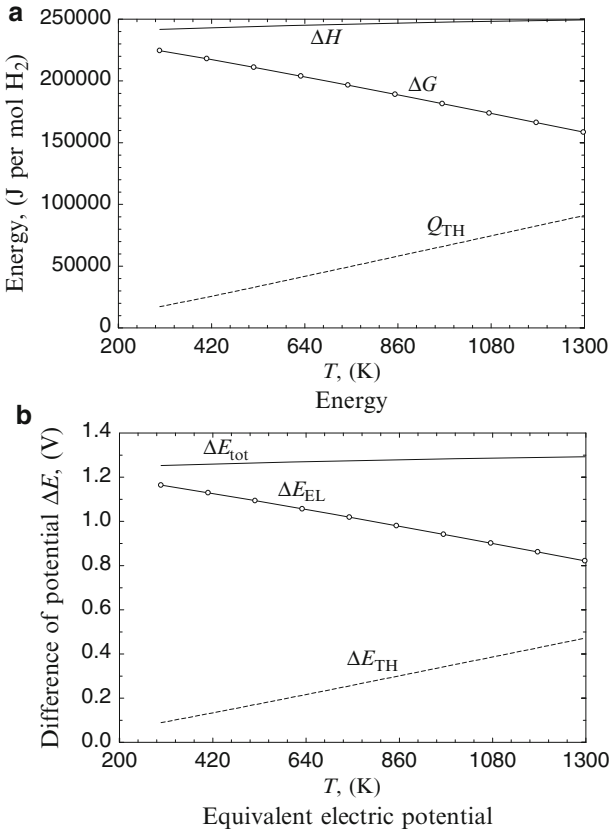


**Fig. 13.3** The energy and the equivalent electric potential needed to drive the water electrolysis process for a range of temperatures and standard pressure

$$\eta_{EL} = \frac{\Delta G + Q_{TH}}{\Delta G/\eta_E + Q_{TH}} = \eta_E \times \frac{\Delta G + Q_{TH}}{\Delta G + \eta_E Q_{TH}} > \eta_E, \tag{13.9}$$

where $\Delta G/\eta_E$ is the amount of thermal energy needed to generate the electricity amount equivalent to $\Delta G$. It can be observed in Eq. (13.9) that the factor $(\Delta G + Q_{TH})/(\Delta G + \eta_E Q_{TH}) > 1$; thus, $\eta_{EL} > \eta_E$, which demonstrates that the theoretical efficiency of HTSE is necessarily higher than the theoretical efficiency of liquid water electrolysis.

The ideal/minimal energy needed to drive the water electrolysis process can be calculated as $\Delta H(T)$, $\Delta S(T,P)$, and $Q_{TH}$ using the thermodynamic properties of water, hydrogen, and oxygen. These energy components are presented in Fig. 13.3a) and their corresponding electric potential equivalents in Fig. 13.3b). Many energy losses occur in electrolyzers due to various reasons such as over-potentials, ohmic losses. Consequently, the energy required to drive the electrolysis process is much higher than that calculated with $\Delta H(T)$.

The energy efficiency, defined as the energy retrieved in molar HHV of hydrogen, is divided into the total energy consumed to drive the process $\Delta H_{in}$,

$$\eta_{EL} = \frac{HHV_{H_2}}{\Delta H_{in}}, \tag{13.10}$$

and the corresponding exergy efficiency then becomes

$$\psi_{EL} = \frac{ex^{ch}_{H_2} + 0.5ex^{ch}_{O_2}}{Ex_{in}}. \tag{13.11}$$

$\eta_{EL}$ and $\psi_{EL}$ are of the order of 55% and 50%, respectively, for liquid water electrolysis; note that the chemical exergy of oxygen is very much smaller than that of hydrogen; also note that Eq. (13.11) is written for 1 mol of hydrogen produced. For HTSE, the energy efficiency achieves 80% while the exergy efficiency achieves 60%.

The total efficiency of the electrolysis, considering the electricity generation process, becomes the product $\eta^{TOT}_{EL} = \eta_{EL}\eta_E$ and $\psi^{TOT}_{EL} = \psi_{EL}\psi_E$. Based on these considerations, the hydrogen generation efficiency through water electrolysis is 15% (energy) and 10% (exergy). The corresponding figures for high-temperature electrolysis become 24% (energy) and 12% (exergy). Note also that high-temperature electrolysis is very favorable at 1,000 to 1,200 K and does not require expensive catalysts because the reaction rate is naturally accelerated at high temperature. Applications of HTSE are discussed below as electrothermal methods for hydrogen production.

Basically, any electricity generation process can be connected to a water electrolyzer to generate hydrogen using electricity only. All sorts of renewable energy, nuclear energy, and fossil energy plus energy recovered from other processes can then be used to generate electricity. Therefore, specific methods were developed to produce hydrogen through electricity from all these various routes.

#### 13.4.1.2 Solar–Electrical Routes for Hydrogen Production

Solar radiation is a source of high-quality energy that can be converted through two major methods to electric energy, that is, either directly, through various kinds of photovoltaic (PV) systems, or indirectly, by first concentrating thermal radiation to generate high-temperature heat and then converting the heat into mechanical energy through a heat engine, which further is converted into electric energy by power generators. The solar-generated electric energy can be further used to drive electrolysis, which produces hydrogen, as suggested in Fig. 13.4.

There is one additional electricity-based method that makes use of solar radiation to generate electricity; this is photoelectrolysis, which is conducted in an electrochemical cell. The electrochemical cell represents a compact device that

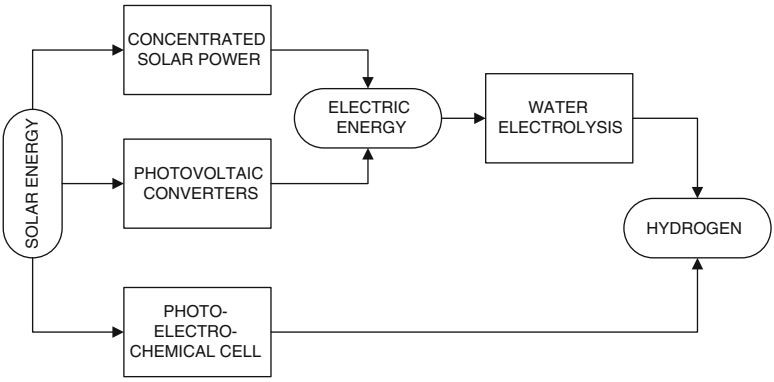


**Fig. 13.4** Two major routes for solar-electrical hydrogen production

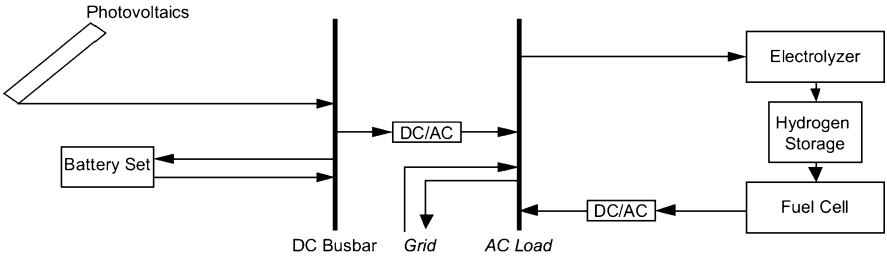


**Fig. 13.5** System for PV-driven water electrolysis [modified from Yilanci et al. (2009)]

combines the photovoltaic cell with an electrolyzer. Several interesting concepts were developed for generating electricity from solar energy; they are reviewed in detail in Chapter 9, where we analyze solar energy. Here, we discuss some relevant methods using solar energy for water electrolysis, without entering into the details of solar electric power generation, and we discuss the photoelectrochemical cell (PEC).

Photovoltaic-driven water electrolysis is a reference system that can be assembled with off-the-shelf components. Such system is described schematically in Fig. 13.5. It comprises PV panels, a DC bus bar, a AC grid, an accumulator battery set, an electrolyzer, and hydrogen storage canisters. The cost of PV-generated electricity is in continuous decline; for example, in 1998 the average cost was $12 per installed watt and in 2008 it was $8. This technology is currently a $10 billion business, growing by 30% per annum. This fact shows an encouraging trend for PV hydrogen production cost. The efficiency of the solar cell can range from 12% to 15% for the silicon solar cell. However, it is as high as 25% to 30% for a GaAs solar cell. The total efficiency of solar radiant energy transformed to chemical hydrogen energy is nearly 16% (Yilanci et al. 2009). The exergy efficiency of the PV-electrolyzer system is calculated as the product of exergy efficiency of the PV system $\psi_{PV}$ and the exergy efficiency of the electrolyzer $\psi_{EL}$ is

**Table 13.3** Efficiencies of the solar-$H_2$ generator components from Pamukkale University

| Components | Energy efficiency (%) | Exergy efficiency (%) |
|---|---|---|
| PVs | 11.2–12.4 | 9.8–11.5 |
| Charge regulators | 85–90 | 85–90 |
| Batteries | 80–85 | 80–85 |
| First inverter | 85–90 | 85–90 |
| Electrolyzer | 56 | 52 |
| Hydrogen tanks | 100 | 100 |
| Fuel cells | 30–44 | 24.5–38 |
| Second inverter | 85–90 | 85–90 |

Data from Yilanci et al (2009)

$$\psi = \psi_{\mathrm{PV}}\psi_{\mathrm{EL}} = \frac{V_{\mathrm{m}}I_{\mathrm{m}} - \left(1 - \frac{T_0}{T_{\mathrm{cell}}}\right)hA(T_{\mathrm{cell}} - T_0)}{\dot{E}x_{\mathrm{solar}}} \times \frac{\dot{E}x_{\mathrm{H_2}} + \dot{E}x_{\mathrm{O_2}}}{V_{\mathrm{m}}I_{\mathrm{m}}}, \qquad (13.12)$$

where $V_{\mathrm{m}}I_{\mathrm{m}}$ is the electrical power accounting for all electrical losses of the PV panel, associated electronics, and electrical lines. This power is the same as that retrieved at the input of the electrolyzer. The quantity $hA(T_{\mathrm{cell}} - T_0)$ represents the heat losses between the PV panel and the ambient air due to heat transfer; some exergy losses are associated with this heat as indicated in the numerator of the above equation.

### Illustrative Example: PV-Electrolyzer System

This example is a hybrid PV-based hydrogen production system, based on the principle introduced in Fig. 13.5, which was installed in February 2007 in the Clean Energy Center (CEC) on the campus of Pamukkale University in Denizli, Turkey, and is equipped with 5-kWe PV panels. For the purposes of our example, one-half of the photovoltaic modules are on a fixed tilt, and the other half are mounted on solar trackers. The fixed tilt (45° south) photovoltaic modules are located on the roof of the building. Each tracker consists of ten modules with nominal power of 1.25 kWp.

A line feed deionizer was selected to supply the quality of water needed for the electrolyzer. A basic particle water filter was also used before the deionizer. A PEM-type electrolyzer was used in the system. A metal hydride (MH) storage tank was used for hydrogen. The downside is that the hydrogen produced for MH storage must be of very high purity. Six OVONIC 85G250B storage tanks were chosen. The system includes also a fuel cell to generate electricity from the produced hydrogen and is connected to the grid. Table 13.3 lists the efficiencies of the individual system components. Average hydrogen production of the system for a week is 4.43 kg.

As for the solar concentrators, there were many test performed in the last 50 years to develop such electric generators. In a typical configuration (see Chapter 9), a parabolic mirror concentrates the solar radiation in the focal point, where it generates high-temperature heat. This heat is captured and used to drive

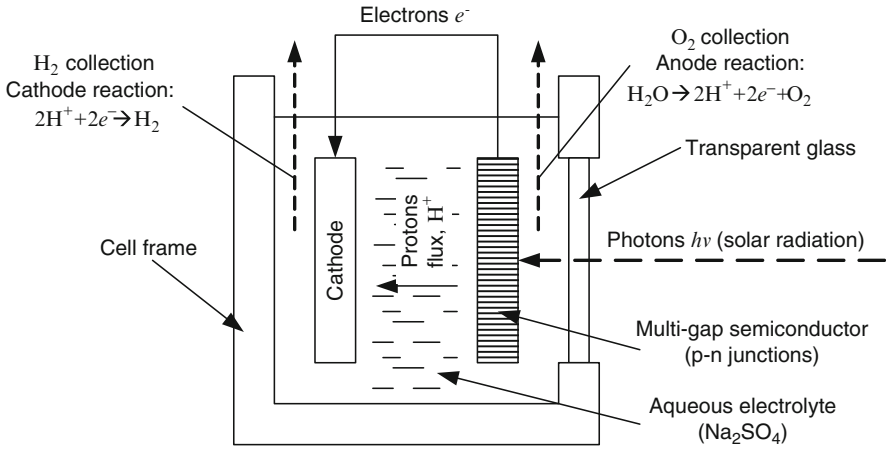


**Fig. 13.6** Sketch illustrating the operating principle of the photoelectrochemical cell

a heat engine that turns an electric generator. The typical efficiency of these electric power generating devices is 20% to 25%. When coupled with a water electrolyzer, the total solar-to-hydrogen efficiency becomes on the order of 10% to 15%.

Another electric-solar method for hydrogen production is photoelectrochemical water splitting. In this method, the photonic energy carried by solar radiation is used to generate an electric current that in turn drives the water electrolysis. This method is also called photoelectrolysis. It uses the so-called photoelectrochemical (PEC) cell, which may comprise photosensitive semiconductors immersed in an aqueous electrolyte and counter electrodes.

Figure 13.6 presents a possible configuration of the PEC cell, which was first proposed by Fujishima and Honda (1972). The semiconductor operates similarly to a photovoltaic cell, and it uses the photons with energy greater than the semiconductor band gap to generate electron-hole pairs that are split by the electric field that traverses the electrolyte. The water splitting reaction through the PEC cell becomes

$$H_2O \xrightarrow{hv} H_2(g) + 0.5O_2(g), \tag{13.13}$$

where $hv$ represents the photonic energy consumed for driving the process.

One remarkable advantage of the PEC cell is that it actually integrates solar energy absorption and water electrolysis into a single unit. Thus, the device does not require a separate solar power generator (e.g., a PV cell) and electrolyzer, and it is consequently more compact. The technology is in the course of development, and it achieved in the laboratory about 18% efficiency (Licht et al. 2001). The lifetime of a PEC cell was shown to be short because water corrodes the electrolyte. Many kinds of photosensitive semiconductor electrodes were investigated, one of the most promising being titanium dioxide ($TiO_2$); the other kinds are strontium titanate, carbonate oxides, NaOH oxides, tantalum oxynitride, other niobates and titanates, and cadmium sulfide.

**Table 13.4** Some projects of geothermal hydrogen production

| Location | Geothermal capacity (MW) | Electrolyzer capacity (MW) | $H_2$ production (ton/day) |
|---|---|---|---|
| Hawaii | 3.0 | 2.6 | 0.5 |
| Hawaii | 2.4 | 1.9 | 0.3 |
| Portugal | 250 | 234 | N/A |

Data from Balta et al. (2009)

#### 13.4.1.3 Hydrogen Production Through Electric Renewable Energy Other Than Solar

It is noted in Fig. 13.1 that energy sources such as hydro, wind, biomass, geothermal, ocean thermal, tides, and waves, and the energy recovered from human activity (industrial heat waste, municipal waste, landfill gas, etc.) can all be converted ultimately to electric energy. This energy can be further used for water electrolysis to produce hydrogen.

Biomass can be converted to electricity by either combustion or heat transfer to a power cycle (e.g., steam engine, organic Rankine cycle, or other engine). It is also possible to convert biomass into biogas or biofuel that further can generate electricity through internal combustion engine generator sets. Again Chapter 9 detailed the methods of electricity generation from biomass. The efficiency of electricity generation in this case ranges from 10% to 15% for a steam engine to 50% to 60% for a combined fuel cell/gas turbine cycle with gasification and heat recovery. Therefore, hydrogen efficiency production with biomass–electricity is of the order of 5% to 30%.

Geothermal energy can be used to generate electricity through various kinds of flash cycles and organic Rankine cycles. Depending on the level of temperature of the geothermal source, the energy efficiency of the electricity generation process may vary between 5% and 25%; correspondingly, if a geothermal generator is coupled with an electrolyzer, the expected hydrogen production efficiency is expected to be in the range of 3% to 12%. Some recent projects demonstrating geothermal hydrogen production are described briefly in Table 13.4.

Hydroelectric power generation is an established technology that uses the potential energy of water to generate electricity. The main components of the hydropower plants are a dam/retaining wall, a water turbine, and an electrical generator. A dam or retaining wall is built along the width of a river so that the water level can rise on one side of the wall. On the other side of the dam/retaining wall, water turbines coupled with electricity generators are installed. The potential energy of water is then used to run turbines, and then turbines run generators and produce electricity. Water turbines are available in a large variety and depending upon the different water head the flow rate turbines can be selected. A Pelton wheel and Francis turbines are generally used for high water heads, and the Kaplan turbines can be used for low water heads. Some intermediate water head turbines that can be used for both high and low water heads are the Michel Banki and Deriaz turbines. The electricity produced is then supplied to the grid from where

it is distributed to its users. Mini-hydropower stations can also be built to fulfill the electricity demand of a community that is situated near small rivers and where the water head is not enough for large hydropower plants. Hydro energy is used essentially to produce electricity, and then the electricity can be used for hydrogen production via electrolysis. Hydropower plants are more eco-friendly than the thermal power plants, as they cause less harm to the environment, but as they require large civil structures and community relocation for those who live near the river, they sometimes face substantial public resistance. Because of the high efficiency of hydroelectric power generation (90%), the expected hydro-to-hydrogen efficiency is around 45%.

Wind mills and horizontal-axis and vertical-axis turbines are used to convert the kinetic energy of the wind into electricity. It is one of the more cost-effective forms of renewable energy in today's technology. The electricity produced by wind energy can be supplied to the grid. The technology is beneficial for the locations, where the wind velocity is high, for example, the coastal and subcoastal areas. For better functioning of a wind energy system, the knowledge of the natural geographical variation in wind speed is important so as to smooth out fluctuations. Similar to the limitations of solar energy, wind energy generation is also affected by the intermittent nature of wind speed. Similar to hydro energy, wind energy also essentially is used to produce electricity first, and then the electricity can be used for hydrogen production. However, the problem with wind energy resides in its fluctuating availability. Fortunately, one of the remarkable features of electrolyzers is that they can adapt fast enough to fluctuations in the supplied voltage so that they are suitable to couple with wind turbines. Taking into account the low-capacity factor (~25%), the expected efficiency of wind-electricity-hydrogen production is ~10%.

Some other renewable sources are tidal, wave, and ocean thermal technologies that can produce electricity or can help reduce the electrical load of a power plant. Tidal energy utilizes the power of tide to produce electricity, whereas wave energy systems use the waves formed in an ocean or sea. Oscillators are placed in the sea and they oscillate when waves come in contact with them. This oscillatory motion is utilized to generate electricity. The ocean thermal technology uses the temperature difference between the upper and the deep lower level of ocean water. This thermal difference is utilized to generate electricity.

Several human activities waste large amounts of energy; this energy is lost either in the form of heat, some form of biochemical energy as in landfill gas case, or chemical energy waste that can be incinerated to obtain heat. Heat recovered can be applied in such situations, and depending on the temperature level of the heat source, it is possible to generate electricity with a certain efficiency. There are heat engines that operate at a low-temperature differential, as well as many kinds of power plant technologies that use higher—combustion level—temperature. Landfill gas can be supplied to internal combustion engine-driven generators to obtain electric power and therefore hydrogen.

One important aim of producing hydrogen from renewable sources is leveling electricity production. Many renewable sources like wind, solar, hydro, tides, or

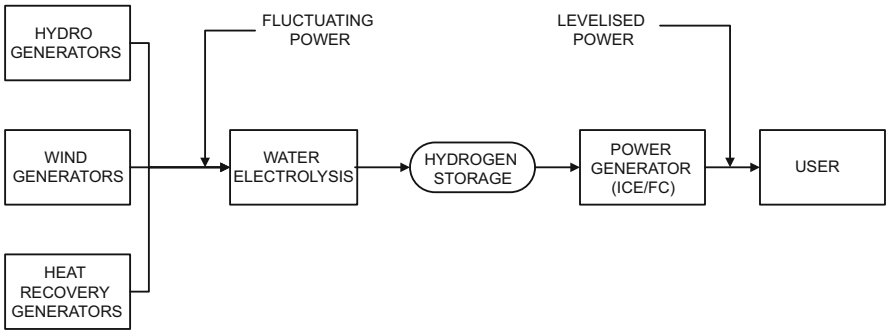


**Fig. 13.7** General concept for $H_2$ generation from renewables for levelized power production

industrial heat recovery are fluctuating in nature or intermittent. A design like the one shown in Fig. 13.7 suggests how, through hydrogen, the power production is levelized. Power generators from various renewable sources can work either separately or in parallel to drive water electrolysis, although with a fluctuating electric capacity. Hydrogen is produced from these sources and accumulated in tankers. The hydrogen may further supply a power generator (e.g., fuel cell, internal combustion engine, etc.) to generate electricity at a levelized rate according to the demand.

#### 13.4.1.4 Fossil Fuel–Based Electricity for Water Electrolysis

The combustion of coal, petroleum, and natural gas is widely used nowadays for electricity production. There is a large number of technologies available to generate electricity from such basic fuel sources. We exclude from our discussion the integrated gasification/gas turbine cycles and fuel cells because such methods already generate hydrogen through thermochemical means, and it does not appear logical to drive an electrolyzer to produce hydrogen in this case. The conventional fossil fuel–based power plants are the steam turbine (Rankine), gas turbine, and diesel engine power plants.

The lowest efficiency is attained by coal power plants, up to 30%, but a combined cycle (topping-bottoming) can reach 50%. Therefore, the expected hydrogen production efficiency from this source is 15% to 25%. This efficiency is degraded if carbon dioxide capture is applied to the power generation plant.

#### 13.4.1.5 Nuclear Power Coupled with Water Electrolyzer

There are two main ways to couple nuclear reactors with water electrolysis stations. In the first and simpler way, all electrical production of a nuclear power plant can be used to drive water electrolysis and to generate hydrogen, as illustrated in Fig. 13.8a. The efficiency of the power plant is indicated in the figure with

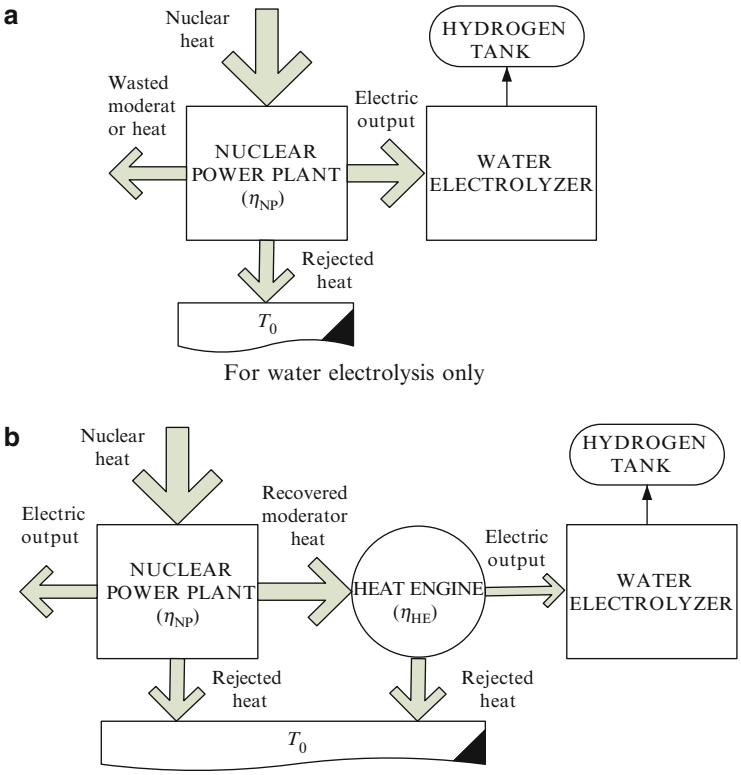


**Fig. 13.8** Ways to couple water electrolysis to nuclear reactors for (**a**) dedicated hydrogen production systems or (**b**) cogeneration systems of electricity and hydrogen

the notation $\eta_{NP}$. The advantage of such a system comes from the possibility of operating at the design load without direct interference with the grid, which can be congested in some periods of time. Another important advantage of nuclear/water electrolysis is that there is no need to modify the reactor. Such systems were applied on nuclear submarines to generate oxygen (for maintaining life) and hydrogen. It is possible to adapt the system to the existent nuclear power plants to generate off-peak electricity.

The generation of hydrogen during off-peak hours at nuclear plants allows for constant load operation at the highest efficiency and lowest electricity production cost. Also, grid congestion that decreases the reliability and efficiency of the electrical grid is avoided. Recall that the maximum expected efficiency of the water electrolysis process is 80% even though studies show less than 55%. Coupled with current light water reactors or advanced light water reactors (ALWRs), the expected thermal-to-hydrogen efficiency is 27%; coupled with a modular helium reactor (MHR) or an advanced gas reactor (AGR), the expected efficiency is ~35%.

The second way to couple nuclear reactors with a water electrolysis system is suggested in Fig. 13.8b. In this case the moderator heat is recovered with

specially designed heat exchangers and supplied to a heat engine able to operate with a low temperature differential. Examples of low differential heat engines are the organic Rankine cycles (ORC) and the Kalina cycle. The efficiency of these cycles is indicated in the figure with $\eta_{\mathrm{HE}}$. Thus the efficiency of hydrogen generation becomes $\eta_{H_2} = (1 - \eta_{\mathrm{NP}}) \times \eta_{\mathrm{HE}} \times \eta_{\mathrm{EL}}$, where the subscript EL stands for electrolyzer.

## *13.4.2 Thermally-Driven Hydrogen Production Methods*

### 13.4.2.1 Water Thermolysis

As indicated in Table 13.2, the hydrogen production methods driven by thermal energy are thermolysis, thermochemical water splitting (TCWS), reforming and gasification, and thermal cracking. All these processes are presented here as well as their coupling with various primary energy and energy recovery sources.

The single-step thermal dissociation of water is known as water thermolysis and can be given as

$$\mathrm{H_2O} \overset{\text{heat}}{\rightarrow} \mathrm{H_2} + 0.5\mathrm{O_2}. \tag{13.14}$$

The reaction requires a high-temperature heat source at above 2,500 K to have a reasonable degree of dissociation, and by the need for an effective technique for separating $H_2$ and $O_2$ to avoid ending up with an explosive mixture. Kogan (1998) tested semipermeable membranes based on $ZrO_2$ and other high-temperature materials at up to 2,500 K. The very high temperature required by the process (e.g., 3,000 K for 64% dissociation at 1 bar) poses severe material problems and can lead to significant reradiation from the reactor, thereby lowering the absorption efficiency.

### 13.4.2.2 Thermochemical Water Splitting

Thermochemical water splitting (TCWS) involves a series of chemical reactions performed in a loop with the general effect of water decomposition into hydrogen and oxygen. One major advantage of a thermochemical cycle is that it normally does not require catalysis to drive the chemical reactions. All chemicals involved in the process are recycled except water, which is the material source from which hydrogen is derived. Water-splitting thermochemical cycles are attractive for the following reasons: (a) there is no need for hydrogen–oxygen separation membranes; (b) the temperature of the required thermal energy source is in a reasonable range (600–1,200 K); (c) there is no or very little requirement for electrical energy to drive the process. If no electricity is needed to drive thermochemical cycles, then an only thermally driven hydrogen production method is possible. If electricity and heat are both needed to drive the thermochemical water process, the associated

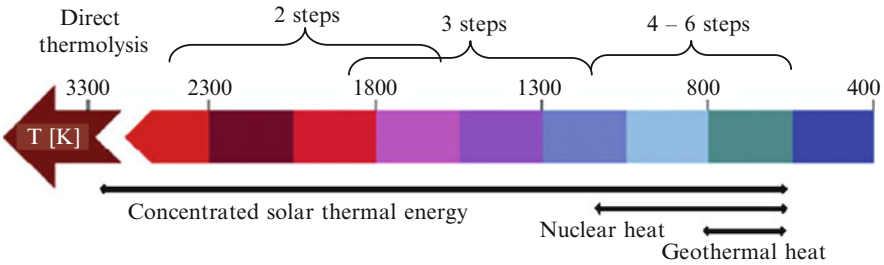


**Fig. 13.9** Correlation between number of chemical steps (cycles) of thermochemical water splitting systems with process temperature [modified from Balta et al. (2009)]

cycle is called a hybrid. Some relevant hybrid thermochemical cycles are reviewed in a subsequent section. Here, we refer only to the thermal-only driven methods.

Balta et al. (2009) noted an interesting finding: the number of chemical reactions involved by the thermochemical water splitting cycles is smaller as the process temperature increases. They correlated the number of cycles with the temperature as indicated in Fig. 13.9. The plot also suggests that concentrated solar energy is suitable for all thermochemical methods.

Abanades et al. (2006) compiled a database with 280 thermochemical cycles referenced in the literature. From those, we will analyze in the subsequent paragraph only two, which are probably the most promising thermal-only cycles. Other hybrid cycles (electro-thermal) will be discussed in Section 13.4.3.1. Various sustainable sources of high temperature heat can be considered to drive these cycles. Nuclear heat probably can be used up to 1,000 K, geothermal heat is available up to 800 K, biomass combustion and concentrated solar radiation may generate heat up to about 1500 K.

The sulfur–iodine (S–I) cycle operates at a maximum temperature of 1000 K to 1075 K, which is needed to drive the oxygen-evolving reaction. The S–I cycle has been fully demonstrated in both Japan and the United States, and has been shown to be technically viable. However, the commercial viability has yet to be demonstrated. The equipment cost of an S–I plant with 790 tons/day of hydrogen production capacity is $125 million. Membrane technology was developed to enhance the separation efficiency for this cycle. The maximum attainable one-pass S-I conversion rate was reported to exceed 90% with membrane technology, whereas the equilibrium rate is about 20%.

The first reaction of this cycle is the sulfuric acid decomposition to release water; this reaction is thermally driven, noncatalytic, and conducted at 300° to 500°C:

$$H_2SO_4(aq) \xrightarrow{\text{heat @ } 300-500^\circ C} H_2O(g) + SO_3(g). \tag{13.15}$$

The resulting steam is separated from $SO_3(g)$ and by further heating up to 800° to 900°C the sulfur trioxide is decomposed thermally to release oxygen:

$$SO_3(g) \xrightarrow{\text{heat @ } 800-900^\circ C} SO_2(g) + 0.5O_2(g). \tag{13.16}$$

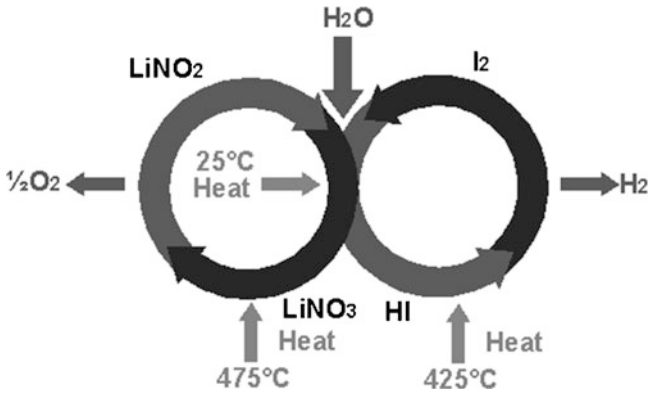


**Fig. 13.10** The $LiNO_3$ water splitting process [modified from Balta et al. (2009)]

The so-called Bunsen reaction follows, which combines the sulfur dioxide $SO_2(g)$ separated from oxygen with iodine and water. The reaction is exothermic and occurs at low temperatures, spontaneously, to produce sulfuric acid:

$$SO_2(g) + I_2(g) + 2H_2O(l) \rightarrow 2HI(g) + H_2SO_4(aq). \tag{13.17}$$

The hydrogen iodine is further decomposed thermally at 425° to 450°C and generates hydrogen:

$$2HI(g) \xrightarrow{\text{heat @ } 425-450^\circ C} H_2(g) + I_2(g). \tag{13.18}$$

One major advantage of the S–I cycle consists of the fact that there are no side reactions occurring during the process, and the separation of chemicals is relatively straightforward. The drawback of the process is that it occurs at a rather high temperature. Thus, a relatively lower number of sustainable thermal energy sources is available to drive this process. Among such possible sources are nuclear heat from high-temperature gas-cooled reactors, concentrated solar thermal heat, and biomass combustion heat. Note that the S–I cycle has a hybrid version also in which the hydrogen evolving reaction is conducted electrochemically.

An interesting process, but less well developed, is the $LiNO_3$ cycle for water splitting. This thermally driven cycle evolves completely at lower temperatures. The highest temperature required is 475°C for the $LiNO_3$ decomposition reaction that releases oxygen. Also, the hydrogen iodine decomposition reaction is evolving at 425° to 450°C. The cycle is represented schematically in Fig. 13.10.

The first reaction occurs at a temperature close to the ambient and is endothermic:

$$LiNO_2(g) + I_2(g) + H_2O(l) \xrightarrow{\text{heat @ } 40^\circ C} LiNO_3(g) + 2HI(g). \tag{13.19}$$

The other two reactions are also endothermic evolving at higher temperature and releasing hydrogen and oxygen:

$$\left.\begin{aligned} 2\mathrm{HI(g)} &\xrightarrow{\text{heat @425–450°C}} \mathrm{I_2(g) + H_2(g)} \\ \mathrm{LiNO_3} &\xrightarrow{\text{heat @475°C}} \mathrm{LiNO_2(g) + 0.5O_2(g)} \end{aligned}\right\}. \tag{13.20}$$

#### 13.4.2.3 Reforming and Gasification

When water is the primary source, the thermochemical processes for hydrogen production are called thermochemical cycles, suggesting that the involved chemicals, except water, are recycled. If other chemicals like hydrocarbons, fossil fuels, biomass, and alcohols are used as hydrogen sources, the thermochemical processes do not occur cyclically. For example, the process of steam methane reforming can be categorized as thermochemical, and no chemicals are recycled, but they are rather completely transformed; overall, methane and steam enter into the reaction, and it results in hydrogen and carbon monoxide.

We turn now to reforming and gasification processes for hydrogen production. The terminological distinction between reforming and gasification addresses the nature of the consumed fuel by the conversion process. When a solid fuel like coal or biomass or solid waste is converted to hydrogen gas or synthesis gas (hydrogen + carbon monoxide), the process is called gasification. When a fluid fuel (gas or liquid: alcohols, natural gas, petroleum) is converted to synthesis gas, this process called reforming.

The steam-reforming/gasification method requires additional steps for shifting CO and for separating $CO_2$, whereas the thermal cracking accomplishes the removal and separation of carbon in a single step. The schematic of the gasification process is represented in Fig. 13.11. The steam-reforming of natural gas, oil, and other hydrocarbons, and the steam-gasification of coal and other solid carbonaceous materials (e.g., biomass) can be expressed by the simplified net reaction:

$$C_x\mathrm{H}_y + x\mathrm{H_2O} \xrightarrow{\text{high temperature heat}} \left(\frac{y}{2} + x\right)\mathrm{H_2} + x\mathrm{CO}. \tag{13.21}$$

Depending on the reaction kinetics and on the presence of impurities in the raw materials, other compounds may also be formed during the conversion. Among the other possible reactions occurring concurrently at various rates are: $\mathrm{CH_4 + H_2O \rightarrow CO + 3H_2 - 206\,kJ/mol}$, $\mathrm{CH_4 + 2H_2O \rightarrow CO_2 + 4H_2 - 165\,kJ/mol}$, $\mathrm{C + H_2O \rightarrow CO + H_2 - 131\,kJ/mol}$, $\mathrm{C + H_2 \rightarrow CH_4 - 75\,kJ/mol}$, and $\mathrm{C + CO_2 \rightarrow 2CO - 172\,kJ/mol}$. The carbon monoxide content present in the product of the reforming/gasification process can be shifted to $H_2$ via the catalytic water–gas shift reaction ($\mathrm{CO + H_2O \rightarrow H_2 + CO_2}$), and the carbon dioxide can be separated from $H_2$ using various methods as discussed in Chapter 14.

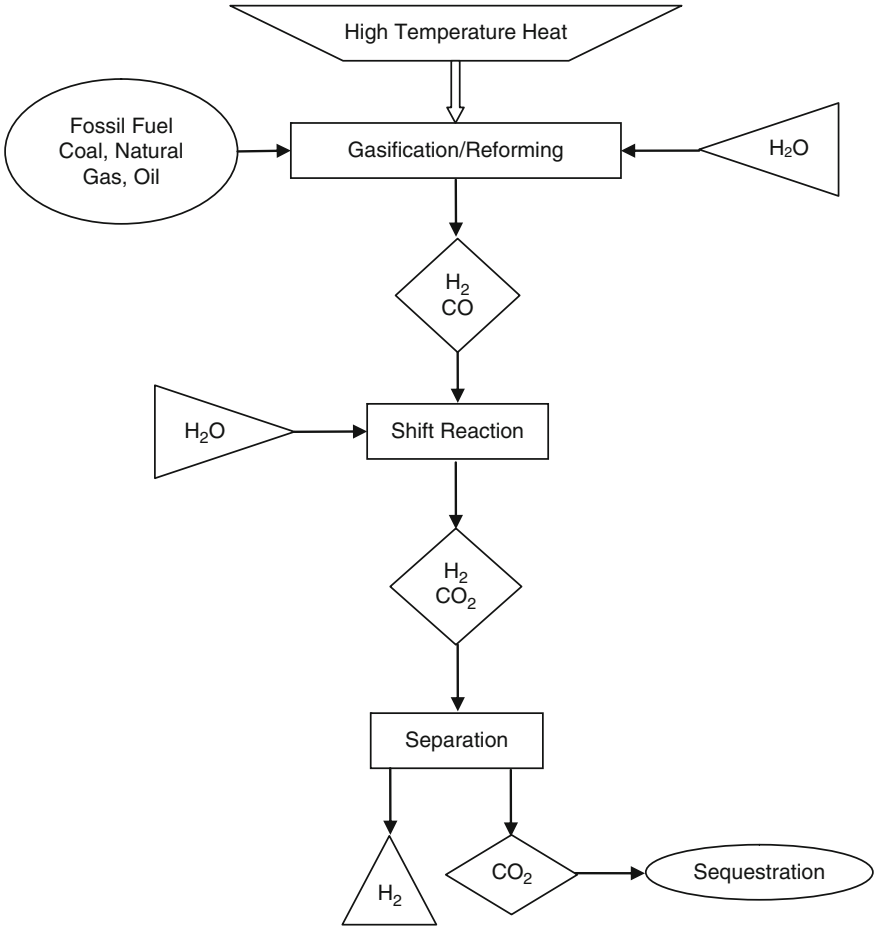


**Fig. 13.11** Schematic diagram of the gasification/reforming process

The gasification agents are described in Table 13.5. Gasifiers and reformers are in general large equipment that operate at high temperature and are exposed to ambient conditions. Consequently, one of the energy losses characteristic of such equipment is the heat leaks through the exterior. If $T_w$ is the temperature of the gasifier, the lost heat can be simply calculated with $Q_{lost} = U_w A(T_w - T_0)$, where $T_0$ is the ambient temperature and $U_w$ is the heat transfer coefficient at the wall, which can be determined with an appropriate equation that considers a combined heat transfer through convection and radiation. One recommended equation for the heat transfer coefficient is that by Isachenko et al. (2004):

$$U_w = 1.9468(T_w - T_0)^{1/2}(2.8633V_{wind} + 1)^{1/2} + 5.75 \times 10^{-8}\varepsilon_{ins}\frac{T_w^4 - T_0^4}{T_w - T_0}, \quad (13.22)$$

**Table 13.5** Gasification agents

| Agent | Process temperature | Remarks |
|---|---|---|
| Oxygen | 1,000–1,400°C | Syngas heating value is high: 10–15 MJ/m$^3$; oxygen handling is expensive and implies safety issues |
| Air | 900–1,100°C | Syngas has low heating value (4–6 MJ/m$^3$) because it contains up to 60% $N_2$ and other contaminants like tars and hydrocarbons; it is the cheapest method and most used |
| Steam | 800–1,200°C | The heating value of product gas is 8–10 MJ/m$^3$ with around 45% H2, 25% of CO and a large quantity of steam (~18%); presence of steam creates problems with corrosion |
| Supercritical water | 400–800°C | Operates at high pressures, around 30 MPa; this process can suppress the formation of tar and char; drying of fuel (like biomass) can be avoided |

where $\varepsilon_{\text{ins}}$ is the thermal emissivity of the insulation and $V_{\text{wind}}$ is the average velocity of the wind in m/s. The temperature of the wall is calculated based on the average temperature of the gasification process $T$, and the thermal conductivity of the wall insulation, $k_{\text{ins}}$, assumed to be of thickness $\delta$:

$$U_{\text{w}}(T_{\text{w}} - T_0) = \frac{k_{\text{ins}}}{\delta}(T - T_{\text{w}}). \tag{13.23}$$

The main parameters affecting the gasification process are listed in Table 13.6. Different gasifiers are employed in the gasification process: fixed bed, moveable bed, and fluidized bed. The process could be either auto-thermal or all-thermal depending on how this heat is provided. In the case of auto-thermal gasification, the necessary heat is generated directly by partial oxidation in the gasifier itself.

#### 13.4.2.4 Thermocatalytic Cracking

Hydrogen can also be produced from hydrocarbons by using thermal cracking processes. The thermal cracking process normally necessitates catalysts, as opposed to thermochemical hydrogen production, which does not. Thermal cracking can be conducted either as an oxidative or nonoxidative process. The nonoxidative process of thermal cracking of hydrocarbons to produce hydrogen can be represented by the simplified net reaction:

$$\text{C}_x\text{H}_y \rightarrow x\text{C(s)} + \frac{y}{2}\text{H}_2\text{(g)}, \tag{13.24}$$

where C(s) represents carbon that is precipitated as a powder or granulate matter.

The thermal cracking reaction produces a carbon-rich condensed phase and a hydrogen-rich gas phase. The carbonaceous solid product can be used as a material

**Table 13.6** Parameters influencing the gasification process

| Parameter | Description | Effects |
|---|---|---|
| Equivalent ratio | The oxygen supplied over the stoichiometric oxygen | Higher oxidant delivered through increased air rate dilutes the product gas and reduces the efficiency; too low air rate does not suffice for partial oxidation, which reduces gas production |
| Steam-fuel ratio | $\mathrm{SBR} = \frac{\dot{m}_{\mathrm{steam}} + \dot{m}_{\mathrm{moist}}}{\dot{m}_{\mathrm{fuel}}(1 - \mathrm{moist}_{\%})}$ | Influences the required energy input and product gas composition; low SBR leads to more methane and solid carbon formation; high SBR means more syngas produced |
| Process temperature | Process temperature is not constant; gasifier temperature is considered that which occurs after the pyrolysis zone | Lower temperatures lead to more solid carbon and methane in the product gas; in general, optimal values are 800–900°C; above these hydrogen yield reduces |
| Process pressure | Gasification occurs at constant pressure in the gasifier | Chemical equilibrium indicates that gasification is favored by low pressures and high temperatures; however, no substantial gain is obtained if the process runs in a vacuum |

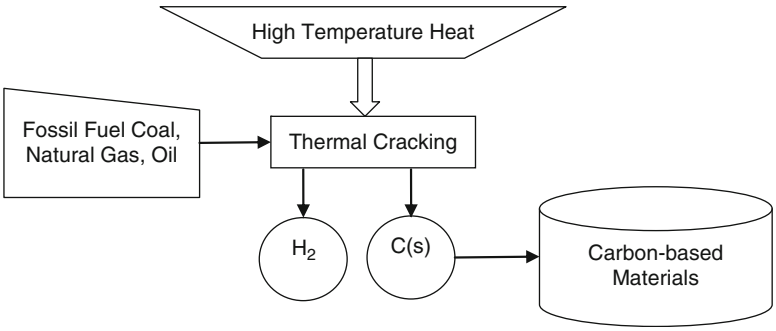


**Fig. 13.12** Schematic diagram of solar cracking

commodity or reducing agent. The process of thermal cracking is illustrated schematically in Fig. 13.12. Thermal cracking may be the preferred option for natural gas and other hydrocarbons with a high $H_2$/C ratio. Oxidative thermal cracking can be implemented as cyclic redox reactions on metals. An efficient two-step thermocatalytic cycle uses metal oxide redox reactions. The first step is the endothermic reduction:

$$\mathrm{M}_x\mathrm{O}_y \xrightarrow{\text{high temperature heat}} x\mathrm{M} + \frac{y}{2}\mathrm{O}_2. \tag{13.25}$$

The second step is the exothermic oxidation:

$$xM + yH_2O \rightarrow M_xO_y + yH_2, \tag{13.26}$$

where M denotes a metal and $M_xO_y$ the corresponding metal oxide. The first, endothermic step is of thermal dissociation of the metal oxide to lower-valence metal oxide. The second process is exothermic hydrolysis of the metal to form $H_2$ and to reform the initial metal oxide. The net reaction is of water splitting ($H_2O = H_2 + 1/2O_2$), but since $H_2$ and $O_2$ are formed in different reactors (reduction and oxidation reactors), the need for high-temperature gas separation is thereby eliminated.

A very well known redox process for hydrogen production is the so-called steam–iron process:

$$\left.\begin{aligned} 2Fe_3O_4 + H_2O &\rightarrow 3Fe_2O_3 + H_2 \\ 3Fe_2O_3 + CO &\rightarrow 2Fe_3O_4 + CO_2 \end{aligned}\right\}, \tag{13.27}$$

which normally evolves at very high temperature (~1,000°C). The carbon monoxide is consumed in this process. Sources of carbon monoxide can be found in metal processing plants. Note that the thermal cracking process can also be electrically driven in plasma produced by electric arcs.

#### 13.4.2.5 Biomass-Thermal Routes for Hydrogen Production

Biomass having moisture content lower than 35% can also be used as primary energy to extract hydrogen from steam. If the moisture content is too high, either the biomass must be dried before gasification or supercritical steam gasification can be applied. Supercritical steam gasification is a process that uses steam at supercritical pressure and temperature, and it is adapted to convert biomass to hydrogen regardless of its moisture content. Wood sawdust, sugar cane, and bagasse are some general forms of biomass that can be used to produce hydrogen.

Abuadala et al. (2010) analyzed a hydrogen production system based on steam gasification of biomass that uses wood sawdust and 4.5 kg/s of steam at 500 K. They found that the hydrogen yield reaches 80 to 130 $gH_2$/kg biomass with 50% molar concentration in the product gas, which reaches a heating value of 15 to 20 MJ/$m^3$. The biomass is introduced to a gasifier at an operating temperature range of 1,000 to 1,500 K. The global reaction of the biomass gasification process to produce hydrogen is as follows:

$$\alpha C_lH_mO_n + \gamma H_2O \xrightarrow{\text{heat}} aH_2 + bCO + cCO_2 + dCH_4 + eC + f\,\text{Tar}, \tag{13.28}$$

where $\alpha C_lH_mO_n$ is the general chemical representation of the biomass. The formation of tars is undesirable because of the negative effect on the pipes, ducts, and

**Table 13.7** Energy and exergy efficiency of biomass gasification process

| Case | Energy efficiency | Exergy efficiency |
|---|---|---|
| Only hydrogen is considered as output | $\eta = \frac{\mathrm{HHV}_{\mathrm{H_2}}}{n_\mathrm{b}\mathrm{HHV}_\mathrm{b} + n_\mathrm{s}\Delta h_\mathrm{s}}$ | $\psi = \frac{\mathrm{ex}^{\mathrm{ch}}_{\mathrm{H_2}}}{n_\mathrm{b}\mathrm{ex}^{\mathrm{ch}}_\mathrm{b} + n_\mathrm{s}\mathrm{ex}_\mathrm{s}}$ |
| All product gas (PG) is considered as output | $\eta = \frac{\mathrm{HHV}_{\mathrm{PG}}}{n_\mathrm{b}\mathrm{HHV}_\mathrm{b} + n_\mathrm{s}\Delta h_\mathrm{s}}$ | $\psi = \frac{\mathrm{ex}^{\mathrm{ch}}_{\mathrm{PG}}}{n_\mathrm{b}\mathrm{ex}^{\mathrm{ch}}_\mathrm{b} + n_\mathrm{s}\mathrm{ex}_\mathrm{s}}$ |
| The product gas (PG), tar (T), and char (C) are all considered as useful outputs | $\eta = \frac{\mathrm{HHV}_{\mathrm{PG}} + n_\mathrm{T}\mathrm{HHV}_\mathrm{T} + n_\mathrm{C}\mathrm{HHV}_\mathrm{C}}{n_\mathrm{b}\mathrm{HHV}_\mathrm{b} + n_\mathrm{s}\Delta h_\mathrm{s}}$ | $\psi = \frac{\mathrm{ex}^{\mathrm{ch}}_{\mathrm{PG}} + n_\mathrm{T}\mathrm{ex}^{\mathrm{ch}}_\mathrm{T} + n_\mathrm{C}\mathrm{ex}^{\mathrm{ch}}_\mathrm{T}}{n_\mathrm{b}\mathrm{ex}^{\mathrm{ch}}_\mathrm{b} + n_\mathrm{s}\mathrm{ex}_\mathrm{s}}$ |

**Table 13.8** Indicative parameters and $H_2$ yields of biomass gasifiers

| Biomass | $T$ (°C) | Steam-biomass ratio | $H_2$ yield (%) |
|---|---|---|---|
| Pine and eucalyptus | 880 | 0.8 | 41 |
| Pine sawdust | 750 | 0.5 | 40 |
| Mixed sawdust | 750 | 0.51 | 62.5 |
| Mixed sawdust | 800 | 4.7 | 57.4 |
| Mixed sawdust | 800 | 1.4 | 48.8 |
| Mixed sawdust | 800 | 1.1 | 46 |
| General biomass | 777 | 1.5 | 59 |

*Source:* Abuadala et al. (2010)

equipment by slugging and fouling. Tar formation can be diminished by proper controls and by using various catalysts.

Assuming that the inputs in the steam gasifier are the energy embedded in steam and in the fed biomass, the energy and exergy efficiencies can be defined as in Table 13.7. In the efficiency expressions, $n$ represents the number of mols of biomass (index b), steam (index s), tars (index T), and char (index C) needed to generate 1 mol of product. For the first row in the table, the product is considered to be hydrogen only; for the other two cases, the number of mols corresponds to the generation of 1 mol of product gas. The enthalpy difference $\Delta h_\mathrm{s}$ is calculated based on the molar specific enthalpy of the steam at gasifier inlet conditions and the enthalpy of the water at the reference state, $\Delta h_\mathrm{s} = h_\mathrm{s} - h_0$. The thermomechanical exergy of the steam is given by $ex_\mathrm{s} = \Delta h_\mathrm{s} - T_0(s_\mathrm{s} - s_0)$, where $s_\mathrm{s}$ is the specific molar entropy of steam. The notation $\mathrm{ex}^{\mathrm{ch}}$ stands for the specific molar chemical exergy; the HHV are the respective molar higher heating values. Table 13.8 indicates the $H_2$ yield and operating parameters of typical gasifiers.

### Illustrative Example: Biomass Gasification for Hydrogen Production

This example entails steam biomass gasification for hydrogen production according to the results by Abuadala et al. (2010), in a gasifier with 80 cm outside diameter and 50 cm height, insulated with a material with $k_\mathrm{ins}/\delta = 12\,\mathrm{W/m^2\,K}$ and $\varepsilon_\mathrm{ins} = 0.01$, exposed to an average wind condition of 2 m/s and fed with sawdust wood biomass at a rate in the range of 10 to 32 kg/s. Steam is fed at 500 K, while the temperature of the gasifier is kept in the range of 1,000 to 1,500 K. For modeling purposes, the chemical formula of tars is assimilated to that of benzene.

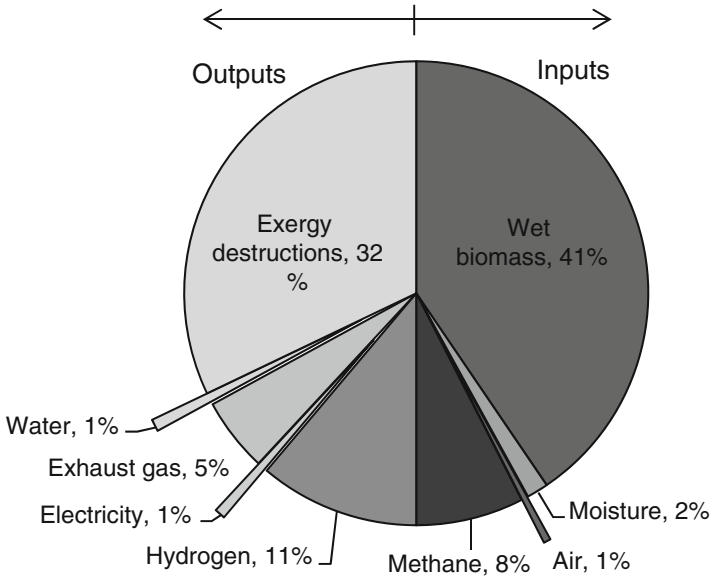


**Fig. 13.13** Typical exergy balance on a biomass gasifier [data from Cohce et al. (2010)]

At these conditions, the simulations performed by Abuadala et al. (2010) with Engineering Equation Solver (EES) software indicate the variation of the product gas concentration with the biomass feed rate in the range of 50% to 60%. It is interesting to note that the hydrogen concentration behaves in an opposite manner to the carbon monoxide concentration. These results indicated that only 7% to 11% of the fed biomass is converted to hydrogen. If the steam feed rate is increased in the same conditions (from 4.5 to 6.3 kg/s), the hydrogen concentration in the product gas increases by about 4%, which indicates the beneficial effect of adding steam. It has been found that the rise of the gasification temperature from 1,000 to 1,500 K led to the decrease of hydrogen concentration by 2%.

The order of magnitude of energy inputs and outputs in a gasification process is indicated in Fig. 13.13, which is constructed based on the results of Cohce et al. (2010) that simulated palm oil gasification with ASPEN Plus software. Note also that a biomass gasifier is a complex system involving many types of equipment such as heat exchangers, particle–gas separators (cyclones), gas–gas separation devices (membranes), gas turbines, compressors, pumps, blowers, biomass feeders, and so on. Figure 13.14 illustrates the biomass gasifier as programed in ASPEN Plus software.

#### 13.4.2.6 Hydrogen Extraction from Hydrogen Sulfide

Hydrogen sulfide, with chemical formula $H_2S$, embeds 76 g of hydrogen per liter at standard atmospheric conditions, which is about 1,000 times more than the mass

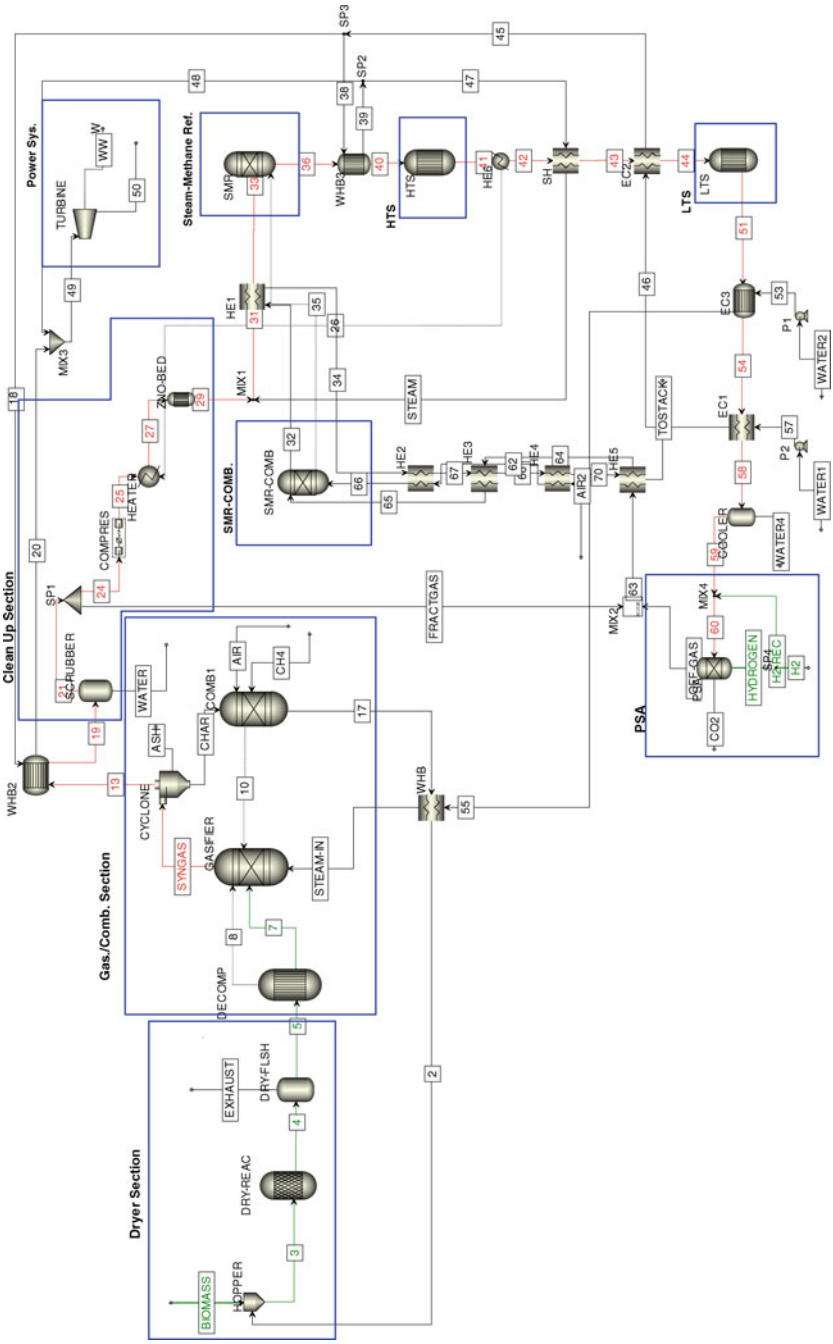


**Fig. 13.14** ASPEN Plus diagram of a biomass gasifier [modified from Cohce et al. (2010)]

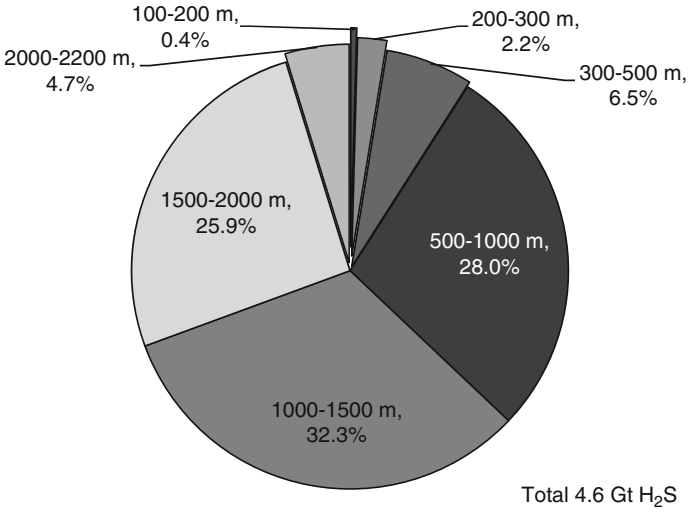


**Fig. 13.15** Hydrogen sulfide distribution in Black Sea deep sea waters [data from Midilli et al. (2007)]

of pure hydrogen per unit of volume in the same conditions. Hydrogen sulfide occurs naturally in various environments, such as regions with volcanic activities, hot springs, well water, oil wells, and in certain lakes and seas.

Thus, hydrogen sulfide can be seen as a natural resource from which hydrogen and sulfur can be extracted. A recent study by Midilli et al. (2007) demonstrates that deep waters of the Black Sea have a resource of 4.6 billion tons of $H_2S$, which offer the potential of extracting 270 million tons of hydrogen; in energy terms, this amount is equivalent to 851 millions tons of natural petroleum (or $7 \times 10^9$ barrels). Exploited properly, this resource can be made renewable, since the bacterial activity could in principle be maintained. Extraction of hydrogen from hydrogen sulfide can be made via thermal cracking at high temperatures or by special membrane technology.

The Black Sea is unique in the sense that most microbial activity that it hosts (90%) is anaerobic. This facilitates the proliferation of sulfur-reducing bacteria, which generate hydrogen sulfide. It has been observed that the anaerobic activity is more intense in deep water (at depths of over 150 m), where the concentration of $H_2S$ increases steadily; close to the sea bottom at 1,000 to 2,000 m depth the concentration reaches 8 to 8.5 ml/l (Midilli et al. 2007). The hydrogen sulfide distribution in the Black Sea depths is presented as percentages in Fig. 13.15, which is constructed based on the data published in Midilli et al. (2007). Hydrogen sulfide can be extracted from (sea) waters through various methods, including distillation, and further cracked.

Cracking of hydrogen sulfide generates hydrogen and sulfur according to the decomposition reaction $H_2S \rightarrow H_2 + 0.5S_2$. The thermal cracking of the hydrogen sulfide molecule occurs at about 900 to 1,200 K. Other methods of decomposition include plasma cracking (see Gutsol and Fridman 2008), and photochemical and electrochemical methods. However, presently there is no commercially available

method to produce hydrogen from $H_2S$. The available laboratory methods known to date and the potential to develop a commercial process were analyzed by Zaman and Chakma (1995).

One of the cited possibilities is to use catalytic separation membranes made from a combination of glass and alumina, which allow permeation of hydrogen from the $H_2S$ decomposition reactor. The membrane is doped with catalysts. Among tested catalysts, those based on molybdenum ($MoS_2$) showed excellent yield; other catalysts are based on $WS_2$, NiW, NiMo, and alumina (Zaman and Chakma 1995). Two-step thermochemical cycle extracting hydrogen from $H_2S$ with the help of metals of various valences were also investigated; they operate as follows (see Zaman and Chakma 1995):

$$\left.\begin{aligned} &M + zH_2S \rightarrow MS_z + zH_2 \\ &MS_z \rightarrow M + zS \end{aligned}\right\}, \tag{13.29}$$

where M represents a metal; some encouraging results were obtained with transition metals such as vanadium. Other thermochemical cycles for hydrogen sulfide decomposition can operate with iodine or carbon monoxide:

$$\left.\begin{aligned} &\text{Iodine cycle: } H_2S + I_2 \rightarrow 2HI + S; \quad 2HI \rightarrow H_2 + I_2 \\ &\text{Carbon monoxide cycle: } H_2S + CO \rightarrow COS + H_2; \quad COS \rightarrow CO + S \end{aligned}\right\}. \tag{13.30}$$

All these processes are still in the development phase as they entail several technical problems with controlling the reactions, improving yields and reaction rates, and diminishing the formation of nondesired products. For example, as cited in Zaman and Chakma (1995), the thermochemical cycle operating with carbon monoxide, though very attractive because its hydrogen releasing reaction evolves at very low temperature (373–473 K), is difficult to cycle because of the formation of $CS_2$ in a concurrent reaction, namely $2COS \rightarrow CO_2 + CS_2$.

#### 13.4.2.7 Solar–Thermal Hydrogen Production

Concentrated solar energy, being a source of high-temperature heat, can be used to drive many thermal methods of disassociating water into hydrogen and oxygen or extracting it from other materials like hydrocarbons or hydrogen sulfide. Figure 13.16 shows the main paths to produce hydrogen from solar energy using thermal methods. Among these, one notes that solar gasification/reforming of fossil fuels can be accompanied by carbon dioxide capture and sequestration.

The sulfur–iodine TCWS cycle also can be driven by high-temperature steam generated by solar concentrators. Considerable work has been done on solar-driven thermal cracking via redox reactions, where at the focal point a solar concentrator is placed as the chemical reactor. Solar energy also can be applied to extract hydrogen from fossil fuels. For coal and other solid carbonaceous materials, the

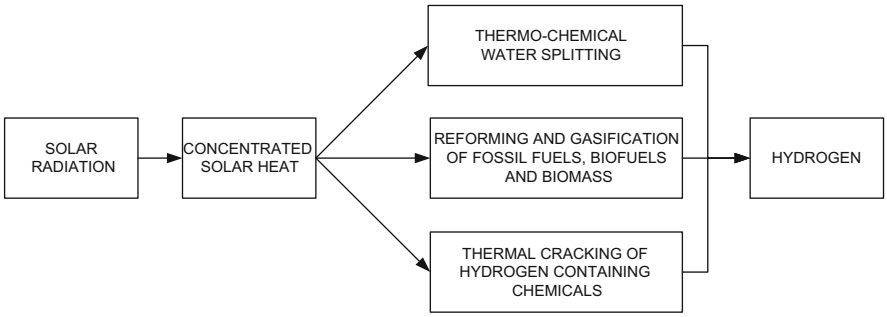


**Fig. 13.16** Solar thermal paths for hydrogen production

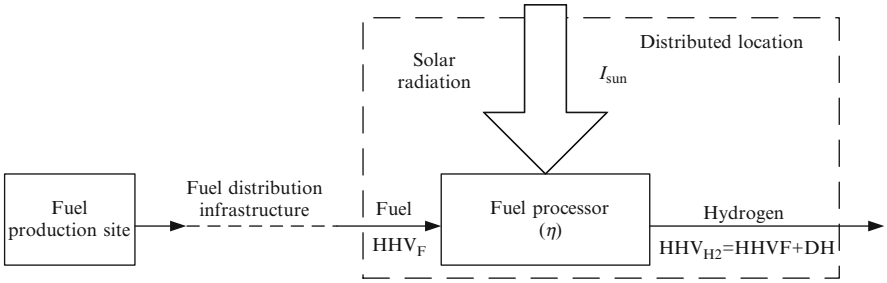


**Fig. 13.17** Solar reforming of fuels or hydrogen carriers to generate hydrogen at distributed locations

solar gasification via steam methane reforming reaction has the additional benefit of converting a solid fuel traditionally used to generate electricity in Rankine cycles into a cleaner fluid fuel—cleaner only when using solar process heat—that can be used in highly efficient fuel cells. In addition, liquid and gaseous fuels and biofuels can be reformed to generate hydrogen using solar energy. In such a system, a fossil fuel, hydrocarbon (e.g., propane, butane), biofuel, or a hydrogen carrier (e.g., ammonia, ammonia borane) can be converted to hydrogen under the proper exposure to high-temperature solar heat. The principle of this kind of solar hydrogen generation technique is presented in Fig. 13.17.

By considering a unitary production of transformed energy from the reformation process, say 1 MJ, the usage costs of reforming fuels in addition to an on-site $CO_2$ mitigation factor can be compared to the direct use of the fuels. For direct decomposition of the fuel, such as the ammonia reformation case, the development of a cost index is simple. First, some parameters must be defined:

$$\varepsilon = \frac{\mathrm{HHV}_{\mathrm{H}_2}}{\mathrm{HHV}_{\mathrm{F}}}, \tag{13.31}$$

where $\mathrm{HHV}_{\mathrm{H}_2}$ is the higher heating value of the reformed fuel, in this case hydrogen, and $\mathrm{HHV}_{\mathrm{F}}$ is the higher heating value of the original fuel. Next, the

molar ratio of product fuel to reactant fuel must be determined from the chemical equation:

$$\mathrm{MR}_{i/\mathrm{H}_2} = \mathrm{kmol}_i/\mathrm{kmol}_{\mathrm{H}_2}. \tag{13.32}$$

The cost index for the reformation is now shown, where the value of the index is between 0 and 1, clearly showing the cost reduction for reformed fuel:

$$\mathrm{CI} = \frac{1}{\varepsilon}(\mathrm{MR}_{i/\mathrm{H}_2}). \tag{13.33}$$

It also should be noted that in terms of the equilibrium reactions, water may be recycled in the system, but by analyzing the stoichiometric reaction, we can see that water is consumed in the process. First, the molar ratio of water to the final fuel product must be determined from the chemical equation:

$$\mathrm{MR}_{\mathrm{w}/\mathrm{H}_2} = \mathrm{kmol}_{\mathrm{w}}/\,\mathrm{kmol}_{\mathrm{H}_2}, \tag{13.34}$$

where the subscript $w$ indicates water. Cost parameters must also be added on a per unit mass basis for the consumption of the original fuel as well as water: $C_{\mathrm{i}} = \$/(\mathrm{kg\ initial\ fuel})$, and $C_{\mathrm{w}} = \$/(\mathrm{kg\ water})$. The cost index for steam reformed fuels, such as methane or propane, then becomes

$$\mathrm{CI} = \frac{1}{\varepsilon}\left(\mathrm{MR}_{i/f} + \mathrm{MR}_{w/f}\frac{\mathrm{MM}_{\mathrm{H_2O}} \cdot C_w}{\mathrm{MM}_i \cdot C_i}\right). \tag{13.35}$$

For carbon-based fuels that may be reformed, and for every quantity of initial fuel used, the same amount of $CO_2$ is released during the reformation process as would be released during combustion. However, the solar energy that is added to the system results in a diluted release of $CO_2$. As such, a $CO_2$ mitigation index is defined as follows. This time, there must be a direct comparison of the reformation reaction to the combustion reaction. The first molar ratio is the ratio of $CO_2$ released upon combustion of the initial fuel to the amount of initial fuel burned: $\mathrm{MR}_{\mathrm{CO_2}/i} = \mathrm{kmol}_{\mathrm{CO_2}}/\mathrm{kmol}_i$. The second molar ratio is the ratio of $CO_2$ released upon reformation of the fuel to the amount of final fuel produced: $\mathrm{MR}_{\mathrm{CO_2}/\mathrm{H_2}} = \mathrm{kmol}_{\mathrm{CO_2}}/\mathrm{kmol}_{\mathrm{H_2}}$. It follows that the $CO_2$ mitigation index shown below is once again a value between 0 and 1, where for example an index of 0.85 represents a mitigation of 15%:

$$\mathrm{CO_2}I = \frac{1}{\varepsilon}\left(\frac{\mathrm{MR}_{\mathrm{CO_2}/\mathrm{H_2}}}{\mathrm{MR}_{\mathrm{CO_2}/i}}\right). \tag{13.36}$$

The above analysis is meant to quantify in terms of cost and carbon mitigation the benefits of distributed hydrogen production through fuel/carriers reforming.

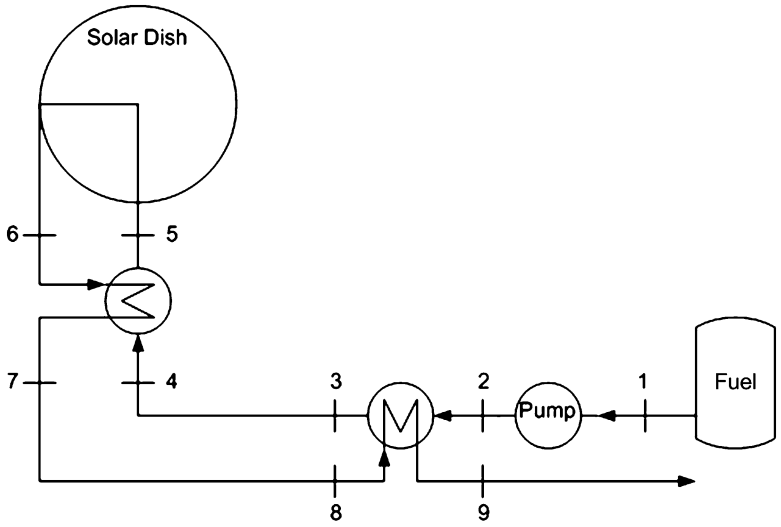


**Fig. 13.18** Simplified diagram of a solar-driven fuel reforming system for hydrogen production

The system, shown in Fig. 13.18, comprises a number of stages: 1–2, pumping; 2–3, first preheating; 3–4, fuel pipeline transport; 4–5, second preheating; 5–6, solar-driven fuel reforming; 6–7, heat recovery; 7–8, reformate pipeline transport; 8–9, second stage of heat recovery.

#### 13.4.2.8 Nuclear–Thermal Routes for Hydrogen Production

Using nuclear energy as the primary energy source for hydrogen production is attractive because (1) the greenhouse gas emissions associated with nuclear energy production are much lower than those with conventional fossil fuel combustion, and (2) nuclear energy is adaptable to large-scale hydrogen production. Progress has been made in nuclear-based hydrogen production in recent years as evidenced by many research studies published in the literature.

The typical utilization of nuclear reactors has been for electricity generation with steam power plants. Studies indicate that more benefits can be obtained if in addition to electricity a sustainable fuel such as hydrogen is produced. The efficiency of power generation normally increases with increasing temperature of the working medium, which, in the case of the nuclear energy utilization, leads to increased nuclear reactor coolant temperatures and pressures. However, increases in the power generation efficiency of nuclear power plants are mainly limited by the permissible temperatures in nuclear reactors and the corresponding temperatures and pressures of the coolants. Coolant parameters are limited by the corrosion rates of materials and nuclear reactor safety constraints.

**Table 13.9** Progress in high-temperature reactor design for hydrogen production

| Reactor type | Progress description |
|---|---|
| Advanced gas reactor (AGR) | – Commercially available in the UK; 14 units in operation with 1,500 MW thermal each<br>– Coolant temperature 650°C to be upgraded to 750°C<br>– Subcritical carbon dioxide coolant at 43 bar to be upgraded at supercritical pressures |
| High-temperature gas-cooled reactor | – Developed by Japan Atomic Energy Research Institute (JAERI)<br>– Prototype power 30 MW cooled with helium at maximum 950°C<br>– Adaptable to drive the S-I thermochemical water splitting cycle<br>– Advantageous concept for efficient, economic, and safe nuclear energy |
| Secure transportable autonomous reactor (STAR-$H_2$) | – Not available yet commercially; based on proven technology from Russian submarine propulsion<br>– Demonstrated liquid lead coolant at 500°C to be upgraded to 800°C<br>– 400 MW thermal capacity in compact units transportable by rail |
| Modular helium reactor (MHR) | – Based on demonstrated German and the U.S. technologies<br>– Helium coolant at 850°C at 70 bar, upgradable to 1,000°C<br>– Meets the requirements for hydrogen production<br>– Proposed as a basis for a nuclear energy source |
| Sodium-cooled fast reactor (SFR) | – Demonstrated technology in Russia, the U.S., and France<br>– Sodium coolant at 500°C upgradable to 550°C<br>– Closed fuel cycle with efficient management of actinides and conversion of fertile uranium |
| Molten-salt-cooled advanced high-temperature reactor | – Only in design phase; not yet built<br>– High-temperature (750–1,000°C) heat<br>– Molten fluoride salts coolant and a pool configuration<br>– Efficient low-cost thermochemical $H_2$ and electricity<br>– Coated-particle graphite-matrix fuel |
| Supercritical water cooled CANDU reactor | – Coolant (supercritical water) pressure of about 25 MPa<br>– Coolant temperature 625°C<br>– Expected power generation efficiency 45% |

Many studies address nuclear reactor modifications and the progress needed to meet the requirements for producing cheap electricity and high-temperature heat by efficiently coupling the heat with a hydrogen production plant. The envisaged reactor technologies and the progress in their development are listed in Table 13.9. With respect to the process heat temperature level that these technologies offer, gas-cooled reactors, molten-salt-cooled reactors, and heavy-metal-cooled reactors appear to be the most promising technologies for hydrogen production. The various nuclear reactor technologies combined with thermally driven hydrogen production processes adaptable to nuclear reactors complement but do not compete with heat in shaping the future nuclear-based hydrogen generation capability. Table 13.10 lists the envisaged thermally driven hydrogen production methods that can be integrated with nuclear reactors.

**Table 13.10** Envisaged hydrogen production methods coupled with nuclear reactors

| $H_2$ production method | Description and remarks |
|---|---|
| Thermochemical cycles | Best candidate is the S–I cycle. It allows for centralized, base-load production of hydrogen and the utilization of waste heat from nuclear power plant provided that suitable temperature level upgrade methods are elaborated. Potential efficiency of the overall process can be higher than 40%. The technology is proven at lab scale but requires development to achieve commercialization phase. |
| Nuclear coal gasification | European research led by Germany since 1999. Requires temperatures higher than 700°C. The gasification technology is mature, and coupling with nuclear reactors can show overall efficiency over 60%. The main advantage: carbon dioxide emissions are reduced as compared to auto-thermal processes. |
| Nuclear steam reforming of fossil fuels using membranes | Chemical reactions, the required heat for reactions, fuel savings, and $CO_2$ emission reductions were investigated for natural gas and petroleum. The process temperature can be reduced to 550°C. High efficiency (>60%) and lower $CO_2$ emissions are achievable. |

#### 13.4.2.9 Fossil Fuel–Based Thermally Driven Hydrogen Production

When hydrogen is produced from fossil fuels via thermal methods, the energy associated with fuel combustion is used to drive the conversion process in which the hydrogen atoms are extracted from steam and/or from the fuel itself. For example, by adding oxygen in a steam methane reformer, the reaction becomes exothermic:

$$4CH_4 + 2H_2O + O_2 \rightarrow 10H_2 + 4CO, \tag{13.37}$$

which can generate syngas at 1,200 to 1,400 K and 72.2 kJ/mol of hydrogen. This reaction can be conducted at higher pressure—up to 100 bar—producing thus compressed hydrogen. The water gas shift reaction can be subsequently applied so that the overall reaction of auto-thermal methane conversion is $4CH_4 + 6H_2O + O_2 \rightarrow 14H_2 + 4CO_2$, which delivers hydrogen at 500 K and an exothermic reaction heat of 20.8 kJ/mol of hydrogen.

The auto-thermal fossil fuel reforming or gasification process is one of the most well known and widely applied hydrogen processes in industry. With natural gas as the starting fuel, 4 mol of carbon dioxide are released in the atmosphere for each 14 mol of hydrogen produced. In principle, the hydrogen production from fossil fuels can be assisted by carbon dioxide sequestration. This is a path toward cleaner hydrogen production and is called fossil fuel decarbonization (see Muradov and Veziroglu 2008); sometimes the process of decarbonization of fossil fuel to generate hydrogen and possibly to produce electricity is called precombustion, meaning that the decarbonization of the fossil fuel is done prior to the combustion process; what is combusted is the produced carbon-free fuel—the hydrogen.

An alternative to auto-thermal fossil fuel conversion to hydrogen, which emits carbon dioxide, is the process of thermal cracking of the hydrocarbons, which is not supposed to emit any $CO_2$ but rather to generate carbon. Thermal cracking is a process of decomposition. It can be successfully applied to the hydrocarbons with the smallest molecular mass for which more desirable products are formed. Thermal decomposition of methane, $CH_4 \rightarrow C(s) + 2H_2$, is an endothermic reaction with the associated heat of 75.6 kJ/mol. Methane can be decomposed through catalytic or noncatalytic processes that can be conducted thermally or under the influence of plasma. The advantage of the method comes from the fact that the resulting carbon powder can be viewed as a by-product. Carbon is very much needed by industry to construct carbon fibers and nano-materials.

## *13.4.3 Electrothermally-Driven Hybrid Hydrogen Production*

The processes studied in Section 13.4.2 are categorized as thermally driven because the energy needed to generate hydrogen is in the form of high-temperature heat. When implemented in practice, such processes need electricity to run pumps, compressors, conveyers, fans, and so on. Thus, in a practical implementation, most of the hydrogen production methods are electrothermally driven. Another aspect to mention is that the thermally driven methods require very high temperature heat. In contrast, the electrochemical processes do not require high temperature. Because the sustainable high-temperature sources are limited mainly to solar and nuclear, it is desirable to devise hybrid methods that are driven electrically/electrochemically and thermally. Some thermochemical cycles are hybrid and can operate at temperatures below 550°C as compared to the S–I cycle, which runs at close to 1,000°C. Another process of interest is the high-temperature electrolysis in which part of the energy needed by the process is transferred thermally and part is transferred electrically. In this section, the major electrothermal processes and systems for hydrogen production are discussed.

### 13.4.3.1 Hybrid Thermochemical Water Splitting Cycles

Apart from thermally driven TCWS cycles, mentioned above, three other TCWS cycles—called hybrid—draw special attention because they operate at lower temperatures. Hybrid cycles use thermal and electrical energies to conduct certain endothermic and electrochemical reactions. As a consequence of their lower operating temperatures, other sustainable thermal sources in addition to solar, high-temperature nuclear, and biomass combustion can be used to drive the involved processes. The additional heat sources are nuclear reactors of the present generation operating at 250° to 650°C and entailing geothermal and waste heat recovery. Figure 13.19 presents in a schematic manner the operation of the Mg–Cl cycle (a) and the $H_2SO_4$ cycle (b)—both being driven electrothermally. The flux of

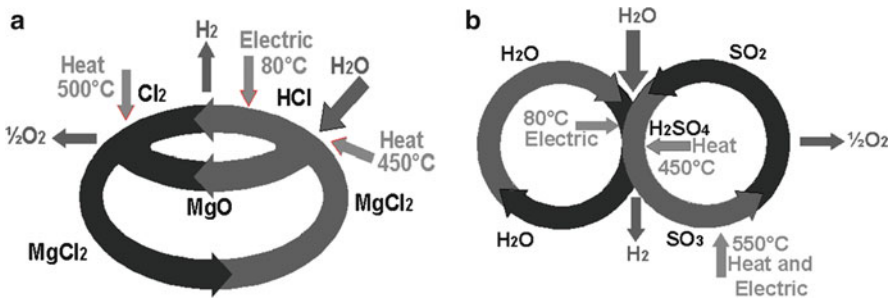


**Fig. 13.19** Low-temperature thermochemical water splitting cycles: (**a**) Mg–Cl cycle, and (**b**) $H_2SO_4$ cycle [modified from Balta et al. (2009)]

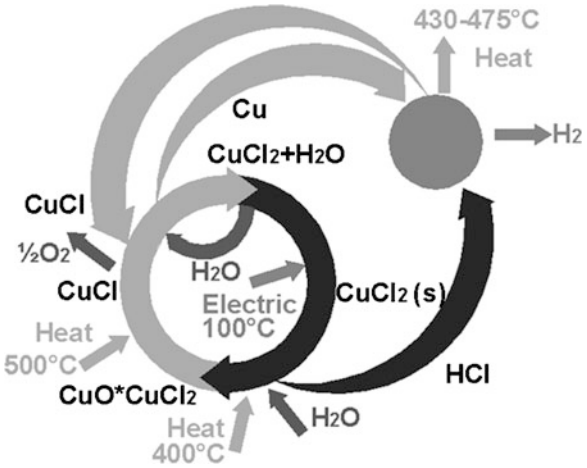


**Fig. 13.20** The Cu-Cl thermochemical water splitting cycle [modified from Balta et al. (2009)]

the recycled chemicals is shown as well as the energy inputs and temperature level; a distinction is made between electrical and thermal energy inputs.

Recently, a group of institutions led by the University of Ontario Institute of Technology, the Atomic Energy of Canada (AECL) Limited, and the Argonne National Laboratory in the U.S., with other participants, is developing a pilot scale prototype of the Cu-Cl TCWS plant. The maximum temperature level required from the heat source is about 550°C, which is needed to drive the oxygen generation reaction. There are several variants of the Cu–Cl cycle; the one that is most studied is called the "five-steps" version. The five-step Cu–Cl cycle comprises three thermally driven chemical reactions, one electrochemical reaction, and one physical step of drying. According to the study by Orhan et al. (2009a), the energy efficiency of hydrogen production by a Cu-Cl plant is close to 60%, while the energy efficiency is about 11%. The processes involved in the five-step cycle are indicated in Fig. 13.20.

The copper chlorine cycle for TCWS has advantages over the other cycles regarding hydrogen generation from low-grade temperature sources, especially those sources that can be considered sustainable thermal energy. These categories include nuclear heat, industrial heat, heat recovered from power plants, concentrated solar heat, heat resulting from municipal waste incineration, geothermal heat, and other sources. The current stage of development of this cycle is reviewed in Naterer et al. (2009).

Among the topics under investigation are kinetics of the hydrogen production reaction, development of the electrochemical step for copper particulate generation, drying of the aqueous cupric chloride, transport processes in hydrolysis reactor, modeling the molten salt reactor for oxygen production, scale-up study and economic analysis of the plant, thermochemical data compilation for the involved materials (see Zamfirescu et al. 2010a), development of appropriate materials, linkage of nuclear and other sustainable thermal sources, and the hydrogen plant.

The process diagram of the Cu-Cl TCWS cycle is shown in Fig. 13.21. Low-pressure superheated steam is extracted from a steam turbine and supplied to the Cu–Cl cycle, which decomposes water into hydrogen and oxygen. The superheated steam fed in line 0 is expanded with work recovery to 1 bar of pressure, where it is assumed that saturated or nearly saturated steam exists. The saturated steam is superheated to 400°C at the state labeled 2 on the figure using a heat pump (details are given later). The extracted amount of steam is replaced by supplying an equal amount of water back into the cycle.

Liquid water at 20°C is supplied into the cycle and then boiled and superheated to 400°C. This process induces a number of losses. The steam is injected into a fluidized bed reactor $CR_1$, where it chemically reacts with copper (II) chloride ($CuCl_2$) under heat addition $Q_{CR1}$ (endothermic reaction). This step dissociates the water molecule and forms hydrochloric acid (HCl). An additional compound is formed, which is a metallic solution of copper oxide and copper dichloride. This chemical reaction and others in the Cu–Cl cycle are summarized in Table 13.11, which gives the reactor, reaction, temperature, and heat per kmol of hydrogen produced. Hydrogen is a product of the fifth chemical reactor ($CR_5$), involving the exothermic combination of particulate copper with HCl at 450°C.

In the second reactor ($CR_2$), oxygen is produced by thermal dissociation of copper oxide at about 500°C. Step 3, called the copper production step, is driven electrochemically. The third reactor ($CR_3$) is an electrochemical cell containing an aqueous solution of copper chloride. The reaction heat is shown in Fig. 13.21, with $W_{CR_3}$ designating the electrical power.

The copper precipitate is removed from $CR_3$ and transferred to $CR_5$. In reactor $CR_4$, there is no chemical reaction, but rather water is removed (by drying) from the aqueous solution of $CuCl_2$ that was produced by electrolysis. Table 13.12 shows the substances circulated within the Cu–Cl cycle, together with their state and temperature. The entire Cu–Cl cycle operates at atmospheric pressure. Therefore, the products (hydrogen and oxygen) must be compressed for storage. To facilitate compression, the products are cooled first with heat recovery. A blower (indicated

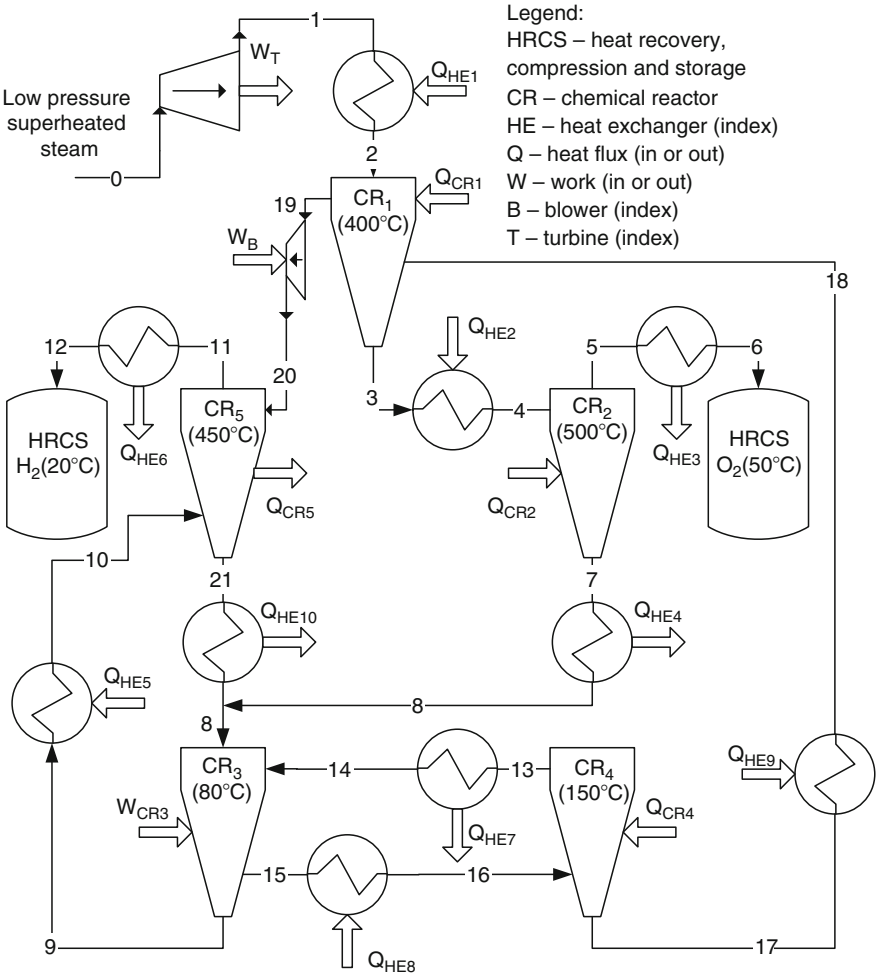


**Fig. 13.21** The five-step Cu–Cl water splitting cycle [modified from Zamfirescu et al. (2010b)]

by $W_B$ in Fig. 13.21) is necessary to extract the HCl from $CR_1$ and to deliver it to $CR_5$. During this process, the circulated HCl is slightly heated.

On Fig. 13.21, one notes that in the Cu-Cl plant there are four chemical reactors that comprise the hydrolysis reactor $CR_1$; the oxygen producing reactor $CR_2$; the hydrogen producing reactor $CR_5$; the copper electrolyzer $CR_3$. With $CR_4$ one indicates the dryer of aqueous $CuCl_2$, which does not actually perform any chemical reaction, but rather conducts a physical process of drying. For the design of these reactors, it is important to have a good understanding of the reaction kinetics and equilibrium, and to determine the optimum parameters that enhance the yields and production rates. We briefly address here some relevant results regarding the chemical reactors.

**Table 13.11** Process steps of the Cu–Cl cycle

| Step | Reaction | $T$ (°C) | $Q$ (MJ/ kmol $H_2$) | $G$ (kcal) | $H$ (kcal) |
|---|---|---|---|---|---|
| 1 | $2CuCl_2(s) + H_2O(g) \rightarrow CuO \cdot CuCl_2(s) + 2HCl(g)$ (endothermic) | 400 | 105.3 | 9.5 | 27.9 |
| 2 | $CuO \cdot CuCl_2(s) \rightarrow 2CuCl(l) + 0.5O_2(g)$ (endothermic) | 500 | 110.5 | −0.71 | 30.9 |
| 3 | $4CuCl(s) + H_2O(l) \rightarrow 2CuCl_2 \cdot H_2O(aq) + 2Cu(s)$ | 80 | 140.4 | | |
| | (i) $4CuCl(s) + 4Cl^- \rightarrow 4CuCl_2^-$ | | | 8.27 | 0.062 |
| | (ii) $4CuCl_2^- \rightarrow 2CuCl_2 + 2Cu + 4Cl^-$ (electrochemical) | | | 14.5 | 2.93 |
| 4 | $CuCl_2 \cdot H_2O(aq) \rightarrow CuCl_2(s) + H_2O(g)$ (drying only) | 150 | 18.3 | 6.0 | 19.9 |
| 5 | $2Cu(s) + HCl(g) \rightarrow 2CuCl(l) + H_2(g)$ (exothermic) | 450 | −55.5 | 0.23 | −11.2 |

Data from Zamfirescu et al. (2010b)

**Table 13.12** Substances circulated within Cu–Cl cycle

| Line | Substance | State | $T$, °C | Remarks |
|---|---|---|---|---|
| 0 | Steam | Superheated | >100 | $P > 1$ bar |
| 1 | Steam | Saturated | 100 | $P = 1$ bar |
| 2 | Steam | Superheated | 400 | – |
| 3 | $CuO{\cdot}CuCl_2$ | Solid | 400 | Metallic solution, powder |
| 4 | $CuO{\cdot}CuCl_2$ | Solid | 500 | Metallic solution, powder |
| 5 | $O_2$ | Gas | 500 | – |
| 6 | $O_2$ | Gas | 80 | – |
| 7 | CuCl | Liquid | 500 | Liquid metal |
| 8 | CuCl | Solid | 80 | Precipitated, particulate |
| 9 | Cu | Solid | 80 | Particulate, powder |
| 10 | Cu | Solid | 450 | Particulate, powder |
| 11 | $H_2$ | Gas | 450 | – |
| 12 | $H_2$ | Gas | 80 | – |
| 13 | Steam | Superheated | 150 | Pressure 1 bar |
| 14 | Water | Liquid | 80 | Pressure 1 bar |
| 15 | $CuCl_2$ | Slurry | 80 | Aqueous solution |
| 16 | $CuCl_2$ | Slurry | 150 | Aqueous solution |
| 17 | $CuCl_2$ | Solid | 150 | Metallic powder |
| 18 | $CuCl_2$ | Solid | 400 | Metallic powder |
| 19 | HCl | Gas | 400 | Acid |
| 20 | HCl | Gas | 430 | Slightly compressed |
| 21 | CuCl | Solid | 450 | Particulate |

Data from Zamfirescu et al. (2010b)

Hydrogen is generated through an exothermic reaction that combines particulate copper with gaseous hydrochloric acid at about 400°C. The kinetics of this reaction, in the context of reactor design has been studied parametrically by Zamfirescu et al. (2010e). The involved reaction is $Cu(s) + HCl(g) \rightarrow CuCl(l) + 0.5H_2(g)$.

The suggested residence time of copper particles varies between 10 and 100 seconds, depending on the operating conditions, while the conversion varies between 55% and 85%.

The noncatalytic gas–solid reaction that occurs in the hydrolysis reactor $CR_1$, where $CuCl_2$ reacts with steam to obtain hydrochloric acid and copper oxychloride, assumes the following:

- The reactor is a fluidized bed comprising two regions: bubble and emulsion.
- The temperature gradient within the bed reactor is negligible.
- Only one reaction occurs: cupric chloride particles react with superheated steam.
- The reaction takes place in the emulsion phase.
- The conversion of particles at the inlet of the reactor is zero.
- The hydrolysis reaction is first-order.

The results by Haseli et al. (2009) indicate that the gas conversion ranges from 20% to 50% and the solid conversion ranges between 30% and 60% with a recommended interface velocity of 0.4 to 0.8 m/s. The optimum temperature in this reactor is around 500° to 550°C. According to Orhan et al. (2009b) the exegy efficiency of the hydrochloric acid production reactor is around 65% at about 400°C. The oxygen production reactor has been analyzed by Orhan et al. (2009c). It has been found that at 500°C the exergy destruction in this reactor is around 5,300 kJ/kmol of hydrogen. The exergy destruction of the electrochemical step for copper production is, according to the calculations by Orhan et al. (2008b), 140 MJ/kmol hydrogen at 45°C.

The coupling between the Cu–Cl cycle and a sustainable energy source must consider necessarily various opportunities for heat recovery and heat upgrading. Depending on the temperature level of the temperature sources, one can either upgrade the temperature via heat pumps or use internal heat recovery within the cycle. Granovskii et al. (2008a) proposed a chemical heat pump based on the reversible steam methane conversion reaction, and Zamfirescu et al. (2010b,f) analyzed some vapor compression heat pumps.

The thermodynamic calculations of heat requirements and heat ejection from the Cu–Cl cycle lead to the determination of the *T*–*H* in Fig. 13.22, where *H* is total enthalpy. This diagram shows the required heat inputs and outputs and their associated temperature levels. The continuous line refers to heat input streams, and the dashed line refers to heat outputs. The streams requiring heat are identified with the line 1–2–3–4–5–6–7–8 and those releasing heat with 9–10–11–12–13.

It is desirable to apply heat recovery as much as possible and upgrade the temperature of the ejected heat so that it reaches the temperature level needed for heat input. The heat released by stream 9–10–11–12 should be received by a heat pump that, at the expense of additional power, upgrades the temperature and enthalpy content and delivers a hot stream to the Cu–Cl cycle that matches the profile 3–4–5–6–7–8. The work required to operate such a heat pump can come from a sustainable heat source available at an intermediate temperature $T_m$, which drives a heat engine operating between $T_m$ and the ambient air at $T_0$. This heat engine also delivers power to the Cu–Cl cycle.

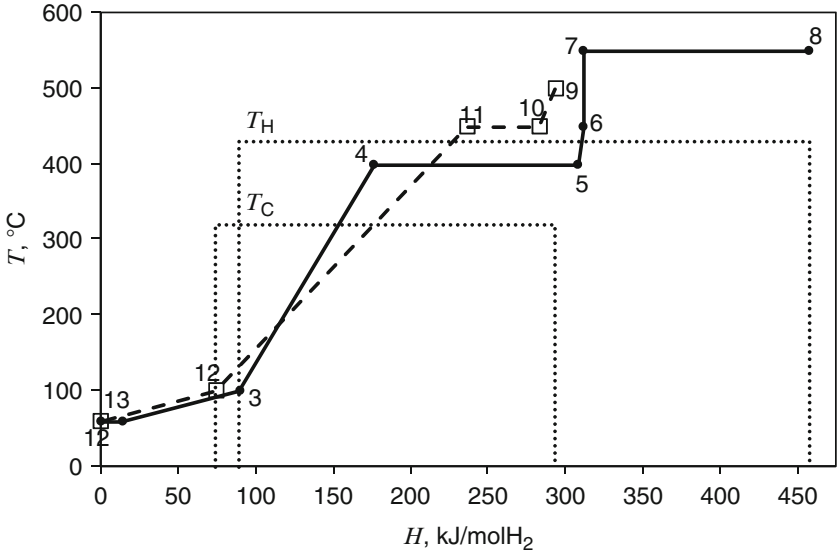


**Fig. 13.22** T-H diagram of heat inputs and outputs associated with the Cu–Cl cycle [modified from Zamfirescu et al. (2010b)]

It is useful to transpose the *T–H* presented in Fig. 13.22 in *T–S* coordinates, where *S* is the stream entropy expressed in kJ/K and mol $H_2$. The streams are thermodynamic systems that interact with the exterior by heat transfer only. Consequently, for any stream, $\delta Q = \mathrm{d}H$, thus,

$$\mathrm{d}S = \int \frac{\delta Q}{T} = \int \frac{\mathrm{d}H}{T}. \tag{13.38}$$

The area embraced by the lines 1–2–3–4–5–6–7–8 and that indicated by "Heat Source" in Fig. 13.23 represent the ideal/minimum work needed by the heat pump to upgrade the temperature of the heat source and deliver useful heat to the Cu–Cl cycle. The area embraced by the lines 9–10–11–12–13 and that indicated with "Heat Sink" in Fig. 13.23 represent the ideal/maximum work that can be obtained from the heat recovered by the Cu–Cl cycle. The engineering challenge regarding the integration of the Cu-Cl plant with the thermal energy source $T_m$ consists of finding suitable working fluids and processes that allow for the construction of a heat pump and heat engine cycle operating like the one presented in Fig. 13.23.

One original idea is to use the CuCl as working fluid in a vapor compression heat pump that recovers heat from the hydrogen production reactor and other hot stream, upgrades the temperature level, and delivers the heat to the oxygen production reactor. Zamfirescu et al. (2010f) proposed such a system, as shown in Fig. 13.24.

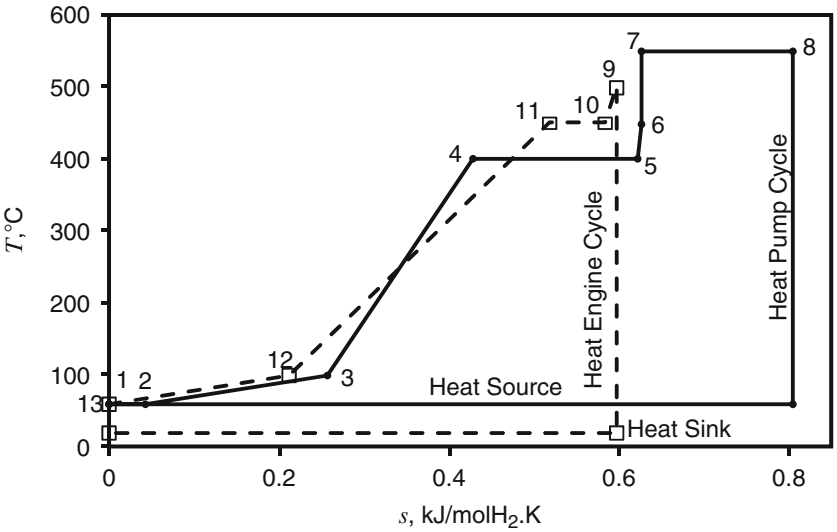


**Fig. 13.23** T-S diagram of ideal power and heat pump cycles coupled to the Cu-Cl plant [modified from Zamfirescu et al. (2010b)]

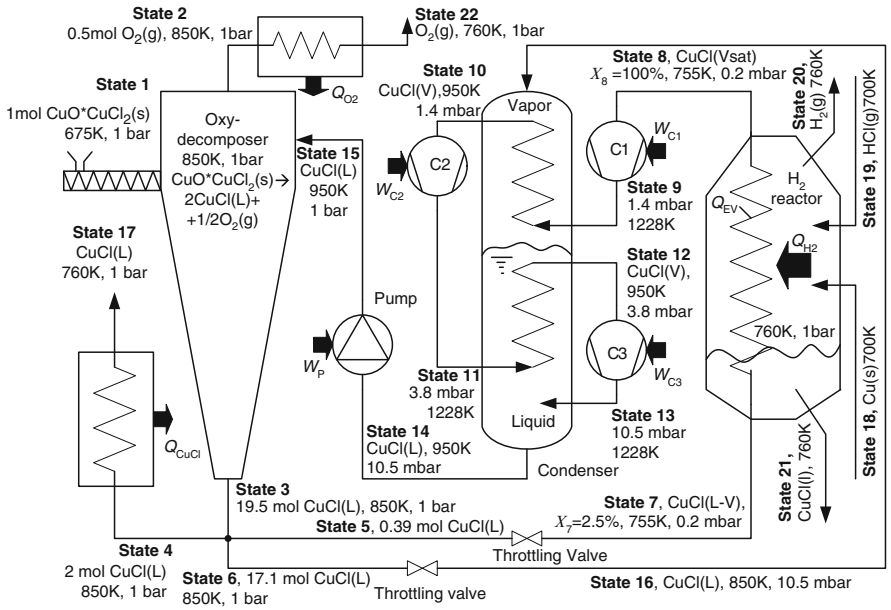


**Fig. 13.24** Heat pump with CuCl vapor compression for internal temperature level upgrading within the Cu-Cl water splitting cycle [modified from Zamfirescu et al. (2010f)]; *g* gas; *L* liquid; *V* vapor; *Vsat* saturated vapor; *X* vapor quality; *W* work; *Q* heat; *C* compressor

The copper oxychloride is fed at state 1 into the oxy-decomposer at 675 K. The temperatures, pressures, and other parameters indicated in Fig. 13.24 correspond to the reference case. Inside the reactor, the particulate $CuO \cdot CuCl_2$ is heated by direct contact with molten cuprous chloride, which is injected at state 15 at 950 K. The molten salt delivers its sensible heat and cools down to the average reactor temperature, which is assumed to be 850 K for the reference case considered in this study.

The heat delivered by the hot stream at state 15 makes copper oxychloride decompose thermally and release oxygen, while forming molten cuprous chloride (CuCl). At the top of the reactor, oxygen gas is expelled at state 2, while at the bottom, molten CuCl is collected and drained out at state 3. The molten CuCl product is split into three parts at the reactor exit (state 3): one part (state 4) is sent for further processing within the plant (quantitatively, state 4 flows 2 mol of CuCl for 1 mol of copper oxychloride); and the remaining two parts (streams in states 5 and 6) are further processed thermomechanically within the heat pump.

The stream in state 5 is expanded through a throttling valve in a vacuum, down to 0.2 mbar and reaches a two-phase state at state 7 at a saturation temperature of 755 K. This stream is further heated and reaches 100% saturated vapor at state 8. The vapor is then compressed in three stages with intercooling in order to reduce compression work. The final pressure is 10.5 mbar, for which the corresponding saturation temperature is 950 K. A design of the condenser that embeds a direct contact heat exchanger is indicated in the figure. The condenser consists of a vessel that incorporates two coils, where superheated vapors are cooled after stages 1 and 2 of compression. During the operation, at the bottom of the condenser, saturated CuCl is collected. The superheated vapor at the final stage of compression—state 13—is injected into this liquid, and thus cooled by direct contact and condensed. The condensation heat is transferred to an additional stream of molten CuCl. This stream flows as follows:

- From state 6, the liquid is throttled and its pressure is reduced from 1 bar to 10.5 mbar, wherein the CuCl is still in a subcooled thermodynamic state; therefore, the liquid temperature does not change sensibly during the throttling (state 16).
- The subcooled liquid (state 16) is injected into the condenser at the top.
- Inside the condenser, the enthalpy of stream at state 16 is increased such that it takes all condensation heat of the vapor stream at state 9.
- The saturated liquid collected at the bottom of the condenser (state 14 at 950 K) incorporates all condensation heat.

Furthermore, the pressure of stream at state 14 is increased up to atmospheric pressure and then the heated flow is injected into the oxy-decomposer at state 15. The CuCl stream is one of the products of the oxy-decomposer, and therefore injecting this substance in excess does not affect the chemical species present in the oxy-decomposer, even though it may affect the chemical equilibrium. However, because oxygen is drawn constantly out of the reactor, there is a tendency to shift the equilibrium toward the right, which compensates the tendency of shifting toward the left due to excess CuCl present in the reactor.

Figure 13.24 shows the heat and mechanical power fluxes associated with various components. The heat flux $Q_{O_2}$ rejected by the heat exchanger cools the oxygen from state 2 to state 16. The heat flux $Q_{CuCl}$ of cooling the molten cuprous chloride from state 4 to state 17 can be recovered and used internally to provide heat to the heat pump's evaporator. A part of the evaporation heat, $Q_{EV}$, can be supplied by these two sources. Additional sources of heat to deliver to the evaporator can be found within the water splitting plant. For example, the hydrogen production reaction, which combines particulate copper with gaseous hydrochloric acid, is exothermic and rejects heat at over 725 K. This reactor can operate also at 760 K, and the rejected heat is recovered and used to drive the heat pump. Figure 13.24 suggests that the evaporator coils of the CuCl heat pump can be embedded in the hydrogen production reactor. For the proposed settings, the heat flux received by the evaporator is the summation of heat fluxes recovered from the hydrogen production reactor and from the heat exchangers for oxygen and CuCl(L) product cooling ($Q_{EV} = Q_{H_2} + Q_{O_2} + Q_{CuCl}$).

The theoretical calculations indicate that the coefficient of performance (COP) of the heat pump is much higher than 2.5, being possible to reach the value of 10. The explanation of such a high COP is that the working fluid is rather easy to compress, and the temperature lift of the heat pump is reasonable. The work needed to drive the heat pump is about 10 to 15 kJ/mol of $H_2$.

The capital cost of Cu-Cl plant, as estimated by Orhan et al. (2008a) is roughly $10–50 million for a capacity range of 1 to 10 tons of hydrogen per day. The cost of produced hydrogen by such a large-scale plant must account for many production cost components apart from the direct production costs such as taxation, depreciation, insurance, rent, overhead, administrative expenses, distribution and marketing expenses, research and development costs, financial allocations, and gross-earning expenses. A rough estimation of the contribution of individual costs in the hydrogen product price is shown in Fig. 13.25. Table 13.13 compares the hydrogen production costs with other methods.

#### 13.4.3.2 Solar-Driven Electrothermal Systems

Solar energy can be converted into high-temperature heat and electricity to supply electrothermal processes for hydrogen production. Figure 13.26 suggests two possible routes to do this. The first route entails simultaneous generation of electricity (through photovoltaic panels) and high-temperature heat from concentrated solar radiation.

Both the high-temperature heat and the electricity are then used to fuel a hybrid process for hydrogen production, such as the thermochemical copper chlorine cycle of HTSE. The second route proposes to concentrate solar radiation first and then obtain high-temperature heat, which is supplied to the hybrid process for hydrogen production. The process rejects heat—such as that associated with high-temperature products that must be cooled—which can be recovered and used to run a heat engine to generate electricity for the hybrid process. Solar energy converted in high-temperature heat is suitable for all kinds of hybrid processes.

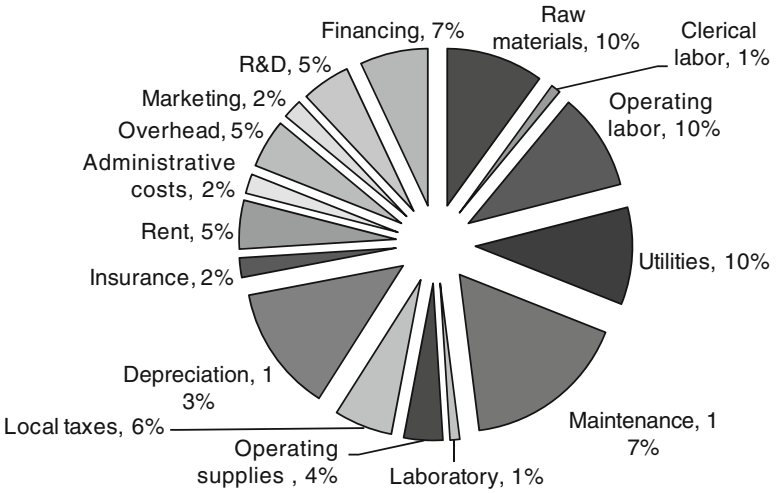


**Fig. 13.25** Various contributions to the total product cost of a Cu-Cl water splitting plant for hydrogen production [data from Orhan et al. (2008a)]

**Table 13.13** Comparison of Cu-Cl hydrogen cost with other methods for 10 tons of hydrogen per day

| Cost item ($/GJ) | Cu-Cl plant | Off-peak electrolysis | Steam–methane reforming |
|---|---|---|---|
| Capital cost | 7.7 | 3.2 | 3.1 |
| Energy charge | 0.5 | 1.0 | 0.8 |
| Carbon charge | 0 | 0 | 1.6 |
| Hydrogen cost | 2.71 | 2.41 | 2.67 |

Data from adapted from Orhan et al. (2008a)

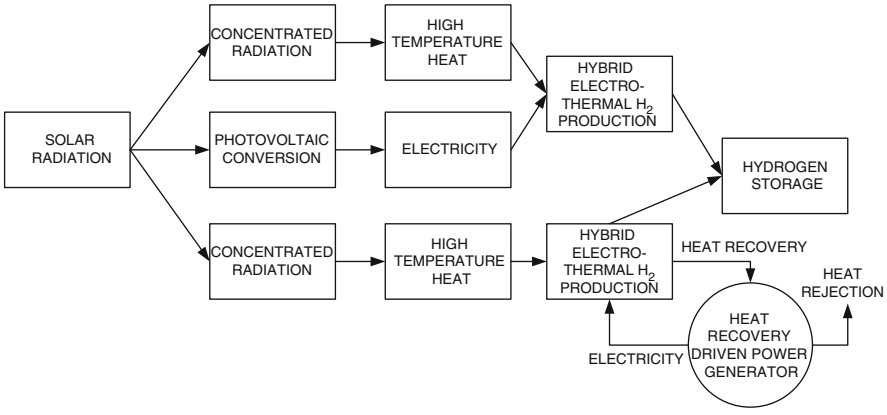


**Fig. 13.26** Routes for supplying electrothermal $H_2$ production processes with solar energy

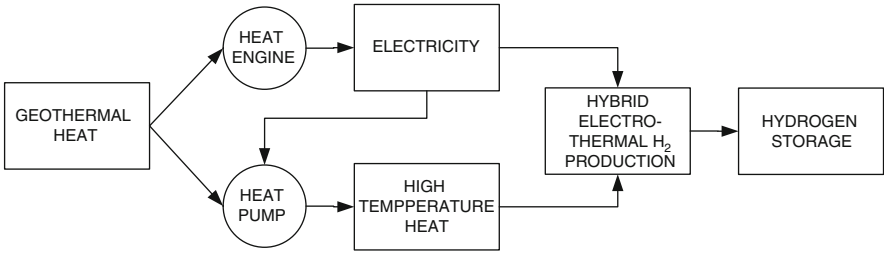


**Fig. 13.27** Geothermal hydrogen production through electrothermal methods

### 13.4.3.3 Geothermal Electrothermal Hydrogen Production

The temperature range of geothermal heat is narrower than that of solar, with typical temperatures of about 50°C to 450°C. Few geothermal sources reach temperature over 500°C. Thus, most of the geothermal sources available need to be coupled to heat pumps to upgrade the temperature to a suitable level for hybrid processes for hydrogen production. Figure 13.27 shows a system for driving a hybrid electrothermal process for hydrogen production with geothermal energy.

In this approach, the geothermal heat is used to supply a heat engine that converts heat into electricity. The generated electricity is used partially to "fuel" the hybrid process for hydrogen production and partly is supplied to a high-temperature heat pump. The role of the heat pump is to lift the temperature level of the geothermal source. Therefore, the heat pump is supplied with heat from the geothermal source and delivers high-temperature heat to the hybrid process.

The configuration of the geothermal hydrogen production system intimately depends upon the available temperature range. Say, for example, it is very high temperature (500°C); it can be used to provide heat directly in hybrid thermochemical cycles for water splitting, and there is no need for temperature level upgrading. If it is moderate temperature range, then electricity and heat upgrading can be applied, or if the level of temperature is too low, hybrid thermochemical cycles may not be applicable; rather in this condition geothermal energy can be used to drive cold water electrolysis process.

Figure 13.28 suggests a possible diagram of a geothermal-driven steam electrolysis system operating at very high temperature that uses the opportunity of heat recovery from the hot product streams. The heating of water is done in three stages, whereas at low temperatures regular materials are used for heat exchangers. At intermediate temperatures water is boiled, and at high temperature water is superheated in heat exchangers that make use of expensive materials with appropriate thermal behavior and durability. The temperature that steam has to reach before entering in the electrolyzer should be higher than 1,000°C. The geothermal energy is converted into electricity and used to drive the electrolysis. The same arrangement can be used for other thermal energy sources.

Depending on the geothermal source characteristic, the efficiency of electric power generation varies greatly, with typical values of energy efficiency between

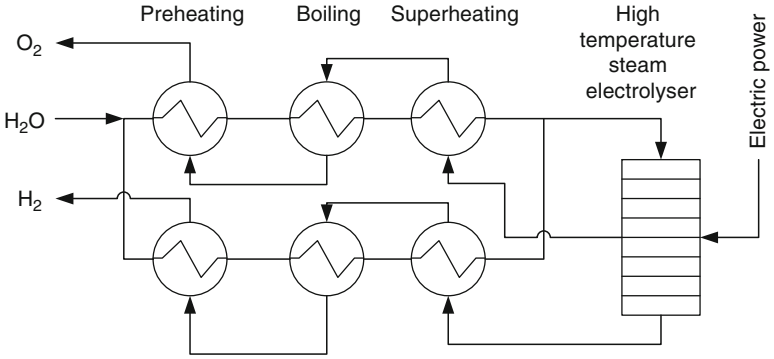


**Fig. 13.28** Arrangement for high-temperature steam electrolysis

5% and 50%. Assuming 80% energy efficiency of the HTSE systems, the expected energy of geothermal hydrogen production may be in the range of 4% to 40%. Geothermal-based hydrogen production can also be implemented by coupling thermochemical cycles with geothermal heat, power generators, and heat pumps for temperature upgrading.

#### 13.4.3.4 Biomass-Based Electrothermal Systems

Another option to generate good-purity hydrogen by using biomass energy is by coupling a biomass combustion facility with an HTSE system. A possible implementation is shown in Fig. 13.29. The system uses an SOEC and two biomass furnaces. The SOEC is basically the reverse of a solid oxide fuel cell (SOFC), which contains a solid electrolyte permeable to oxygen ions. Various types of solid oxide electrolytes were tested, but the technology is in development. The electrolyte can be formed on a porous support made of calcium-stabilized zirconia $ZrO_2$ (CSZ), whose porosity may be about 35%. Other approaches use yttrium-stabilized zirconia (YSZ), containing about 10% molar $Y_2O_3$. The operation range of SOEC is of about 900° to 1,100°C, respectively.

The main furnace (line 14–15–16–17 in Fig. 13.29) is supplied with wet biomass and operates at a relatively low exhaust gas temperature. The function of the main furnace is to generate heat to drive a steam power plant and to dry some biomass. The well-dried biomass is fed in a second furnace, of smaller capacity, that, with dry biomass, can generate exhaust gases with very high temperature (around 1,000 K). The hot exhaust gases transfer heat to the SOEC, which generates hydrogen and oxygen.

The oxygen generated by SOEC is used to enhance the combustion efficiency in the high-temperature furnace. Because the heat needed for the water splitting reaction is supplied completely via heat transfer, it is said that the SOEC operates above the "thermo-neutral point." At 1,000°C and 20% $H_2$ conversion, the SOEC efficiency $\eta_{Cell}$ can be estimated conservatively at 80%. A possible, highly efficient,

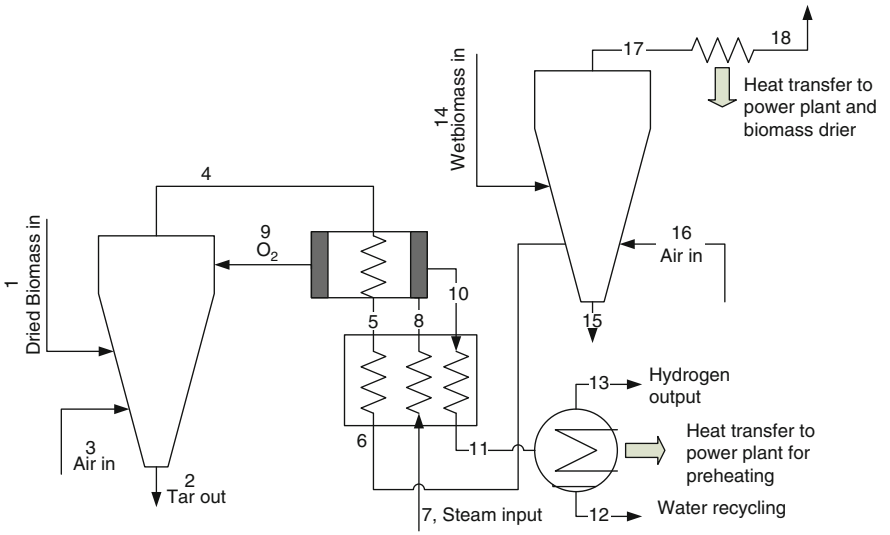


**Fig. 13.29** Biomass-driven high-temperature steam electrolysis system

steam Rankine cycle driven by the low-temperature furnace is shown in Fig. 13.30. The cycle allows for the extraction of process steam and is designed especially for coupling to the above steam electrolysis system.

Another possible system is the biomass-driven hybrid thermochemical water splitting to generate hydrogen. Figure 13.31 shows a possible design. In this system, a low-grade (wet) biomass is used and there is no need for drying because the temperature required of the exhaust gases is slightly below 700°C to supply the thermochemical cycle. The kind of thermochemical cycle considered here is the Cu-Cl one. There is also enough heat in the exhaust gases to supply a steam power plant that produces the required amount of electricity.

The steam power plant is detailed in Fig. 13.32. The steam cycle features a two-phase steam expander at line 7–8 that helps increase the exergy efficiency by allowing for a perfect match of temperature profiles of the exhaust gas and the working fluid (steam). The required heat inputs and outputs in the Cu–Cl cycle can be calculated from energy balances and it results in the temperature-total enthalpy in Fig. 13.33.

### Illustrative Example: Comparison of Two Water Splitting Systems

The biomass-driven HTSE system and the biomass-driven TCWS system introduced above were compared with respect to energy and exergy efficiencies and biomass utilization. It was assumed that heat losses from the system are 0.5% from the reaction heats. The results were obtained by Zamfirescu et al. (2010d) based on standard thermodynamic analysis conducted according to the first and second laws of thermodynamics.

Since the required temperature level is available anyway for the flue gas produced by biomass combustion, internal heat recovery within the Cu-Cl plant is applied. The plot in Fig. 13.33 shows with dashed lines the temperature level and

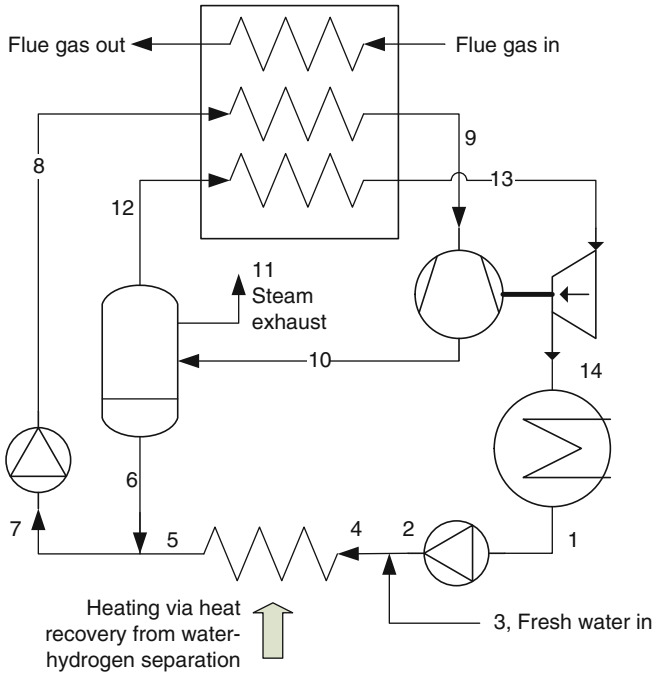


**Fig. 13.30** Efficient Rankine cycle with steam extraction used in conjunction with the high-temperature steam electrolysis system shown in Fig. 13.29

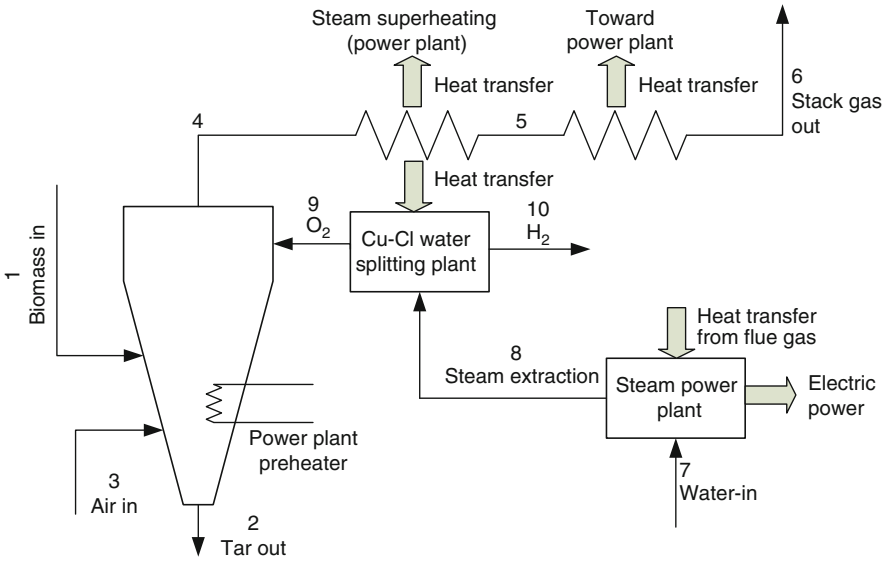


**Fig. 13.31** Biomass-driven thermochemical water splitting system

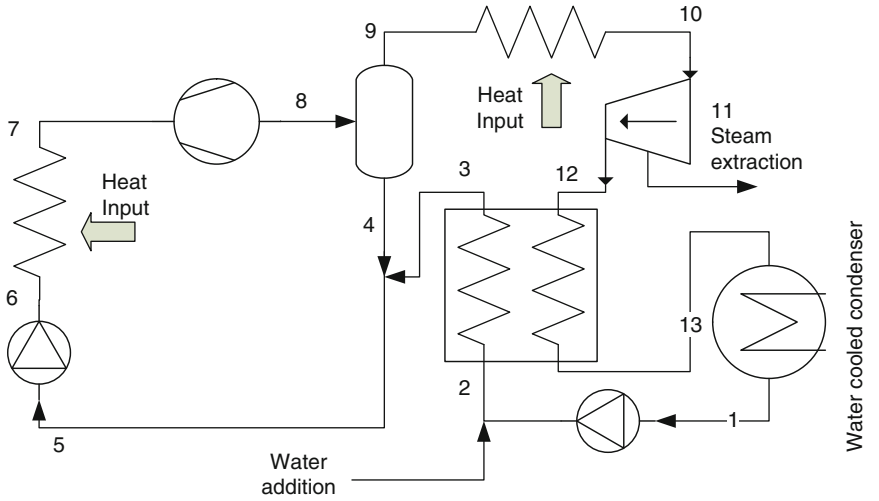


**Fig. 13.32** Steam power plant coupled with the biomass-driven thermochemical water splitting system suggested in Fig. 13.31

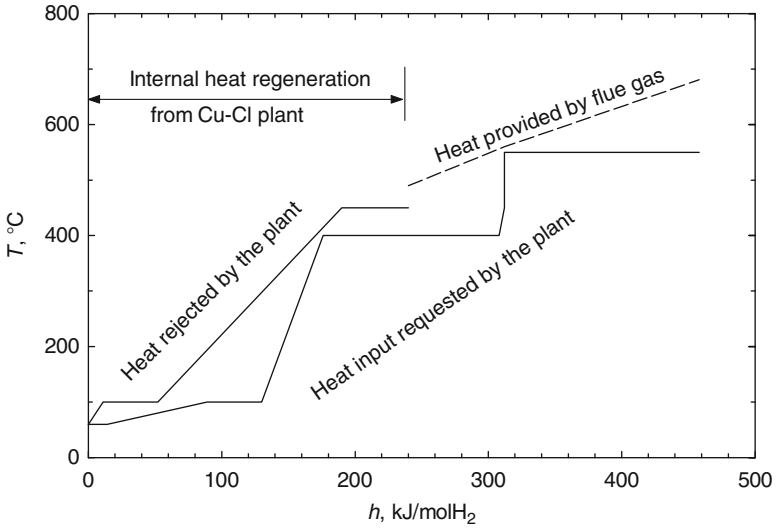


**Fig. 13.33** Heat input and heat rejected by the Cu-Cl plant per 1 mol of $H_2$

enthalpy range of the flue gas delivering heat to the Cu-Cl plant. The highest temperature of the flue gas is 680°C. Figure 13.34 shows the energy and exergy efficiencies as a function of biomass moisture content. The definitions of these efficiencies are shown on the same figure.

The last result indicates in Fig. 13.35 the biomass utilization as a function of technology and biomass quality. *N* represents the number of mols of biomass

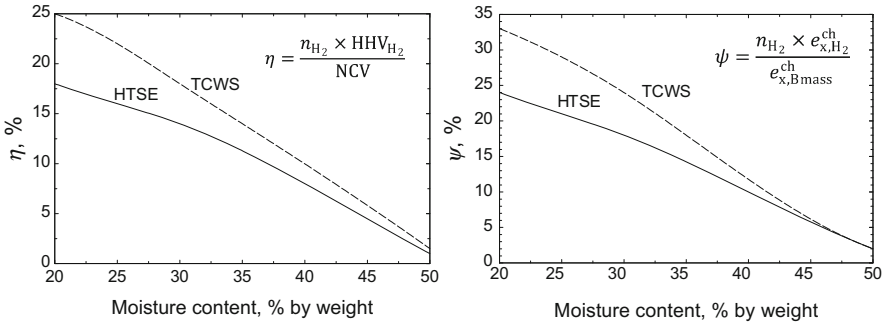


**Fig. 13.34** Energy ($\eta$) and exergy ($\psi$) efficiencies of HTSE and TCWS driven by biomass energy [data from Zamfirescu et al. (2010d)]

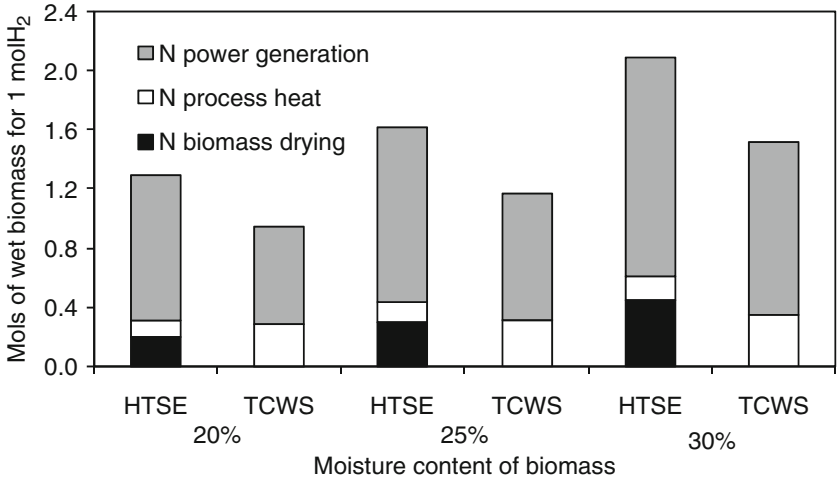


**Fig. 13.35** Biomass utilization at hydrogen production via HTSE and TCWS [data from Zamfirescu et al. (2010d)]

used per mol of hydrogen produced. The result demonstrates that the TCWS consumes less biomass than HTSE because (1) the requirement of electrical energy is reduced and (2) there is no need to dry the biomass before utilization. The conclusion is that TCWS appears more attractive than HTSE.

### 13.4.3.5 Energy Recovery Routes for Electrothermal Hydrogen Production

Energy recovery can be applied in various instances to generate high-grade or low-grade temperature heat. Municipal waste incineration and landfill gas combustion are typical examples of high-temperature heat recovery obtained from human

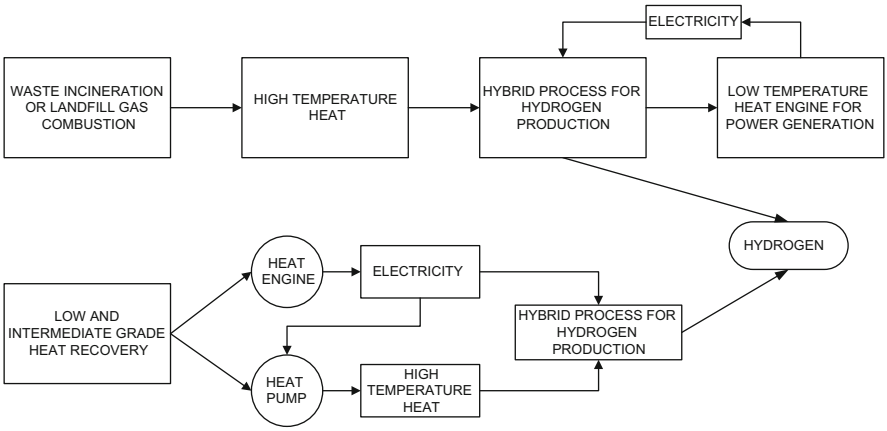


**Fig. 13.36** Routes to hybrid hydrogen production processes driven by energy recovery

activity. Also, various industries eject a large amount of heat into the surroundings. In general, such heat comes at a lower grade, typically from 60°C to 150°C, or at intermediate temperatures that are up to 400°C.

Figure 13.36 presents some possible routes to generate hydrogen through hybrid processes starting from energy recovery. The recovered energy is present or it is eventually converted into heat at high, intermediate, or low grade. The high-temperature heat can be directly used to feed hybrid processes; in this case, the heat ejected by the processes can be used to drive electricity generation through heat engine power generation, which is fed back to the hybrid process. Additional heat possibly can be obtained from the high-temperature heat by using appropriate power cycles. In the case when low or intermediate heat is recovered, heat engine generators and heat pumps may be used simultaneously to obtain electricity and higher temperature heat appropriate for the process. It may be economically advantageous to drive a hybrid process in this way instead of producing electricity only and conducting water electrolysis. The economic advantage of the system depends on the temperature level of the heat source. If the level is too low, upgrading the temperature is not beneficial.

#### 13.4.3.6 Fossil Fuel–Based Electrothermal Systems

Fossil fuels can be used to generate high-temperature heat and electricity to supply hybrid processes for hydrogen production. Figure 13.37 illustrates some ways to do this. Electrothermal plasma methods are emerging technologies for hydrogen generation. In this approach, fossil fuel feedstock is supplied to a plasma reactor. The plasma process can be of two kinds: (1) steam–hydrocarbon reforming and (2) plasma hydrocarbon decomposition. In the first kind, preheated fuel and superheated steam are fed into the reactor. In the second kind, only hydrocarbon is fed.

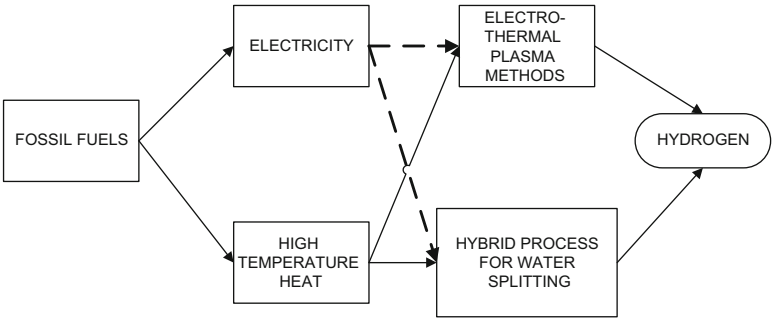


**Fig. 13.37** Thermoelectrical routes for hydrogen production supplied by fossil fuel energy

The feedstock is subjected to a high-voltage electric arc that increases the process temperature up to 5,000°C, enough to dissociate chemicals and generate hydrogen. For plasma steam reforming, the resulted syngas contains 50% to 75% hydrogen and the rest is mostly CO.

If steam is not fed in the plasma process, carbon is separated from the hydrocarbon material. The advantage of the plasma decomposition is its high electrical efficiency (80–90%) and hydrogen purity (98% or more). One of the major technical problems with plasma reactors comes from the carbon deposits on the electrodes, which often must be replaced.

The second route shown in Fig. 13.37 involves electricity and high-temperature heat generation from fossil fuels, followed by a hybrid process for water splitting. In the preferable arrangement, high-temperature combustion heat is used to supply the process, while heat recovery can be applied to generate electricity. The involved hybrid processes can be the HTSE and the hybrid thermochemical water splitting cycles. Therefore, in this route, fossil fuels are used only to generate thermal and electric energy to drive the process, while the feedstock of hydrogen is the water.

#### 13.4.3.7 Nuclear Electrothermal Routes for Hydrogen Production

The HTSE can be coupled with nuclear reactors. The required temperature level for the process is 500° to 1,200°C. SOEC can obtain an electrical-to-hydrogen efficiency of over 90%, provided that the process temperature is higher than 1,000°C. The estimated overall efficiency in conjunction with Advanced Light Water Reactor (ALWR) is around 30%. The efficiency is over 45% with Modular Helium Reactor (MHR) and Advanced Gas Reactor (AGR). The technology requires more research and development before it can become commercially available.

Much attention is paid to the development of heat-upgrading solutions of nuclear heat generated by reactors of the current generation so that one can raise the efficiency of the hydrogen-generation process. Most nuclear reactors generate heat at two levels: high temperature (which is transferred by the reactor coolant) and low temperature (which is ejected through the moderator fluid). Typically, the

**Table 13.14** Heat-upgrading solution of nuclear heat to drive hydrogen production

| Method | Description |
|---|---|
| Chemical heat pumps | Heat pumps operating based on the reversible steam methane reaction can deliver heat up to about 650°C with a source at around 500°C. Magnesium oxide/steam-based chemical heat pumps, operating according to the reversible reaction $MgO(s) + H_2O(g) \leftrightarrow Mg(OH)_2$ can upgrade the heat source temperature from about 250°C to 550°C. Ammonia/salt chemical heat pumps based on reversible reactions, such as $MnSO_4 \cdot 6NH_3 \leftrightarrow MnSO_4 \cdot 2NH_3 + 4NH_3$, can upgrade the heat source temperature from about 80°C to 260°C. In principle, several kinds of chemical heat pumps can be cascaded to upgrade the low-level temperature heat ejected by the moderator of the nuclear power plant reactors and to obtain heat at over 600°C, which eventually can drive a thermochemical water splitting cycle. |
| Vapor compression heat pumps | Novel working fluids were investigated by Zamfirescu and Dincer (2009a), Zamfirescu et al. (2009a), and Zamfirescu et al. (2010f). Siloxane-base can upgrade the source temperature with about 100°C and deliver heat at maximum 400°C, showing a heat pump COP higher than 6; special thermodynamic cycles are proposed operating in the dense gas region and two-phase vapor compression. Biphenyl-based heat pump shows potential to upgrade heat source temperature from about 250°C to 450°C with COP higher than 2.5. Titanium tetra-iodide-based heat pumps are an attractive technical solution to upgrade the source temperature from 350°C to 650°C with a COP higher than 3. A cascaded cyclohexane-biphenyl heat pump upgrades the heat recovered from moderator at 80°C and delivers variable temperature heat between 250°C and 600°C, showing a COP around 5. |
| Reversed Brayton cycle heat pumps | Several reversed Brayton cycle-based heat pumps were suggested and analyzed by Marmier and Füterer (2008) operating with helium and/or $CO_2$ at 70 bar and able to upgrade the nuclear heat temperature from 400°C to 850°–1,000°C. Internal work recovery between the turbine and compressor is applied to enhance the COP. |

moderator heat comes at temperatures in the range of 40° to 80°C and the process heat at temperatures of 250°C up to 650°C.

It is justifiable in view of financial efforts and safety issues not to change the nuclear reactor design but rather to adapt the external cooling loop in such a way that it can be coupled thermally with hydrogen production facilities. Two possibilities can be envisaged for coupling the current nuclear reactors to hydrogen production facilities, without requiring reactor modifications. The first is to recover the heat ejected by the moderator fluid and use this thermal energy for hydrogen generation. In this case, the reactor cogenerates hydrogen and electricity. The second possibility is to dedicate the reactor to hydrogen production only. In this case, the reactor coolant transfers the thermal energy to the hydrogen production facility. In both described situations, heat pumps may be necessary to upgrade the source temperature to a higher level, appropriate for driving the hydrogen production process via thermochemical cycles. Some possible heat-upgrading solution with heat pumps are described in Table 13.14.

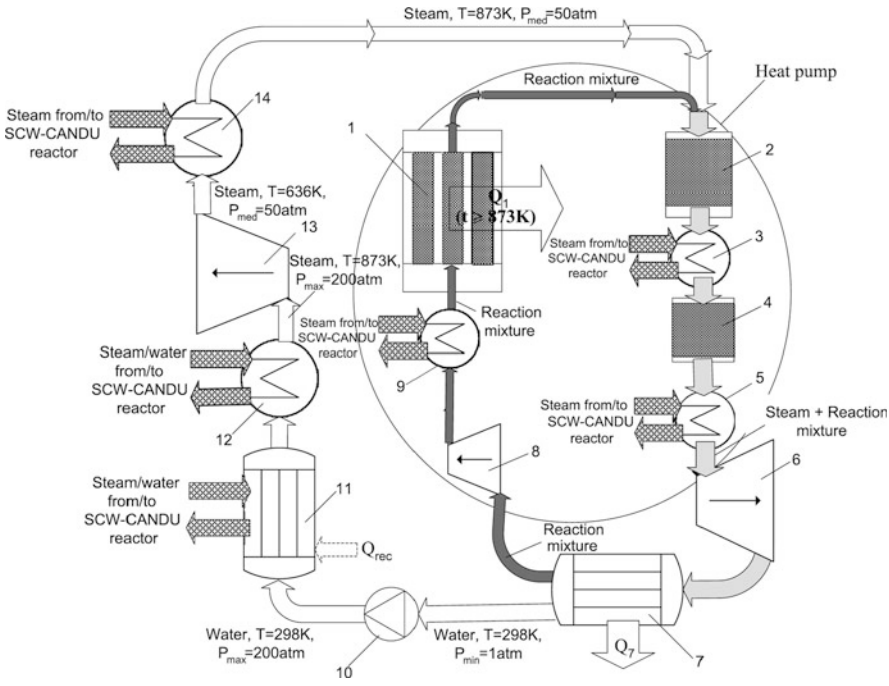


**Fig. 13.38** Chemical heat pump coupling a thermochemical water splitting cycle with the SCW-CANDU nuclear reactor [modified from Granovskii et al. (2008a)]

### *Case Study*: Chemical Heat Pump Integrated with the SCW-CANDU Reactor

This case study presents the solution proposed by Granovskii et al. (2008a) to couple a Cu-Cl TCWS plant with a supercritical water-cooled CANDU reactor for hydrogen generation. The proposed heat pump is of the chemical type, performing cyclically the reversible methane–steam reaction. This is a known process that is used largely for hydrogen production, according to $CH_4 + H_2O + Q \rightarrow CO + 3H_2$ which is favored at low pressure. The reverse reaction is favored at high pressures, and it can deliver heat at higher temperatures according to $CO + 3H_2 \rightarrow CH_4 + H_2O + Q$. The system studied by Granovskii et al. (2008a) to conduct cyclically these reactions is presented in Fig. 13.38.

The high-temperature heat is generated in the methanator (1), where the methane synthesis reaction is conducted at higher pressure. The heat absorbing reaction occurs as slightly lower pressure in two stages in reactors 2 and 4. The heat is transmitted to the heat pump through a heat exchanger 3 inserted between the two steam–methane conversion stages. The reaction products are expanded in turbine 6 after reheating using nuclear heat in the heat exchanger 5.

The water is condensed in the condenser 7 and the noncondensed gases, containing reaction products are recompressed by compressor 8, reheated at point 9, and delivered to the high-temperature reactor 1 to close the heat pump cycle. In the Rankine power cycle, water is pressurized up to 200 atm, then boiled at point 11 and

superheated at point 12 prior to the first stage of steam expansion in the turbine system at point 13. Reheating of intermediate pressure steam is applied at point 14. Within the chemical heat pump loop the reversible water gas shift reaction occurs rapidly and concurrently with the other reactions according to $CO + H_2O \leftrightarrow H_2 + CO_2$. The calculated hydrogen generation efficiency with a nuclear and chemical heat pump and a copper chloride TCWS plant is calculated to be between 45% and 50%.

### *13.4.4 Photonic Energy-Driven Hydrogen Production Methods*

Solar radiation is in essence a source of photonic energy. It is known that photonic energy is proportional to the frequency of the radiation and given by $hv$, where $h$ is the Planck constant and $v$ is the frequency. Photons can be used by various living or "non-living" processes to dislocate electrons by their interaction with matter. While electrons are dislocated, the obtained electrical charge can be used either to generate electricity (viz. photovoltaic effect) or to manipulate the valence electrons of chemical species in order to conduct chemical reactions. These kinds of reactions, called photochemical or electrophotochemical depending upon the context, can lead to hydrogen generation. The following methods of hydrogen production, discussed here, are light-driven: photoelectrochemical water splitting, photocatalytic water splitting, and biophotolysis.

#### 13.4.4.1 Photocatalytic Water Splitting

Photocatalytic water splitting uses various kinds of supramolecular complexes capable of capturing photons from incident solar radiation and that release energy to dislocate electrons that in turn either reduce water to hydrogen or oxidize water to produce oxygen; when reduction and oxidation reactions are coupled, a complete water splitting process is performed. The supramolecular catalysts possess active centers and photosensitive centers. The photoreduction and photo-oxidation of water molecule occur as follows:

$$\left.\begin{array}{l}\text{Photoreduction: } 2H_2O + 2e^- \xrightarrow{hv} H_2 + 2OH^- \\ \text{Photo}-\text{oxidation: } 2H_2O \xrightarrow{hv} 4H^+ + 4e^- + O_2(g)\end{array}\right\}. \tag{13.39}$$

It is a major technological challenge to maintain photoelectrons for a sufficiently long duration at the supramolecular level. A recently declassified proprietary technology developed by Brewer and Elvington (2006) demonstrated at laboratory scale the water photoreduction reaction, with nonsacrificial supramolecular complexes capable of generating multiple electrons and maintaining them at the active center for a long enough duration. In this process, water is exposed to an

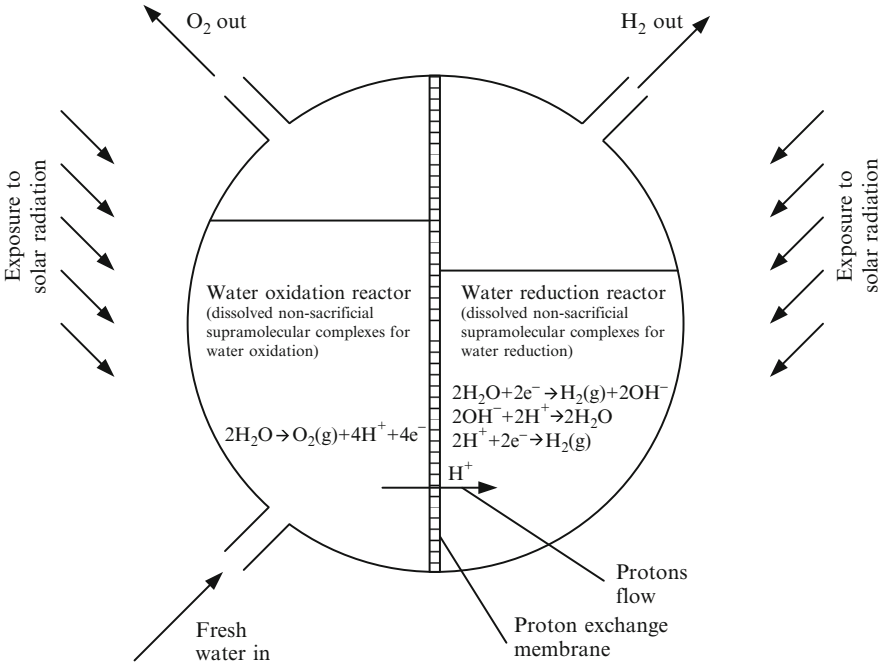


**Fig. 13.39** Conceptual design of a photochemical water splitting reactor [modified from Zamfirescu et al. (2010c)]

electrically charged supramolecular complex that reduces water to hydrogen at the active center. Simultaneously, the supramolecular complex is exposed to solar radiation, during which the incident photons dislocate multiple electrons. Electrons propagate along a molecular chain within nanoseconds and "recharge" the supramolecular complex with electrons. The supramolecular complex can be placed on a support or dissolved in water.

A possible conceptual design of a photocatalytic water splitting system is proposed in Fig. 13.39 and consists of a vessel comprising two photochemical reactors separated by a PEM. Both reactors are exposed to solar radiation. On the left side, the water photo-oxidation reactor is located, in which selected supramolecular photocatalysts are dissolved at a proper quantity to generate electrical charges that oxidize water and generate oxygen gas and protons. Fresh water is continuously supplied to this reactor, while the photocatalysts remain in solution. The flow rate of fresh water is adjusted such that the water level in the vessel remains constant. The protons released by the photochemical oxidation reaction are driven by a concentration gradient and they cross the proton exchange membrane. In the water reduction reactor, selected supramolecular complexes for photocatalytic reduction of water to hydrogen are dissolved in the proper concentration. The water from this reactor is not consumed in a steady-state operation because the only overall reaction is that of proton reduction to form hydrogen gas. Above the

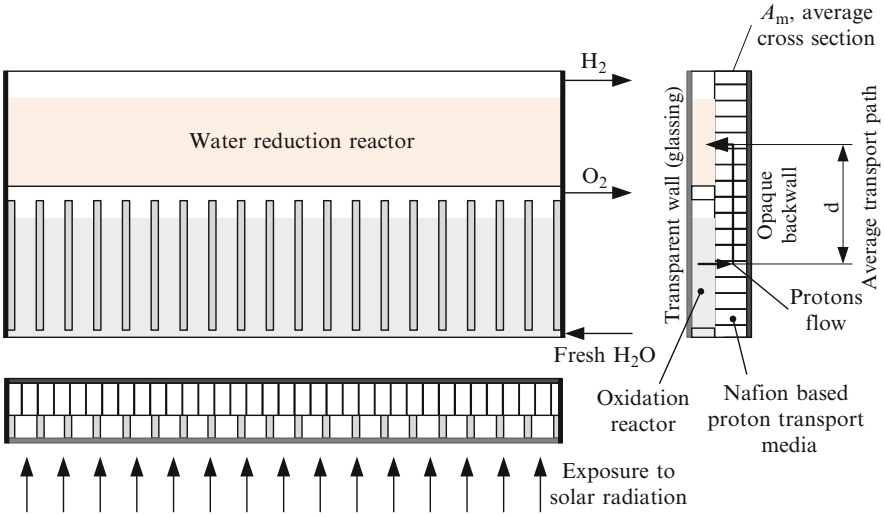


**Fig. 13.40** Possible implementation of the reactor as a flat-plate type [modified from Zamfirescu et al. (2010c)]

liquid level, the product gases (oxygen and hydrogen) are continuously extracted with the use of external fans, which maintain low pressure in the system. In order to avoid water migration through the proton exchange membrane, the pressure is maintained at about the same level on both sides.

In a practical implementation, the photochemical reactor can be constructed with a flat-plate–type geometry. Figure 13.40 suggests a possible practical construction. The system possesses a transparent glassing divided in two sections: below is the water oxidation reactor and above the water reduction reactor. The PEM is placed behind the glassing in the lower reactor. In the lower part, there are a number of vertical channels on both sides, which support the proton exchange membrane.

A water distribution channel and an oxygen collection channel are placed below and above the water oxidation reactor. The space above the water reduction reactor is free of liquid and hydrogen is collected from one of the sides. A flat-plate–type photochemical reactor, as illustrated in Fig. 13.40, can be mounted on a tilted position to capture 4 to 7 kWh of incident solar radiation per day.

There are many catalysts based on complex organic molecules and rare metal active centers that are capable of splitting water, photocatalytically. A brief summary of past results is given here based on Zamfirescu et al. (2010c). Ruthenium-based complexes based on 4-picoline and 2,2′-bipyridine were synthesized; they promote photochemical water oxidation. Bipyridine is a key chemical compound that can be linked to a ruthenium metal active center to have the role of photosensitizer, which dislocates electrons each time when the active center is hit by photons of appropriate energy. Bipyridine is derived from pyridine $C_5H_5N$, which is an aromatic heterocyclic organic compound. Bipyridine comprises two pyridine rings. It has the chemical formula $(C_5H_4N)_2$. A typical photosensitizer embeds a ruthenium atom in three bipyridine molecules, and it is known as $[Ru(bpy)_3]^{2+}$.

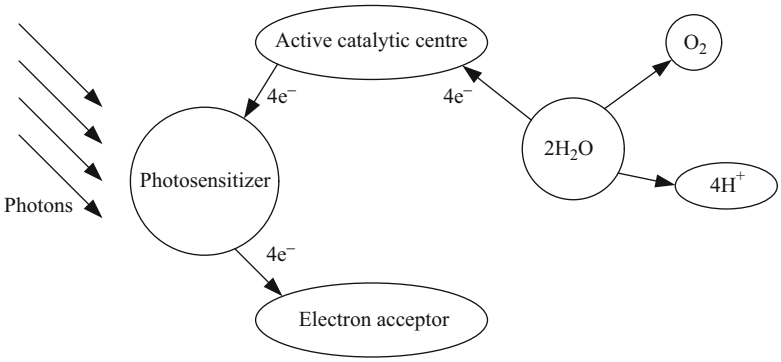


**Fig. 13.41** Mechanism of photocatalytic water oxidation [modified from Zamfirescu et al. (2010c)]

The mechanism of photocatalytic water oxidation is demonstrated in Fig. 13.41. When the ruthenium atom is photoexcited, it enters into a metastable state (it increases its valence by one), characterized by the ability to lose one valence electron. The valence electron is transferred to an adjacent molecule that serves the role of electron acceptor. After losing one valence electron, the ruthenium atom takes one electron from the active catalytic center (typically a metal), which is now activated. The active center is then capable of accepting electrons from adjacent water molecules and oxidizing them. Therefore, at the active center, an oxygen molecule and four protons are formed for each oxidizing cycle, which consumes two water molecules. The crucial issue with the operation of this oxidation mechanism is the nature of the electron acceptor. The majority of electron acceptors developed in the past are consumed in the reaction, so one must continuously supply the process with fresh electron acceptors and remove the ones that are consumed. Many types of electron acceptors are known: $[Co(NH_3)_5Cl]Cl_2$, $Na_2S_2O_8$, $K_2S_2O_8$, $AgNO_3$, $S_2O_8$ or $[Co(NH_3)_5Cl]^{2+}$. For example, if the persulfate $S_2O_8{}^{2-}$ is used as an electron donor, the photoexcitation yields

$$2[Ru(bpy)_3]^{2+} + S_2O_8{}^{2-} \xrightarrow{h\nu} 2[Ru(bpy)_3]^{3+} + 2SO_4{}^{2-}. \tag{13.40}$$

The persulfate is consumed as it transforms in sulfate ($SO_4{}^{2-}$). Once the photosensitizer is excited, it is able to react with the water molecule at the active center ($RuO_2$):

$$4[Ru(bpy)_3]^{3+} + 2H_2O \xrightarrow{RuO_2} 4[Ru(bpy)_3]^{2+} + O_2 + 4H^+. \tag{13.41}$$

As observed in reaction (13.41), the photosensitizer takes one electron from the catalyst ($RuO_2$), which then during four catalytic cycle charges with a charge of +4e, becomes able to split the water molecule. In general, the catalyst is in the form of a colloidal suspension in water.

**Table 13.15** Preparation and performance characteristics of the selected water oxidation reaction

| Parameter | Characteristics | Remarks |
|---|---|---|
| Photosensitizer | Tris(2,2′-bipyridil) ruthenium-II; $[Ru(bpy)_3]^{2+}$ | $6.8 \times 10^{-4}$ mol/dm$^3$ |
| Catalyst | Colloidal $RuO_2 \cdot 2H_2O$ | $4.8 \times 10^{-5}$ mol($RuO_2$)/dm$^3$ |
| Electron acceptor | Nonsacrificial Fe-III in the form of $NH_4Fe(SO_2) \cdot 12H_2O$ | 0.1 mol (Fe-III)/dm$^3$ |
| Ionic strength fixer | $NaSO_4$ | 0.1 mol/dm$^3$ |
| Illumination | Filtered light with $\lambda$>400 nm | 3,333 W/dm$^3$ |
| pH | pH adjuster $H_2SO_4$ | 1.9 (optimized) |
| $O_2$ yield rate | At quantum efficiency of 48% | 0.043 $\mu$mol/dm$^3$ s |

Data from Christensen et al. (1985)

There is a limited number of recyclable electron acceptors. A possible acceptor is methylviologen ($MV^{2+}$), a chemical molecule based on the bipyridine structure. However, coupling ruthenium–bipyridine systems with methylviologen as a reversible electron acceptor, in order to oxidize water, is improbable because the oxidation process is slower than the electrical charge lifetime in the system. Another recyclable (nonsacrificial) electron acceptor is mercury-II. Oxygen generation with mercury-II as an electron acceptor show, that upon irradiation of water containing $[Ru(bpy)_3]^{2+}$ at pH 3 and 0.01 mol/dm$^3$ $Hg(NO_3)_2$ and colloidal $RuO_2$ of $3.2 \times 10^{-5}$ mol/dm$^3$, the rate of oxygen production was about $(1.3 \pm 0.3) \times 10 - 9$ mol/dm$^3$ min. However, the quantum efficiency of oxygen production was rather low, that is, 0.25%.

An interesting photo-oxidation system has been proposed by Christensen et al. (1985), which is based on iron-III as nonsacrificial electron acceptor. This was demonstrated experimentally with a quantum efficiency of oxygen production of about 48%. The system is based on reaction (13.41), where the recycling of the photosensitizer is performed:

$$\begin{cases} 4[Ru(bpy)_3]^{2+} \xrightarrow{h\nu} 4[Ru(bpy)_3]^{3+} \\ 4[Ru(bpy)_3]^{3+} + 4Fe^{2+} \rightarrow 4[Ru(bpy)_3]^{2+} + 4Fe^{3+} \\ 4[Ru(bpy)_3]^{2+} + 4Fe^{3+} \xrightarrow{h\nu} 4[Ru(bpy)_3]^{3+} + 4Fe^{2+} \end{cases} \tag{13.42}$$

In the first reaction of set (13.42), the ruthenium atom increases its valence under the influence of photonic radiation. Furthermore, the ruthenium atom recharges the electron acceptor $Fe^{2+}$ by giving one electron to it. Next time, when the ruthenium atom is hit by the photonic radiation, it takes an electron from the active center ($RuO_2$) and gives it to the electron acceptor. In this mechanism, the electron acceptor is recycled. The preparation and performance characteristics of reactions (13.41) and (13.42) are listed in Table 13.15. The proton production rate is four times higher than the oxygen yield rate. Based on the data reported in Table 13.15, this is 0.172 $\mu$mol($H^+$)/dm$^3$ s. The rate of fresh water to be added to the system is

**Table 13.16** Preparation and performance characteristics of the selected water reduction reaction

| Parameter | Characteristics | Remarks |
|---|---|---|
| Molecular device | $[\{(bpy)_2Ru(dpp)\}_2RhBr_2](PF_6)_5$ dissolved in $CH_3CN$ | 65 μmol/dm$^3$ |
| Electron donor | *N*,*N*-dimethylaniline (DMA) | 1.5 mol/dm$^3$ |
| Illumination | Monochrome light with $\lambda = 470$ nm and $\lambda = 520$ nm | 400 W/dm$^3$ |
| pH | pH adjuster CF3SO$_3$H | 9.1 (optimized) |
| $H_2$ yield rate | Maximum achieved during 3 tests at $\lambda = 470$ nm | 0.085 $\mu$mol/dm$^3$ s |
| $H_2$ yield rate | Maximum achieved during 3 tests at $\lambda = 520$ nm | 0.024 $\mu$mol/dm$^3$ s |
| $H_2$ yield rate | Averaged for solar radiation | 0.054 $\mu$mol/dm$^3$ s |

Data from Brewer and Elvington (2006)

double the moles of produced oxygen. According to reaction (13.22), it is then 0.086 $\mu$mol/dm$^3$ s.

For photocatalytic water reduction, the method by Brewer and Elvington (2006) attracts much attention because of its ability to generate multiple photoelectrons with specially designed molecular complexes. With a 5-W monochromatic LED array, the yield of hydrogen was a maximum 10.9 μmol in 4 hours for a wavelength of 470 nm (blue light). Brewer and Elvington measured the produced hydrogen, both in the gas phase (above the reactor) with a chromatograph, and dissolved in liquid, which was calculated using Henry's law, with the reported solubility of hydrogen in various solvents.

In total, Brewer and Elvington investigated seven molecular complexes, of which four have been dissolved in water and three in a solution of acetonitrile ($CH_3CN$). The molecular compound that showed the maximum yield was $[\{(bpy)_2Ru(dpp)\}_2RhCl_2](PF_6)_5$ in a basic aqueous solution of pH 9.1. This molecular complex has two 2,2′-bipyridine (bpy) branches that embed one ruthenium (Ru) atom each. The Ru atom is the light absorber (LA), and it transfers one electron each time it is hit by a photon. Table 13.16 show the parameters of a selected water reduction system based on Brewer and Elvington's work.

Bipyridine has the role of a terminal ligand (TL) that possesses the quality of long-lived metal-to-ligand charge transfer excited states. This facilitates the presence of an electrical charge in the system for enough time to react with the water molecule (as mentioned also above). The complex (dpp) represents 2,3-bis (2-pyridil)pyrazine, which has the role of a bridging ligand that transfers the electrical charge to an electron collector, which is a metal atom, in this case rhodium (Rh). This molecular complex is unique and shows effectively the water reduction to hydrogen. The two-branch complex with Ru light-absorbing atoms can collect up to four electrons and convert trivalent Rh to monovalent Rh, which further reduces the water molecule. This feature is unprecedented and allows for multielectron photochemistry.

The following issues affect the design of the photocatalytic water splitting device:

- The volume (and therefore the content of chemicals) of the reactors must be adjusted so that the two reactors can be coupled by the interface condition. The flow rate of protons produced in the oxidation reactor must be the same as

**Table 13.17** Main geometric design parameters of the water splitting device

| Design parameter | Equation | Value | Remarks |
|---|---|---|---|
| Volume ratio of reactors | $\frac{V_{H_2} \times \dot{n}'''_{H_2}}{V_{O_2} \times \dot{n}'''_{O_2}} = \frac{2}{1}$ | $\frac{V_{H_2}}{V_{O_2}} = 1.6$ | $\dot{n}'''$, mols produced per second and volume |
| Area ratio of exposed surfaces to solar radiation | $\frac{V_{H_2} \times I_{H_2}}{V_{O_2} \times I_{O_2}} = \frac{I_{T0} A_{H_2}}{I_{T0} A_{O_2}}$ | $\frac{A_{H_2}}{A_{O_2}} = 0.2$ | $I_{H_2} = 400\,\text{W/dm}^3$<br>$I_{O_2} = 3{,}333\,\text{W/dm}^3$<br>$I_{T0}$, solar radiation incident |
| Porous media configuration | $\dot{n}_{H_2} = \frac{150 A_m}{\delta} = 0.054 V_{H_2}$ | $\frac{A_m}{\delta} \cong 70 \dot{n}_{H_2}$ | $\frac{A_m}{\delta}$, in $\text{mm}^2/\text{dm}^2$<br>$\dot{n}_{H_2}$, in μmol $H_2$ produced per second |

Data from Zamfirescu et al. (2010c)

the flow rate of protons crossing the membrane, and the same as the number of reduced protons in the water reduction reactor.

- The surfaces exposed to solar radiation of each reactor must be calculated so that the reaction conditions for the illumination are met.
- The parameters of two fans must be specified (flow rate per capacity of reactor) to ensure that the oxygen and hydrogen are swept out at the rate corresponding to the reaction.
- A mass flow controller for dosing fresh water must be programmed to deliver the required water in the oxidation reactor and thus maintain the desired pH.

Based on the above issues, the main parameters characterizing the design geometry are listed in Table 13.17.

The overall result, however, is hydrogen and oxygen generation, without the consumption of any chemicals except the electron donor DMA, which is converted into $DMA^+$ in the photocatalytic water reduction reactor. Recycling of the $DMA^+$ to DMA can be implemented, possibly, through an electron conducting media between the two reactors. In this way, iron-2 could be converted faster to iron-3 in the water oxidation reactor simultaneously with conversion of $DMA^+$ to DMA in the water reduction reactors. In fact, in such a setup $Fe^{2+}$ donates one electron to $DMA^+$. This hypothetical electron transfer process remains to be proved experimentally.

#### 13.4.4.2 Biophotolysis for Hydrogen Production

Another light-driven process is biophotolysis, which is a photonic-driven biochemical hydrogen production process from water. The photosynthesis process used by green plants to convert solar radiation into biochemical energy can be adapted to some extent for hydrogen generation and stands at the base of biophotolysis. Production of hydrogen through biophotolysis can be classified as direct or indirect types and photofermentation type (Kotay and Das 2008).

In biophotolysis, some microorganisms sensitive to light are used as biological converters in a specially designed photobioreactor. The most suitable microorganisms

are microalgae because they exhibit hydrogen evolution and can be cultured in closed systems that can permit hydrogen capture. Microalgal strains can be cultured that exhibit high hydrogen yields. One remarkable advantage of biophotolysis is to produce hydrogen from water in an aqueous environment at standard temperature and pressure. Biophotolysis is not yet developed for commercial use but is demonstrated at laboratory scale. According to Das and Veziroglu (2008), the energy efficiency of the method potentially can reach 10%.

Water molecule can be split through biophotolysis under the action of Cyanobacteria, also known as green microalgae (*Chlamydomonas reinhardtii*) under special conditions. These microorganisms generate and manipulate nitrogenase and hydrogenase enzymes in such a way that they may generate hydrogen and oxygen from water. The bacteria that were found to be hydrogen productive are mainly anabaena variabilis PK84, anabaena cylindica, anabaena AMC 414, gloebacted PCC742, synechococcus PCC602, and aphanocapsa montana; also, the microalgae chlamydomonas reinhardrii cc124 and cc1036 proved to be hydrogen productive. The general reactions producing hydrogen from water with the help of photoactivated enzymes can be written as follows (Das and Veziroglu 2008):

$$\left.\begin{aligned} 12H_2O + 6CO_2 &\xrightarrow{hv} C_6H_{12}O_6 + 6O_2 \\ C_6H_{12}O_6 + 12H_2O &\xrightarrow{hv} 6CO_2 + 12H_2 \end{aligned}\right\}. \tag{13.43}$$

### 13.4.5 Biochemical Methods for Hydrogen Production

Biochemical energy is stored in organic matter in the form of glucose, cellulose, sucrose, and other complex chemicals containing, for example, adenosine triphosphate, and it can be manipulated by microorganisms to extract hydrogen in the absence or presence of oxygen. When oxygen is completely absent or is present in very reduced quantities, the biochemical conversion of organic matter to various forms of biochemical energy is called anaerobic digestion.

Anaerobic digestion is attractive as hydrogen production method for two important reasons: (a) it can generate hydrogen from organic waste, and (b) it stabilizes waste that otherwise may become a source of uncontrolled microbial growth with the potential danger of contamination of biological species. Moreover, the digester hardware is simple and the system is appropriate for mass production. Two types of bacteria are used in anaerobic digestion: mesophilic (which is active at temperatures of 35–40°C) and thermophilic (which is active at 55–60°C). Note that hydrogen production is also possible by aerobic digestion, but this process is less productive and consequently less developed at the present time, and thus is not discussed here.

Experiments were done in both batch and flow reactors, generating hydrogen from various biomass substrates, including sucrose, and maintaining an appropriate

control of the hydrogen-generating and hydrogen-consuming bacteria present in the reactor. The production rate is about 1.5 mol hydrogen per mol of sucrose in the substrate. *Clostridium* bacteria positively affect the hydrogen production rate under certain conditions. One major problem regarding reaction control in anaerobic digestion reactors is the inhibition of methanogens, which represent hydrogen-consuming bacteria. One possibility to eliminate these bacteria, which normally are present in the organic substrate, is to heat the substrate for a short time at about 100°C, which kills all bacterial populations. Further, the biomass is seeded with hydrogen-producing bacteria such as *Clostridium* and *Bacillus* species.

One of the possible chemical reactions favored by the enzymes generated by hydrogen bacteria (viz. hydrogenase) is acetic acid fermentation from sucrose:

$$C_{12}H_{22}O_{11} + 2H_2O \rightarrow 4CH_3COOH + 4CO_2 + 8H_2. \tag{13.44}$$

In an organic substrate, both nitrogenase and hydrogenase enzymes contribute to hydrogen production by reducing free protons according to the following general reactions:

$$\left.\begin{array}{l}\text{Nitrogenase: } N_2 + 8H^+ + 8e^- + 16ATP \rightarrow 2NH_3 + H_2 + 16ADP + 16Pi \\ \text{Hydrogenase: } 8H^+ + 8e^- + 16ATP \rightarrow 4H_2 + 16ADP + 16Pi\end{array}\right\}, \tag{13.45}$$

where ATP is adenosine triphosphate, ADP is adenosine diphosphate, and Pi is inorganic phosphate which is cleaved from the ATP molecule according to the reaction ATP → ADP + Pi, which releases free energy of about 30.5 kJ/mol; this biochemical energy is used to drive the reaction.

Koutrouli et al. (2009) studied hydrogen production from water-diluted (1:4) olive oil using anaerobic digestion. The retention time in the bioreactor was 7.5 to 30 hours as compared to that typical for methane formation from the same substrate, namely, 10 to 20 days. The results show a thermophilic bacteria production rate 1.5 times higher than that of mesophilic ones, and it is at maximum 320 mol of hydrogen per ton of olive pulp.

Another study, Das and Veziroglu (2008), found a hydrogen yield of 7 mol $H_2$ per mol of glucose. The major challenge with aerobic digestion for hydrogen production is the reduced production rate per unit of capital investment in the facility. Remarkable energy conversion efficiency is observed at anaerobic digestion of molasses (which is a by-product of sugar processing), namely 28%. Based on the data compiled by Das and Veziroglu (2008) and Kalinci et al. (2009), the cost per unit of energy content in produced hydrogen via anaerobic digestion is compared with other technologies and with biophotolysis as shown in Fig. 13.42. In this comparison, for anaerobic digestion it has been assumed that the process is "biological water gas shift reaction." This process is a relatively new method for hydrogen production driven by bacteria that perform in anaerobic conditions, and in the absence of light the water gas shift reaction generates hydrogen. The production cost of hydrogen by this method, as reported by Kalinci et al. (2009), is about $24/GJ.

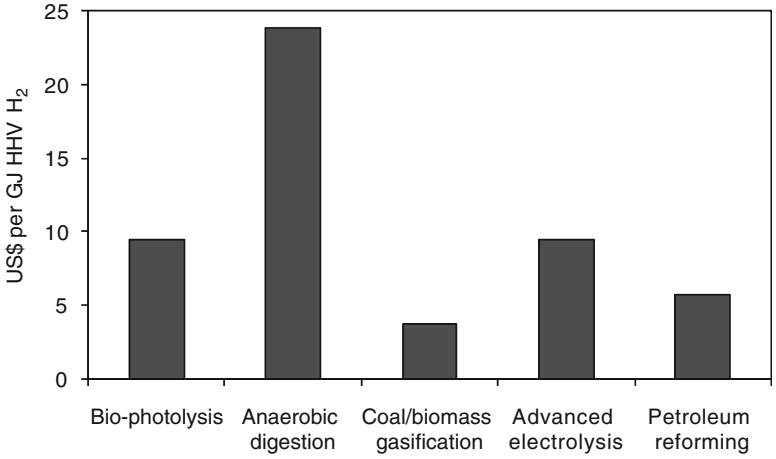


**Fig. 13.42** Cost comparison between biochemical routes and some common methods of hydrogen production

### *13.4.6 Hybrid Methods for Hydrogen Production*

All sorts of methods for hydrogen production can be combined in a complex system aiming to generate hydrogen more effectively. Section 13.4.3 described the electrothermal methods for hydrogen production. It is possible to combine electric, thermal, and photobiochemical methods for better productivity. At the same time, all kinds of primary energy sources (renewables, fossil, nuclear) and recovered energy can be used in various combinations to drive the processes.

Hydrogen can also be produced by combining renewable technologies, for example, photovoltaic and wind. These technologies are not competing with each other; rather, they are complementing and supporting each other. On the one hand, the wind technology can be beneficial for periods without sunshine, on the other hand, solar photovoltaic technology can compensate when there is no wind during the daytime. This symbiotic behavior of the two technologies ensures a better and continuous supply of electricity to the electrolyzer to produce hydrogen. The access power produced by the system can be stored in batteries and can be used in adverse conditions. Another example of coupling two technologies is solar thermal and geothermal.

The hot water from geothermal sources can further heated to the desirable temperature (approximately 550°C) by using solar concentrating collectors and then by using a high-temperature electrolyzer to produce hydrogen. One of the advantages of hybrid renewable technology assisted with fossil fuel and nuclear energy is that it ensures a continuous supply of input energy, which when using these technologies individually sometimes can be challenging. The performance of such hybrid systems can be better than the performance of systems that use the two technologies separately.

**Illustrative Example: Hybrid Artificial Photosynthesis System**

Here is an example of a hydrogen production method that combines photovoltaic electricity generation with electrolysis and artificial photosynthesis. Note that there are many other hybrid systems for hydrogen production; this example is only meant to illustrate the general idea. As a matter of fact, sustainable development requires not only that sustainable energy resources be used, but also that the resources should be used efficiently. Artificial photosynthesis is a concept that not only produces hydrogen (and food), but also improves the environment by removing carbon dioxide and adding oxygen to the environment. This concept is a replica of the photosynthesis of plants and algae. The two reactions involved in photosynthesis, as described before, are the light reaction and the dark reaction:

- *Light reaction*

Light energy is absorbed by special cell membranes and transferred to chlorophylls. Electrochemical reactions generate vital "energy-rich" biological compounds. Oxygen is produced as a by-product of this process and is released to the atmosphere. This is actually nature's own photovoltaic energy conversion system (photosystem), in which the trapped light energy is first converted into electrically stored energy in cell membranes. The light phase requires the cooperation of membrane-bound photochemical assemblies (also called photosystems). Each photosystem operates in series to photochemically "charge" the membrane.

- *Dark reaction*

The products of the light phase, that is, the energy-rich biological compounds, are used within cells for the formation of carbohydrate (sugars) from carbon dioxide, via a series of biochemical intermediates in the presence of some enzymes (catalysts). This process is central to the progressive chemical "assembly" of sugar molecules from carbon dioxide and water. This is the only point at which continued water consumption is absolutely required for carbohydrate formation, and it represents only a tiny fraction of the water supplied conventionally in plant growth. So, the overall reaction of natural photosynthesis, including the carbon fixation process, can be given as $CO_2 + H_2O + \text{Sunlight} = O_2 + \text{Carbohydrate}$.

Artificial photosynthesis is a means of achieving the aims of clean power generation and dry food production as shown in Fig. 13.43, which is a schematic diagram of artificial photosynthesis. The upper half shows the light reaction and the bottom half shows the dark reaction of the photosynthesis.

The main steps in the natural photosynthesis processes of plants and bacteria provide the models and inspiration for a totally biomimetic, industrial-scale technological approach to achieve the following specific goals:

- Electricity generation using photovoltaic systems. The power generated can directly be supplied to the national grid.
- "Dry agriculture," employing enzyme bed reactor systems to fix carbon dioxide from the air or other convenient sources, powered by hydrogen and bioelectric transducers drawing power from the national grid. These produce carbohydrates

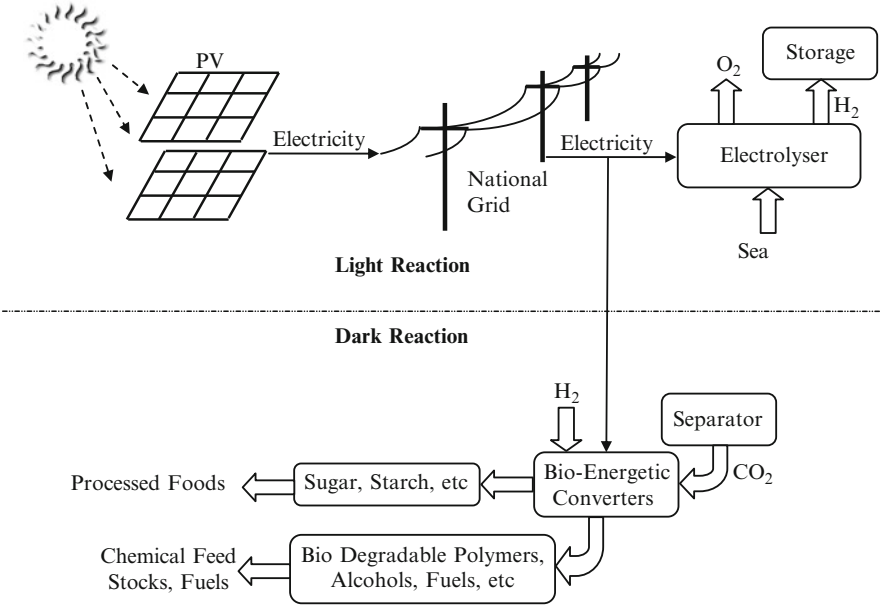


**Fig. 13.43** Schematic of artificial photosynthesis concept [modified from Collings and Critchley (2005)]. *PV* photovoltaic cells

(food), liquid fuels, chemical feed stocks, and polymers for fiber production. Water usage is at or near the absolute chemical minimum and thousands of times lower than in conventional agriculture.

- Hydrogen production from seawater or other suitable water sources. Electrode systems employing catalytic surfaces modeled on the relevant high-efficiency active sites in photosynthetic organisms achieve the electrolytic decomposition of water (into hydrogen and oxygen).

The economical comparison between competing energy systems should be based on the effective costs of the services these fuels provide. The effective costs include the utilization energy, the cost of fuel, and the costs associated with fuel consumption that are not included in its price (so-called external costs). External costs include the costs of the physical damage done to humans, fauna, flora, and the environment due to harmful emissions, oil spills and leaks, and coal strip mining, as well as governmental expenditures for pollution abatement and expenditures for military protection of oil supplies. In economic considerations, it is also important to compare the future costs of hydrogen (which will be considerably lower than they are today because of the assumed market and technology development) with the future costs, both internal and external, of fossil fuels (which unavoidably will be higher than today's prices due to depletion, international conflicts, and environmental impact).

## 13.5 Hydrogen Storage

It is very difficult to store hydrogen in a satisfactorily dense phase so that the packed energy density is similar to that of common fuels used today for vehicles. Based on a higher heating value, 324 g of hydrogen have the same content as 1 kg of gasoline. The corresponding volume of 1 kg of gasoline is about 1.3 L; if 324 g of hydrogen is stored as gas under standard temperatures and pressure conditions, the occupied volume is 3,932 L. At the normal boiling point (20.3 K), under atmospheric pressure the density of the cryogenic liquid hydrogen is 70.77 kg/m$^3$; the volume of 324 g of liquid hydrogen is 4.6 L, which is 3.5 times larger than that of gasoline with the same energy content. Under the standard temperature (298.15 K) and 400 bar pressure, the hydrogen gas density is 25.98 kg/m$^3$ and the gas volume becomes 12.5 L or 9.6 times more than the gasoline volume with the same energy content. The following potential storage methods are considered for hydrogen:

- Compressed gas at standard temperature and very high pressure
- Cryogenic liquid at standard pressure and 20 K
- Physical binding of hydrogen molecule in a solid material matrix
- Chemical binding to synthesize a denser chemical that can later release hydrogen

For storage in any of these methods, hydrogen must be purified to an acceptable degree; for compressed storage 4-ppm impurities are acceptable, while for cryogenic storage 1 ppm is recommended.

For compressed storage, the current target is to develop commercial systems capable of storing hydrogen at 700 bar, at which 5 kg of hydrogen occupy 125 L. Such systems were built and tested for vehicles, but the common storage pressure used today is 300 bar. The adiabatic compression work can be easily calculated under the reasonable assumption of ideal gas behavior of hydrogen:

$$W|_{s=\mathrm{ct}} = \frac{\gamma}{\gamma - 1} RT_1 \left[ \left( \frac{P_2}{P_1} \right)^{\frac{\gamma}{\gamma - 1}} - 1 \right], \tag{13.46}$$

where $\gamma = C_\mathrm{p}/C_\mathrm{v}$. The isentropic efficiency depends on the compression ratio; typical values are 70% to 80% for small compression ratios of the order of 3 to 4 and 50% to 60% for larger compression ratios of 100. For compressing hydrogen at 350 bar, the expected energy consumed is around 10 MJ/kg.

Liquefaction of hydrogen implies its cooling to a cryogenic temperature; this is a well-documented process, and there are mature technologies in industry for obtaining cryogenic hydrogen. But some problems occur in this process:

- It is not possible to obtain a refrigeration effect with hydrogen at a temperature over 190 K because of the "positive" Joule–Thomson coefficient of hydrogen; therefore, liquid nitrogen is used in the first stage of cooling to get hydrogen below 190 K.
- There are two configurations of the hydrogen molecule at ambient temperature: ortho- and para-hydrogen. At cryogenic conditions, all hydrogen converts to the

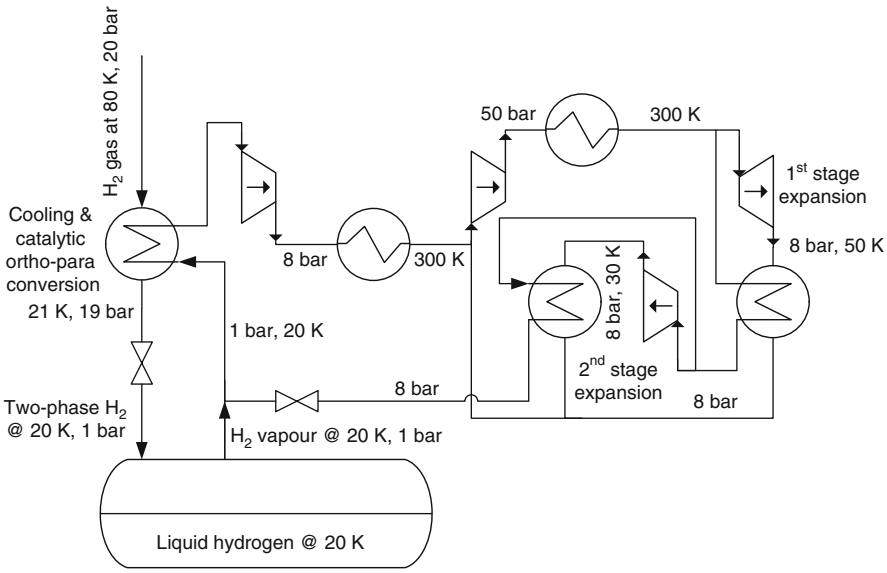


**Fig. 13.44** Simplified diagram of the Claude hydrogen liquefaction process

para configuration. This process is slow, and for an acceptable rate of hydrogen production it must be accelerated by using catalysts. Catalysts (iron-oxide) are normally integrated in the heat exchanger that cools the hydrogen.

- The ortho-para conversion heat of 530 kJ/kg at 20 K adds to the latent heat of condensation, which is about 450 kJ/kg; therefore, an important amount of heat must be extracted at the proper rate in order to obtain liquid hydrogen.
- The evaporation heat of liquid hydrogen (para configuration) is rather low; therefore, the storage tank must be extremely well insulated.

Liquefaction of hydrogen requires expensive materials (e.g., chrome-based) that are suitable for very low temperatures; all the equipment must be placed in a vacuum box and must be thermally very well insulated. In the first stage, liquid nitrogen is used to cool hydrogen down to 80 K. Further cooling of hydrogen from 80 to 20 K is obtained by a special double-stage Brayton refrigeration cycle operating with hydrogen gas. This cycle recycles the hydrogen evaporated from the cryogenic tank; it is drawn, in a simplified way, in Fig. 13.44. After compression to about 20 bar, hydrogen is cooled, down to 80 K. This cooling (not shown in the figure) is done in three stages: cooling with water to 300 K, cooling with a vapor compression refrigeration plant down to ~250 K, and cooling with liquid nitrogen down to 80 K. With further cooling with a cryogenic cooler, the main stream temperature is decreased to 21 K; the throttling process generates colder two-phase liquid–vapor hydrogen introduced in the cryogenic hydrogen tank.

Above the liquid level, hydrogen vapors are always generated because of heat penetrations. They are extracted from the tank at 20 K and 1 bar and used for cooling the main stream of hydrogen down to 21 K; further, the vapor is compressed

in two stages with intercooling, in the first stage, from 1 bar to about 8 bar, and in the second stage from 8 to 50 bar. A part of the compressed hydrogen is expanded to intermediate pressure (8 bar) and reaches 50 K.

The cold stream at 50 K is used to cool the remaining stream prior to the second stage of expansion; before the second stage of expansion, the flow is divided into two streams. Note that the second stage of expansion occurs also from 50 to 8 bar, with the difference being that the flow is much colder prior to expansion. Consequently, the temperature at the end of the second stage of expansion reaches around 30 K. The remaining stream is cooled further down to a little above 30 K prior to the final expansion process that occurs in a throttling valve, after which the temperature of the hydrogen stream reaches 30 K.

Cryogenic hydrogen is normally stored in double-wall stainless steel vessels with vacuum between the walls. The typical evaporation losses due to heat penetration with current storage tank technology vary between 0.3% and 5% per day. The energy associated with the liquefaction process is estimated to be an average of 50 MJ/kg of hydrogen, which adds substantially to the hydrogen cost. It is, therefore, important to reduce the greenhouse gas emissions associated with hydrogen liquefaction. This can be done by using renewable energies to drive the liquefaction process. Kanoglu et al. (2007) studied the ways of using geothermal energy for hydrogen liquefaction. They suggested that the best way of doing this is by using one part of the geothermal energy to drive an absorption cycle that precools the hydrogen gas, and another part of the geothermal energy to generate electricity that drives the liquefaction plant.

There are two processes that can be applied for storing hydrogen in a solid matrix: physisorption (absorption of molecular hydrogen by a solid structure) and chemisorption (dissociation of the hydrogen molecule and bonding of the protons with the metal lattice). Many metal-hydride–based methods were developed for both physisorption and chemisorption of hydrogen. In general, they require some thermal energy at the discharging phase, and some cooling should be applied to enhance the efficiency of the hydrogen charging process.

Some chemical elements such as sodium, lithium, magnesium, and boron can create hydrides (called "chemical hydrides") that store hydrogen more densely than is possible in metal hydrides via physisorption and chemisorption. Decomposition of chemical hydrides is irreversible. Therefore, sophisticated processes must be put in place to recycle the chemical compounds after the hydrogen is released. Two processes are possible for hydrogen evolution from chemical hydrides, namely, thermal decomposition and hydrolysis. Examples of simple chemical hydrides are NaH, LiH, $CaH_2$, $MgH_2$, and various boron hydrides with the general formula $MBH_4$, where M represents a metal from the series Na, K, and Li. A general representation of chemical hydride hydrolysis is $MH_n + nH_2O \rightarrow nH_2 + M(OH)_n$. During hydrolysis, the chemical hydrides release heat. An example, is the hydrolysis of sodium borohydride, which occurs as follows:

$$NaBH_4 + 2H_2O \rightarrow NaBO_2 + 3H_2, \tag{13.47}$$

and which releases heat of 67 kJ/mol of hydrogen. Note that sodium borohydride is nonflammable and nonexplosive and allows hydrogen generation as in Eq. (13.47) at about 80°C over ruthenium or platinum catalysts.

Ay et al. (2006) investigated hydrogen release from sodium boron hydride, which is produced from sodium tetraborate ($Na_2B_4O_7$), which is decomposed at 400° to 500°C under hydrogen atmosphere, endothermically. They found that the release of hydrogen from the formed sodium borohydride can occur under atmospheric pressure and temperature in the range of 25° to 40°C. The reaction of sodium borohydride synthesis, according to Ay et al. (2006), is as follows

$$Na_2B_4O_7(s) + 16Na(s) + 7SiO_2(s) + 8H_2 \rightarrow 4NaBH_4(s) + 7NaSiO_3(s). \quad (13.48)$$

Note that sodium tetraborate (known also as borax) is naturally found as a mineral; the largest borax reserves are in Turkey; other countries having significant borax reserves are the United States, Chile, China, and Romania.

One interesting possibility for storing hydrogen in solid form is to first produce ammonia from it, and then absorb the ammonia gas in metal amines. This solution has been investigated by Sørensen et al. (2008), who found that up to six molecules of ammonia can be bound weakly by magnesium chloride to form $Mg(NH_3)_6Cl_2$, which embeds 109 g/L of hydrogen and 92 g/kg of magnesium ammine; recall that liquid hydrogen density is 71 g/L. The release of ammonia can be obtained by thermal desorption, and the process is reversible; that is, by applying proper cooling, ammonia is absorbed back in the form of ammine.

To completely release the ammonia according to the formula $Mg(NH_3)_6Cl_2 \rightarrow 6NH_3 + MgCl_2$, the associated desorption heat needed is 218 kJ/mol; further, 1 mol of ammonia generates 1.5 mol of hydrogen according to the decomposition reaction $NH_3 \rightarrow 1.5H_2 + 0.5N_2$, which needs at least 68 kJ/mol of ammonia; thus, in order to release 1 mol of hydrogen from the metal amine, the thermal energy must be higher than 191 kJ. This energy can be provided by a heat recovery process or by solar energy (if applicable) or by combustion of the released hydrogen itself. In the last case, accounting for the higher molar heating value of hydrogen of 284 kJ/mol, the remaining energy after the hydrogen that is extracted from the ammine is 93 kJ/mol of hydrogen, a value that reflects the price of generating hydrogen from salt. Nevertheless, metal amines are an attractive solution for hydrogen storage, but one must account for the diminishing of the calorific value due to hydrogen extraction, or alternatively, this method of storage should be applied where some combustion heat can be recovered to drive the ammonia cracking reaction itself.

Hydrogen storage in the form of ammonia has been recognized as an attractive possibility. In this solution, hydrogen can be converted to ammonia by the well-established Haber–Bosch process. The advantages of ammonia as a hydrogen source and storage medium are analyzed in Chapter 7. Storing hydrogen chemically in the form of urea is also an attractive solution, as urea is very stable, can be stored for a very long time, and can be safely transported. Urea is a particulate material delivered in small-size prills. It can be combusted as it has a low calorific value comparable to that of wood, that is, about 10 MJ/kg. The average price of urea is $0.30 per kg.

Urea can be synthesized from biomass or other renewable energy sources so that the result can be a $CO_2$-free fuel. Urea, with the chemical formula $CO(NH_2)_2$, is extensively produced in industry and is used as fertilizer. It is considered a nontoxic substance, and several car manufacturers use it in their passenger vehicles for $NO_x$ exhaust reduction. Currently, urea is synthesized from natural gas or petroleum and is then reformed to produce hydrogen. The hydrogen, therefore, is combined with nitrogen (taken from air) to obtain ammonia, which is eventually combined with $CO_2$ to produce urea. It is simple to produce urea starting only from biomass sources. Another path to synthesize urea is via hydrogen production from renewable sources (e.g., water electrolysis, thermochemical or photocatalytic water splitting, etc.). The hydrogen is then combined with nitrogen to generate ammonia and with $CO_2$ to produce urea.

Carbon dioxide can be recovered from cement factories or power plants, taken from biomass combustion, or extracted from atmospheric air. In any of these cases, the produced urea is either a zero carbon or low carbon hydrogen source. To extract hydrogen from urea is relatively straightforward as discussed in the next illustrative example. A case study demonstrating the benefits of gasoline–urea or diesel–urea co-fueling is demonstrated in Chapter 6.

Ammonia-based compounds, as shown in the above example of urea, have a good capability of hydrogen storage and release. One of the most promising ammonia-based storage methods is ammonia borane with the chemical formula $NH_3BH_3$, which contains 120 g of hydrogen per liter in a weight concentration of 19% (Karkamkar et al. 2007). Ammonia borane releases hydrogen by thermal cracking according to the following reaction evolving at successively higher temperatures:

$$\left.\begin{aligned} 2NH_3BH_3 &\xrightarrow{<120^\circ} C(NH_2BH_2)_2 + 2H_2 \\ (NH_2BH_2)_2 &\xrightarrow{\sim 150^\circ} C(NHBH)_2 + 2H_2 \\ (NHBH)_2 &\xrightarrow{>500^\circ} CBN + 2H_2 \end{aligned}\right\}. \tag{13.49}$$

Therefore, one molecule of ammonia borane can release three molecules of hydrogen if heated at over 500°C. An interesting factor is that ammonia borane can release hydrogen at temperatures lower than 120°C; if properly conducted, the decomposition reaction can release hydrogen even at room temperature. Releasing hydrogen at a low temperature is a crucial characteristic for storage systems used for the cold start-up of engines.

Figure 13.45 presents the hydrogen storage density that is possible with various technologies. The storage density is presented in two different ways. On the horizontal axis, it is the volumetric storage density in kg of hydrogen per unit of volume of storage facility. On the vertical axis, the energy embedded in the quantity of hydrogen that can be released by the storage is presented; this amount is given per unit of mass (kg) of the storage facility (tank). The ammonia-boron compound with the chemical formula $NH_4BH_4$ appears to be the densest hydrogen storage.

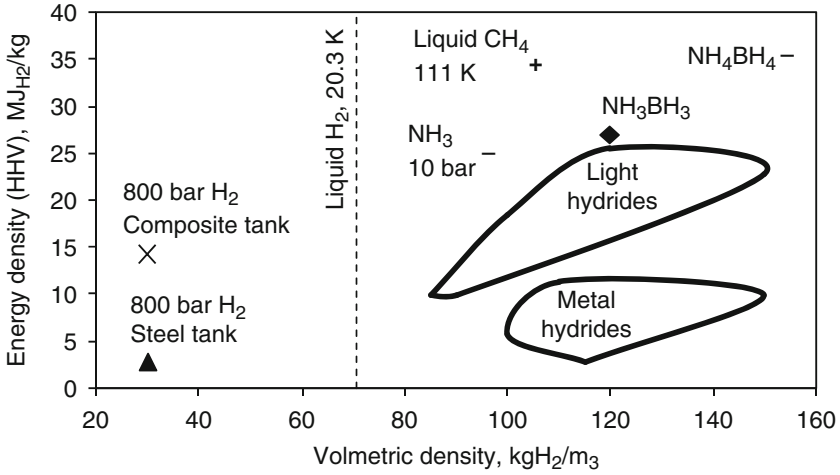


**Fig. 13.45** Density of hydrogen storage with various technologies [data from Kanoglu et al. (2007), Ay et al. (2006), Sørensen et al. (2008), Karkamkar et al. (2007)]

## 13.6 Hydrogen Transportation and Distribution

It is interesting to estimate the total cost of hydrogen, including its production, distribution, and storage. Depending on the production method, the hydrogen costs vary from $1/kg at coal gasification to $9.50/kg using solar energy for electricity generation that in turn is used for water electrolysis (see also Zamfirescu and Dincer 2009b). After production, hydrogen is stored at the manufacturer's location for a certain period prior to delivery. Liquefaction adds at least 30% to the hydrogen price per kg, and on top of that one must add the energy consumed to keep the storage tank at cryogenic temperatures during the storage time.

The minimum cost penalty for hydrogen storage (when hydrogen is stored for 1–3 days) is CN$0.30/kg for compressed $H_2$ and CN$0.70/kg for liquefied $H_2$. Hydrogen distribution to the consumption points is also expensive. If one assumes, for example, that the hydrogen transport is made in pressurized containers at 345 bar, the transported energy content is 8 GJ/$m_3$, that is, a four times smaller amount than for gasoline (32 GJ/$m^3$). The high explosion risk of hydrogen raises the price even more because of the required safety measures. Due to these factors, the estimated minimum cost of hydrogen distribution is ~$1/kg $H_2$. Thus, if one considers the production, storage, and distribution costs, the minimum expected hydrogen price at delivery point should be ~CN$2.50/kg if produced from coal, and ~CN$11/kg if produced from solar energy-driven water electrolysis. Chapter 7 showed that the storage and distribution of hydrogen in the form of ammonia is more advantageous than its storage and distribution as cryogenic or compressed gas.

## 13.7 Hydrogen Utilization

Hydrogen is a basic chemical that is used in many industrial processes in the chemical industry, glass production, oil refining, and metallurgical processes. The projected hydrogen economy is based on hydrogen use as fuel and energy carrier medium. In industry, the use of hydrogen is mostly as a reactant, for ammonia production, methanol production, and petroleum processing. In the electronics industry, hydrogen is used for silicon tetrachloride reduction to silicon, which is needed for semiconductor processing. In the metallurgical industry, hydrogen is used to remove oxygen in annealing, sintering, and furnace brazing. In nuclear power reactors, water dissociates under neutron flux, and hydrogen is used to scavenge the oxygen and impede the possible corrosion that it can produce. The aerospace industry makes significant use of hydrogen as fuel; liquid hydrogen and liquid oxygen propel most rockets. Very promising applications of hydrogen are the fuel cells that can produce clean electricity, without greenhouse gas (GHG) emission at the utilization side. Moreover, hydrogen is proposed as a fuel for internal combustion engines for improved efficiency and to lower the emissions.

Forty million tons of hydrogen are produced worldwide per year for refinery and industrial uses. In Canada, a country highly engaged in hydrogen economy development, hydrogen is utilized in large quantities as a feedstock for various chemical processes in industries and refineries. According to the Canadian Hydrogen Association (CHA), Canada produces more than 3 Mton of hydrogen per annum (CHA 2010). In the past, hydrogen was used in Canada for four main purposes: oil refining, ammonia production, methanol production, and process gas in the metallurgical sector. Presently, there is significant use of hydrogen in Canada for upgrading heavy oil from the oil sand sites of Alberta. Based on statistical data compiled by Taylor (1983) and the CHA (2010), the present, past, and predicted future hydrogen utilization in Canada is shown in Fig. 13.46. In the past, the oil refining sector and ammonia production accounted for 40% of Canadian hydrogen utilization. At present, it is observed that the sectors of oil refining and heavy oil upgrading increased their share of utilization to 46%. It is predicted that by 2025 their share will reach 62%.

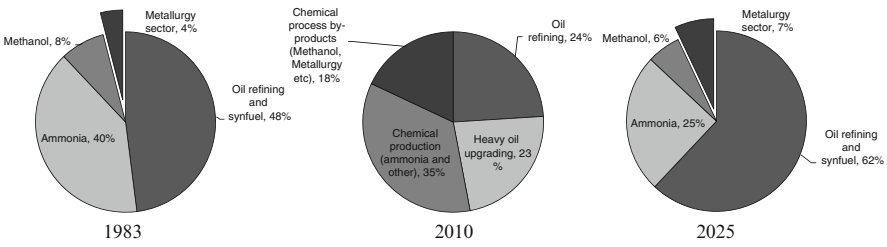


**Fig. 13.46** Evolution of hydrogen utilization in Canada [data from Taylor (1983) and CHA (2010)]

Hydrogen utilization for ammonia production decreased in Canada by 5% in 20 years, and it is predicted to decrease by another 10% in the next 15 years. It appears that by 2025 methanol production will consume 6% of produced hydrogen, while 7% of hydrogen will be used in metallurgy.

## 13.8 Fuel Cells

A fuel cell is a device that conducts the electrochemical reaction between hydrogen and oxygen to produce water and generate electricity. Fuels other than hydrogen can also be used in some special configurations. The primary application of such devices is in sustainable power generation. The basic structure of a fuel cell is represented in Fig. 13.47. It comprises an electrolytic bath and two electrodes. Fuel cells were developed starting in 1838–1839 with phosphoric acid as the electrolyte, and continued in the second half of the nineteenth century. In the twentieth century, various research programs led by the National Aeronautics and Space Administration (NASA) and other spatial agencies further developed fuel cells. Several kinds of fuel cells are available today with both liquid and solid electrolytes.

Hydrogen is fed at the anode of the fuel cell, where it enters in contact with a porous media electrode that is permeable to protons and has a positive charge. Because of the positive charge of the electrode, the valence electrons of the hydrogen molecule are dislocated, and thus the molecule breaks apart, forming two protons, according to the following anodic reaction:

$$H_2(g) \rightarrow 2H^+(aq) + 2e^-. \tag{13.50}$$

The electrode is continuously depleted from electrons by an external circuit that establishes a current of electrons through the electrical load. Since the electrons flow from the anode to the cathode as shown in Fig. 13.47, for the exterior circuit the anode

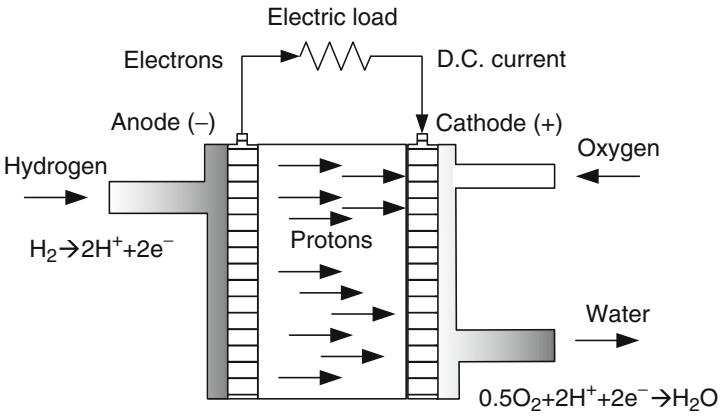


**Fig. 13.47** Schematic illustration of the basic fuel cell principle

appears to be the negative electrode, and the cathode is the positive one. The protons that traverse the porous anode are submerged in an electrolytic solution subjected to a coulomb electric field that drives them from the anode to the cathode. The protons permeate through the cathode, which being at a positive charge allows for the more complex reaction of water formation. During this process, the oxygen molecule that is fed through the oxidant stream at the cathode side (see Fig. 13.47) receives additional electrons that interfere with its valence electrons; consequently, the oxygen molecule is split apart and each of the resulting ions becomes able to react with two protons and form two water molecules; the cathodic reaction can be written as follows:

$$2H^{+}(aq) + 0.5O_2 + 2e^{-} \rightarrow H_2O. \tag{13.51}$$

The above reaction generates energy in the form of heat and electricity. Both these forms of energy are very important commodities for humankind. Conducting the water formation reaction in a fuel cell presents some advantages with respect to direct combustion, namely:

- One can cogenerate electricity and heat more easily.
- The temperature level of the cogenerated heat can be adjusted to correspond to the fuel cell and the application.
- The reaction products are much cleaner than in the case of combustion (no or extremely little $NO_x$ is formed).
- The process is flameless and in general considered safer than combustion.

Several kinds of fuel cell have been developed, from which at least two—proton exchange membrane and SOFCs—have achieved technological maturity. Most of the commercially available fuel cells operate with hydrogen as the fuel. However, due to the fact that the hydrogen's density is extremely low, the fuel cell vehicle technology faces a difficult technical problem, namely, to accommodate a large fuel tank while keeping enough free/useful space onboard. As a consequence, fuel cell vehicle makers are struggled to reduce the size of the fuel cell system while maximizing its power generation capacity. As already mentioned above, it is also possible to use fuels other than hydrogen. This can be done either through specialized fuel cells, or by reforming, directly or indirectly, various fuels to hydrogen.

## 13.9 Fuel Cell Types and Classification

The main types of fuel cells are classified as in Fig. 13.48, and they comprise three main categories based on the level of the operating temperature: low-, intermediate-, and high-temperature fuel cells. The chemical reactions and electrolyte type are explained for each type of fuel cell in Fig. 13.48. Another way to categorize the fuel cell is by the nature of ions that transverse the electrolyte. There are two possibilities: either protons ($H^{+}$) or oxygen ions ($O^{2-}$) migrate from one electrode to the other. If protons migrate, then the water formation reaction occurs

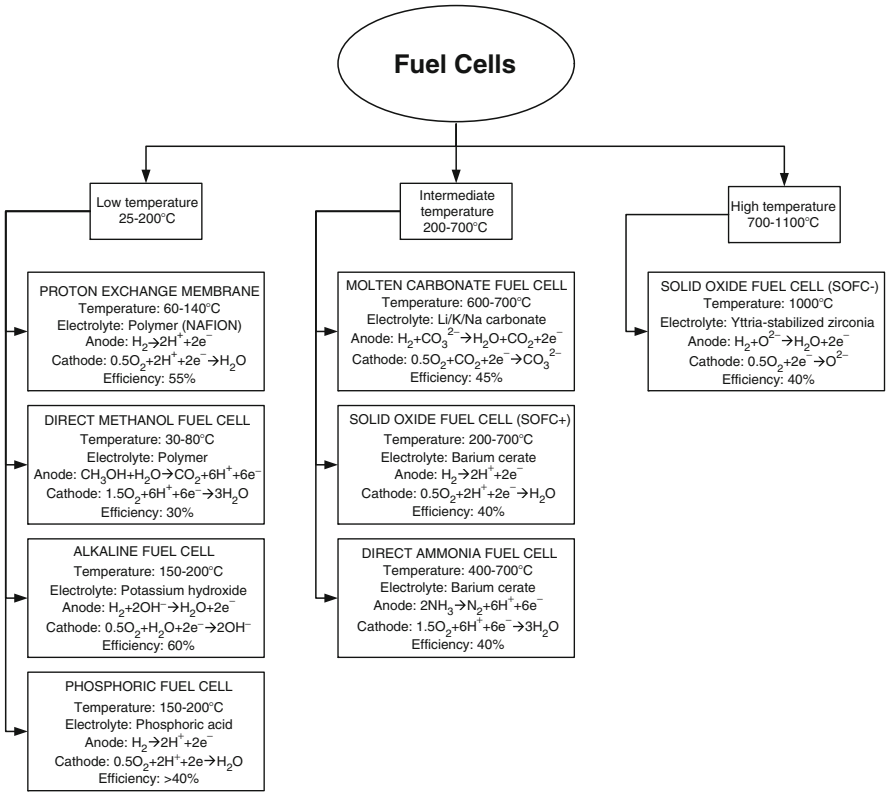


**Fig. 13.48** Classification of fuel cells according to their operating temperature

at the cathode side. Conversely, if the oxygen ions transverse the electrolyte solution, this implies that the water molecule forms at the anode. Looking at the fuel cell types in Fig. 13.48, we see that PEM, direct methanol, and SOFC+ systems have proton conducting electrolytes; also, alkaline, molten carbonate, and SOFC− systems have oxygen ions permeating electrolytes.

The photon exchange membrane (PEM) fuel cell is the most frequently used low-capacity and vehicular power generation system. It has a solid polymer membrane electrolyte from a material known as NAFION. A PEM-based system includes several auxiliary pieces of equipment: an air compressor, heat exchangers, and a rather large and complicated water management subsystem. Note that the NAFION membrane must be continuously humidified with water in order to keep its proton conducting property. Even though PEM systems have a relatively compact stack, they are rather voluminous, and on top of this, their cost is high because they include expensive metal catalysts (platinum) at the electrodes, and their lifetime is relatively short.

Solid-oxide fuels cells (SOFCs) with oxygen ions conducting electrolytes (denoted SOFC− or SOFC-$O^{2-}$) are characterized by stacks of relatively large

size and operate at a very high temperature. Their electrolyte is a solid layer of Yttria-Stabilized Zirconia (YSZ). They may feature a less voluminous and more cost-effective overall system than PEM systems. This fact is due to their high operating temperature, which leads to some important advantages: (a) they are inexpensive and have a long lifetime because no noble metal catalysts are needed for the electrodes, (b) internal reforming of alternative fuels (e.g., methane, syngas, methanol, ammonia) to hydrogen is facilitated so that SOFCs can use a smaller fuel tank, (c) the exhaust gases possess high exergy that can be converted into additional power and low-temperature heating.

One major drawback of SOFC− systems that probably impededs their expansion on low capacity and vehicular applications is represented by their rather long start-up time. It has been suggested that this drawback can be solved by using an SOFC-PEM combination. During start-up, the electricity of an SOFC-PEM system is generated only by the PEM, which has a reasonably short start-up time. At steady operation, when both cells operate, the heat generated by the SOFC is used for reforming the fuel to be delivered downstream to the PEM.

However, as has already been demonstrated, the design of such a system entails a large number of auxiliary components and thus is rather costly, has a short lifetime, and requires a voluminous amount of solution with respect to the generated power. As mentioned above, in SOFC−systems the oxygen ions ($O^{2-}$) traverse the electrolyte from cathode to anode, where they react with the supplied hydrogen to produce steam and release the reaction heat. During this process, at the anode, the hydrogen is consumed and the steam is generated, and thus the hydrogen's partial pressure decreases.

As a consequence of the low partial pressure of hydrogen, the reaction kinetics are degraded and the only solution to compensate for this effect is to supply hydrogen in excess. The excess hydrogen then must be consumed. This can be done in multiple ways. One common method is to combust the excess hydrogen in an afterburner, and the released heat is recovered or converted into work by a gas turbine. Thus, certain amounts of $NO_x$ are formed during the combustion of hydrogen with air.

Recent advances in SOFC technology have led to the development of intermediate-temperature proton-conducting membranes. These are electrolytic membranes based on oxides of a metal such as barium. Therefore, these fuel cells are solid oxide. The proton-conducting solid oxide membranes have the important advantage of letting the protons migrate from anode to cathode. As a consequence, the water formation reaction occurs at the cathode. This type of fuel cell is known as a proton-conducting SOFC, commonly denoted as SOFC+ (or SOFC-$H^+$) to distinguish it from the traditional ion-conducting SOFC.

Complete hydrogen utilization is therefore possible (in principle) in SOFC+ systems with direct implication in increasing the system's simplicity and compactness by eliminating the need for the afterburner. Moreover, because all the hydrogen is reacted electrochemically at the fuel cell cathode, practically no $NO_x$ is formed, and thus the fuel cell emission consists only of steam and nitrogen; thus, it is clean. The SOFC-$H^+$ technology has the potential to replace or complement PEM-FC systems in vehicular applications because it will be inexpensive and

compact, with high power generated per unit of volume, and it may operate at intermediate temperature (e.g., even 300°C), a fact that makes it possible to achieve an acceptable start-up time.

At present, certain efforts are being devoted worldwide to developing proton-conducting membranes. In this respect, barium cerate ($BaCeO_3$)-based materials are identified as excellent solid oxide electrolytes because of their high proton-conducting capability over a wide range of temperatures (300–1,000°C). By letting the protons diffuse through the electrolyte and letting the water-formation reaction occur at the cathode, the electromotive force and conversion efficiency of the fuel cell is significantly increased with respect to the SOFC system.

It is speculated that the governing mechanism of proton conduction is based on the hopping of protons between adjacent oxygen ions that are bound to the atomic structure of the solid oxide electrolytic membrane. The protons, being extremely small, necessitate reduced activation energy as compared to the case of oxygen ion transport through the most advanced SOFC—membranes such as those based on YSZ or doped ceria systems.

Moreover, the electronic conduction of barium cerate materials is much lower than that of doped ceria under operating conditions, and this explains the superior electromotive force, power output, and efficiency obtained with the SOFC+ systems. It also has been shown that proton conduction is enhanced at lower temperatures, such as 300°C. The main problem with barium cerate is the difficulty to sinter it in the form of a solid membrane. One option appears to be doping the barium cerate with samarium (Sm), which allows for sintering thin membranes with a thickness as low as 50 μm and high-power densities in the range of 1,300 to 3,400 $W/m^2$.

Phosphoric acid fuel cells uses platinum-coated porous carbon electrodes and a phosphoric acid electrolyte in the liquid state and kept in a silicon-carbide matrix. The efficiency of this kind of fuel cell is around 40%. The level of temperature required to produce steam is high, and so the fuel cell can be used for cogeneration purposes. As compared with PEM-FC, the phosphoric acid fuel cell is more voluminous for the same generated power.

The alkaline fuel cell potentially can reach an efficiency close to 70%. The electrolyte is an aqueous alkaline solution of potassium hydroxide (KOH) that is embedded in a porous matrix. If air is supplied as the oxidant, the small concentration of carbon dioxide in the intake air is large enough to convert some of the electrolyte (KOH) to potassium carbonate ($K_2CO_3$). In order to lengthen the electrolyte life, air is purified from $CO_2$ with various techniques such as scrubbers or other techniques of carbon dioxide removal (see Chapter 14). In some designs, the liquid electrolyte is replaceable so that after a period of operation, when the fuel cell is gradually poisoned, it can be renewed.

Molten carbonate fuel cells (MCFCs) operate at the upper limit of the intermediate temperature defined in Fig. 14.48 for fuel cells (around 650°C), and it can use fuels other than hydrogen. The fuels are reformed internally to hydrogen using

the high-temperature heat ejected by the cell. The reformation process occurs at the anode. These cells are very efficient, reaching a fuel-to-electricity energy efficiency of around 60%. The MCFCs can be coupled with other thermodynamic cycles that can convert the high enthalpy of steam and nonreacted fuel and carbon dioxide to additional power. Moreover, the MCFCs can be used in cogeneration systems, in which the fuel utilization efficiency can go over 85%. The electrodes do not need to be coated with expensive catalysts; simple carbon-based, inexpensive electrodes operate very well at the high temperature specific to these cells. The electrolyte is a carbonate (e.g., of lithium or potassium) that is suspended in an alumina-based porous matrix. The durability of the fuel cell is low because the electrolyte is highly corrosive.

The direct methanol fuel cell is a low-temperature, proton-conducting, polymer-based membrane fuel cell that is fueled directly with methanol diluted in water at its anode. The methanol is supplied in a proportion of 1:1 molar for the stoichiometric reaction. Direct methanol fuel cells are used for supplying low-power electronics since they are compact and store energy at high density; however, the rate of energy discharge (that is, the power density) is rather low.

Direct ammonia fuel cells have been recently developed as a variant of SOFC+ using ammonia as the fuel, as reviewed in Zamfirescu and Dincer (2009b,c). The high operating temperature of SOFC+ allows for ammonia decomposition at the anode, releasing hydrogen. The protons are formed at the anode and migrate through the solid electrolyte toward the cathode, where the water formation reaction occurs. The reaction products are nitrogen gas and steam. In general the hydrogen utilization is very high, as this characteristic is typical of SOFC+ systems. The energy efficiency of the duel cell stack may reach 55%.

Fuel cells can also be classified according to other criteria:

- Cell and stack design
  - Planar (flat-planar, radial-planar)
  - Tubular (microtubular, tubular)
  - Segmented-in-series (or integrated-planar)
  - Monolithic design
- Type of support
  - Self-supporting (anode-supported, cathode-supported, electrolyte-supported)
  - External-supporting (interconnect-supported, porous substrate supported)
- Flow configuration
  - Co-flow
  - Cross-flow
  - Counter-flow
- Fuel reforming type
  - External reforming
  - Direct internal reforming
  - Indirect internal reforming

## 13.10 Fuel Cell Systems and Applications

Fuel cells have many applications, notably in stationary, mobile, automotive, backup, auxiliary, and portable power generation, transportation technologies, specialty vehicles, small and large distributed generation, district power and heating, various military and space applications, and systems for pure oxygen production. Fuel cell applications can be roughly classified into four categories: power generation; transportation; specialty applications (military, aerospace, medical); and multigeneration applications (Fig. 13.49). In multigeneration applications, the fuel cell system generates multiproducts like power, heating, oxygen, and water.

When used for any application, a fuel cell stack must operate within a more complex system that has the function of supplying fuel and oxidant at appropriate pressure and temperature, recovering heat and work internally (when possible), and expelling heat, water, and reaction products. In many cases, the fuel cell stack must be insulated and maintained at an optimum operating temperature. Also, the balance of the plant has the role of ensuring the start-up and shut-down operations and regulating the system to operate at partial load and full load. In what follows, we present some typical fuel cell systems, including the fuel cell stack and the balance of the plant.

A typical PEM fuel cell power plant (including the fuel cell stack and the balance of the plant) is presented in Fig. 13.50. The diagram comprises a hydrogen tank,

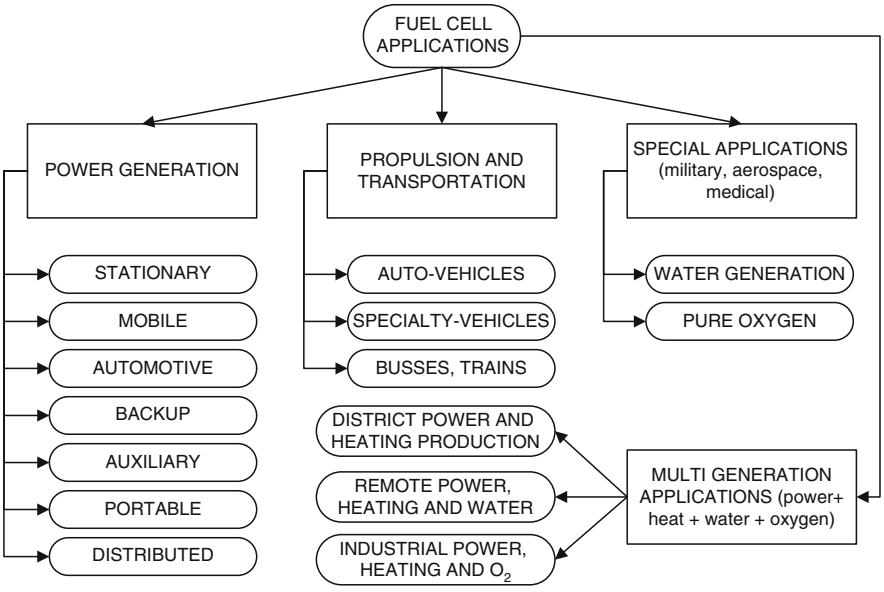


**Fig. 13.49** Classification of fuel cell applications

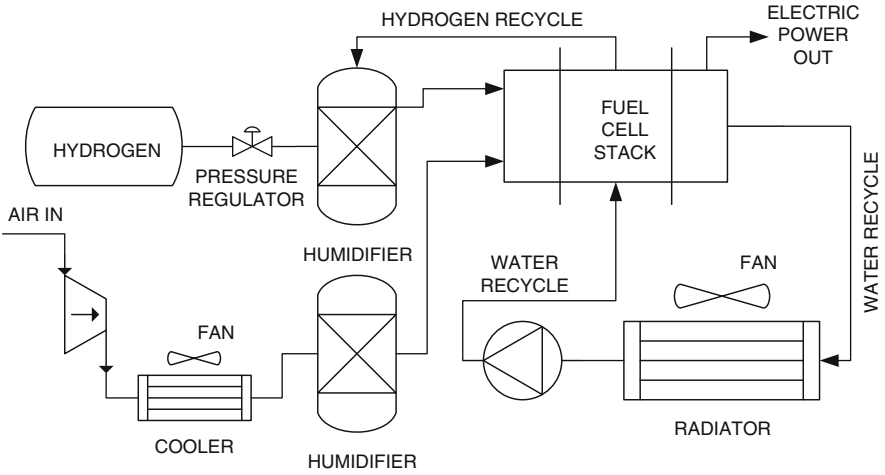


**Fig. 13.50** Simplified diagram of a PEM fuel cell power plant

pressure regulator, humidifiers, fuel cell stack, radiator, cooler, air compressor, and water recycle pump.

Both the hydrogen gas and oxygen gas must be humidified before entering the fuel cell stack because the NAFION membrane works only under humid conditions. The system normally operates at temperatures under 100°C and pressures slightly above the atmosphere. In these conditions, the formed water is in a liquid state. The system continuously generates water when it runs. A part of the water is maintained in the system for hydration purpose. The other part can be expelled (e.g., by spraying it out) or stored. However, storing water may raise problems when the system is applied to an auto-vehicle. The most important feature of the PEM-FC power plant is its fast start-up. Some electric power must be stored in a common accumulator battery as is needed for running the air compressor and the pump at start-up.

Figure 13.51 shows an SOFC+-based system for power generation, which comprises the SOFC+ stack, a turbocharger, four compact heat exchangers, a hydrogen fuel tank, and a pressure regulating device. Hydrogen is provided at state point 11 of the diagram. After the pressure regulator, the hydrogen supplies the power generation system at point 12, and then is preheated in two steps through points 12–13 and 13–14.

Air taken from the surroundings at point 1 is compressed in the turbocharger, delivered to the air-preheater at point 2, and then to the fuel cell stack at point 3. The exhaust of the fuel cell, consisting of oxygen-depleted air and steam, is directed toward the turbine inlet at point 4 and expanded with work recovery up to state point 5. The hot exhaust at point 5 is used to preheat the two reactants: air (point 7–8) and hydrogen (points 6–8 and 8–9), and then either released to the ambient air or used for heat recovery in an additional heat exchanger (point 9–10).

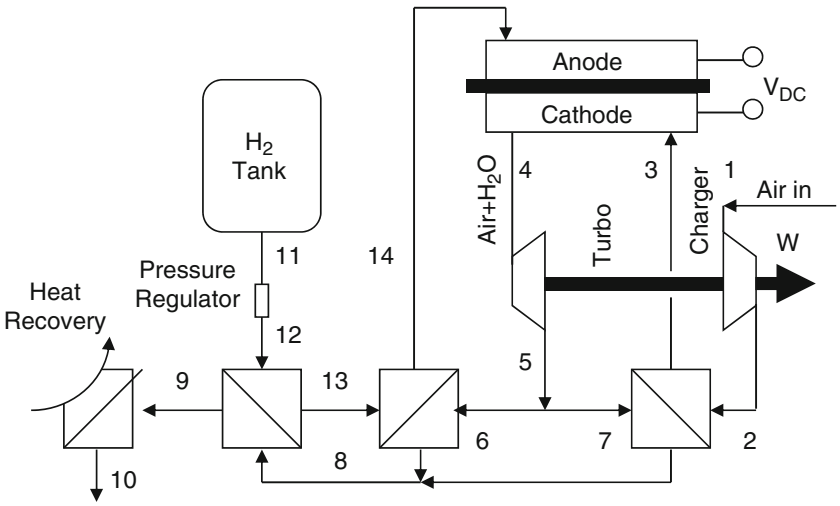


**Fig. 13.51** Fuel cell power plant based on proton conducting SOFC+ technology [modified from Zamfirescu and Dincer (2009c)]

The conceptual design is made so that the two reacting streams, prior to being supplied to the fuel cell stack, are preheated to the same temperature in an equal number of two steps. In fact, the air temperature at point 2 is the same as the hydrogen temperature at point 13, and the air temperature at point 3 is the same as the hydrogen temperature at point 14.

Fuel cells that operate at a higher temperature—like molten carbonate and SOFCs—in general must be coupled with gas turbines in order to achieve satisfactory fuel utilization. Moreover, high-temperature heat is commonly recovered from the reaction product of these kinds of fuel cells and used for reforming of some high-density fuels such as compressed natural gas, alcohols, and others, to hydrogen. An example is given in Fig. 13.52, consisting of an MCFC with reformed natural gas. This is a simplified diagram of a system installed recently by the natural gas provider Embridge Inc. in Toronto, Ontario. The system is connected to the high-pressure natural gas network at point 1.

The high-pressure gas is first preheated (point 1–2) and then expanded to generate about 1 MW electric power from a 6,000 $m^3$/h gas flow rate. After expansion, a part of the low-pressure gas is sent to the distribution network to be used for water/space heating in residences. The other part (point 5) is mixed with water (point 6), preheated (point 7–8) and reformed (point 8–9) and supplied to the MCFC (point 10). The resulting uncombusted anodic gases are further combusted with additional air (point 16) in a catalytic burner (point 11–12) that delivers its produced heat to the reformation process. The $CO_2$-rich combustion gases (point 12) are mixed with air (point 15) and fueled to the MCFC cathode (point 17). The heat carried by the cathode gas is recovered (point 18–19) and used to preheat the high-pressure fuel. Fresh ambient air is used for combustion and fuel cell

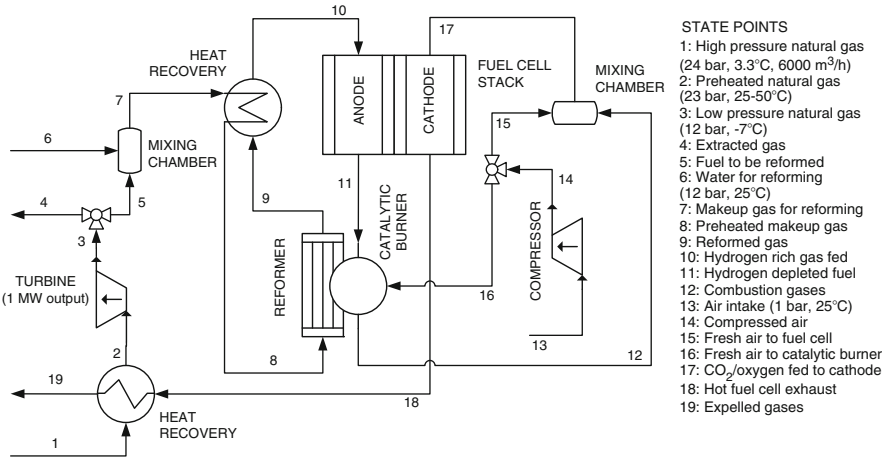


**Fig. 13.52** Natural gas fueled system with molten carbonate fuel cell

processing as it is compressed first (point 13–14) and then split (point 15+16). The energy $(\eta)$ and exergy $(\psi)$ efficiencies of this system, as calculated by Rashidi et al. (2009), are 60% and 50%, respectively. The efficiencies are defined as:

$$\left.\begin{aligned}\eta &= \frac{W_{\mathrm{FC}} + W_{\mathrm{T}} - W_{\mathrm{C}}}{\mathrm{LHV}} \\ \psi &= \frac{W_{\mathrm{FC}} + W_{\mathrm{T}} - W_{\mathrm{C}}}{ex_1^{\mathrm{ch}} + ex_1^{\mathrm{thm}} + n_6 ex_6^{\mathrm{thm}}}\end{aligned}\right\}, \tag{13.52}$$

where $W$ represent the work per mol of fuel consumed, indices FC, T, and C mean fuel cell, turbine and compressor, respectively, indices 1 and 6 represent the respective state points indicated in Fig. 13.52, $ex$ is molar exergy, the exponents "ch" and "thm" mean chemical and thermomechanical, respectively, and $n_6$ is the number of mols of water mixed with 1 mol of fuel.

The SOFC systems have the great advantage of operating at very high temperature, which facilitates steam-assisted reforming of the primary fuel to hydrogen, without the need for expensive catalysts. It was explained above that owing to hydrogen consumption in the anode, its partial pressure decreases, which affects negatively the chemical equilibrium and reaction rate. Thus, hydrogen is fed in excess and is only partially consumed in the fuel cell. One method to improve fuel utilization in the fuel cell is by recycling the product gases as illustrated in Fig. 13.53. Recirculation from ${n_1}^{\mathrm{CH_4}}$ mols of fuel fed results in $(\zeta - 1)$ $({n_2}^{\mathrm{CH_4}} + n^{\mathrm{CO}} + n^{\mathrm{H_2}})$ mol of unused fuel, where $\zeta {n_2}^{\mathrm{CH_4}} < {n_1}^{\mathrm{CH_4}}$.

If product gas recirculation is not applied, then the quantity of noncombustible gases for the system producing the same electric output would be higher $\zeta({n_2}^{\mathrm{CH_4}} + n^{\mathrm{CO}} + n^{\mathrm{H_2}})$. The system with recirculation still requires an additional

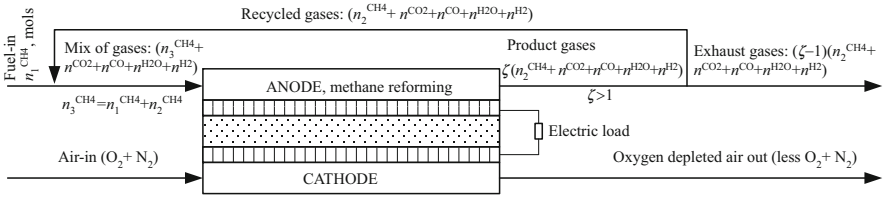


**Fig. 13.53** Product gas recycling in a SOFC system for steam reforming and better fuel utilization

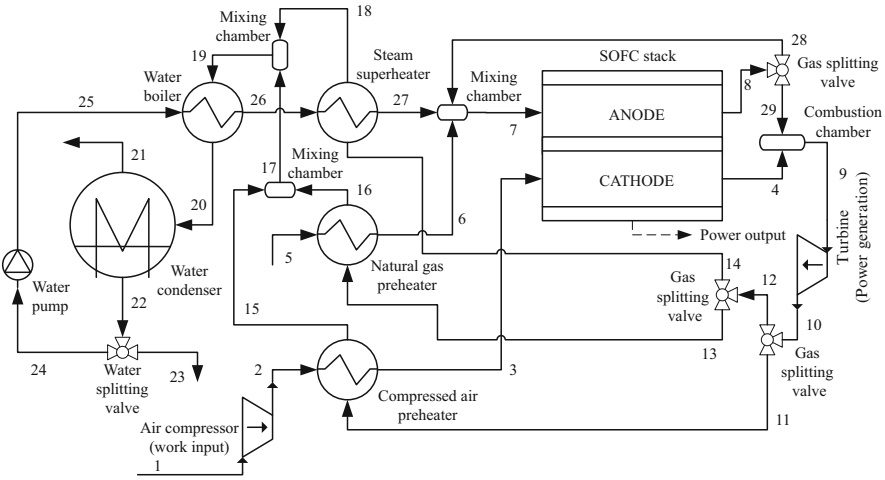


**Fig. 13.54** SOFC/gas turbine power generator with natural gas fuel

afterburner or other system to consume the remaining fuel, but it is a fact that the fuel utilization within the fuel cell is better. Another factor is that steam is needed for reforming the primary hydrocarbon fuel (in the above example, the methane). Through recirculation of product gases, steam is provided to the fuel feed side. Depending on the operating parameter, it is possible that this steam is sufficient for obtaining enough fuel reformation. However, in many practical situations, the steam provided by product gas recirculation is not sufficient. Additional steam then can be provided through water condensation from exhaust gases, followed by water reheating and steam generation. A complete diagram of an SOFC system is presented in Fig. 13.54.

The system use natural gas from municipal distribution lines (assumed at 6–8 bar) which is reformed with steam recovered from the product gas. Air from the ambient is aspired by the air compressor at point 1 and discharged at high pressure at point 2 with further preheating (point 2–3); preheated air is fed in fuel cell at point 3. The oxygen-depleted air is discharged at the cathode side at point 4. Natural gas enters at point 5 and is preheated (point 5–6) and mixed with

superheated steam recycled from the fuel cell stack (point 28) and extracted from the exhaust gases (point 27). The make-up gas consisting of natural gas, steam, uncombusted gases (hydrogen, methane, carbon monoxide) enters at the fuel cell anode at point 7. The product gas exhaust at the anode at point 8 is split into two streams: stream 28 (recycled) and stream 29 directed toward the combustion chamber, where it combusts with oxygen-depleted air from the cathode (point 4), producing hot exhaust gas at point 9.

The exhaust gas at high temperature and pressure at point 9 is expanded with work generation in the gas turbine and retrieved downstream at point 10, where it is split in three streams that are to be used for heat recovery (streams 11, 13, and 14). The enthalpy of these gases is used for preheating air, preheating natural gas, and superheating steam. After this, all three streams are mixed at point 19 and their enthalpy is used for steam generation from recovered water in the water boiler. Colder exhaust gases at point 20 (assumed completely combusted) are further cooled in the water condenser, which condensates water while releasing the non-condensable gases at point 21. The resulting water is partially drained (point 23) (or used for other purposes), and partially recycled at point 24. The recycled water is first pressurized (point 24–25), and then boiled (point 25–26), and the resulting steam is superheated (point 26–27).

Note the essential difference with the MCFC system presented in Fig. 13.52, where the natural gas reforming is done indirectly (outside of the fuel cell stack) because of the lower temperature of the process heat. In that case, more water is needed for the process, and this water is provided from exterior sources. In the SOFC system all water needed by the system is separated from the combustion gases and recycled within the system; there is no need for additional water supply. Consequently, the exergy efficiency of the SOFC system has the potential to be higher than in the MCFC system. The energy and exergy efficiencies can be defined for the SOFC system as follows:

$$\left.\begin{aligned} \eta &= \frac{W_{\mathrm{FC}} + W_{\mathrm{T}} - W_{\mathrm{C}} - \mathrm{W_P}}{\mathrm{LHV}} \\ \psi &= \frac{W_{\mathrm{FC}} + W_{\mathrm{T}} - W_{\mathrm{C}} - W_{\mathrm{P}}}{ex_{\mathrm{NG}}^{\mathrm{ch}} + ex_{\mathrm{NG}}^{\mathrm{thrm}}} \end{aligned}\right\}, \tag{13.53}$$

where the generated work $W$ is given per molar unit of natural gas consumption, indices FC, T, C, P, and NG represent fuel cell, turbine, compressor, pump, and compressed natural gas, respectively, and $ex$ is the molar chemical exergy, and the exponents "ch" and "thrm" mean chemical and thermomechanical, respectively. Granovskii et al. (2008b) calculated the energy and exergy efficiency of an SOFC system like that presented in Fig. 13.57 and showed that depending on the operating condition they can achieve 73% to 85% (energy-based) and 72% to 85% (exergy-based).

## 13.11 Integrated Fuel Cell Systems

Fuel cell systems can be integrated with other cycles, as discussed above, to obtain better fuel utilization efficiency. This is especially the case for fuel cells with oxygen ion-conducting electrolytes, where water is formed at the anode and reduces hydrogen concentration. PEM fuel cell systems do not suffer from this operating deficiency, and, therefore, they can obtain excellent fuel efficiency by themselves; there is no need for a downstream afterburner or other fuel-consuming system.

The need for integration of fuel cell systems with other systems stems from other reasons in addition to that of achieving better fuel utilization. These reasons can be, for example, using fuel other than hydrogen and applying direct and indirect reforming, whichever is the case, or applying heat recovery for cogeneration of power and heat or for driving a bottoming cycle for additional power generation. In addition, fuel cells can be integrated in systems with purposes other than power generation. An example is an oxygen production system as shown in Fig. 13.55. This system combines a fuel cell system with a water/steam electrolyzer system. In this approach, a high-efficiency SOFC power plant is used to drive steam electrolysis. The SOFC system exhaust contains steam at very high temperature along with other combustion products (mainly nitrogen and carbon dioxide). A steam recovery unit cools the exhaust gases, condensates steam, separates water, boils it, and superheats the steam using heat recovery from the gases extensively.

Noncondensable gases are expelled at colder temperature. Thus, high-temperature steam, carrying high enthalpy, is fed into a solid oxide electrolyzer that operates around its thermal neutral point. Consequently, the electrolysis process needs less electricity per mol of water split. The electricity is supplied by the SOFC generator. The hydrogen produced by electrolysis is fed back to the SOFC system in combination with methane. The system is highly effective and can generate hydrogen at a pressure higher than the ambient—at 2 to 6 bar. Having pressurized hydrogen as the output, any further compression as oxygen must be stored at 200 bar or more.

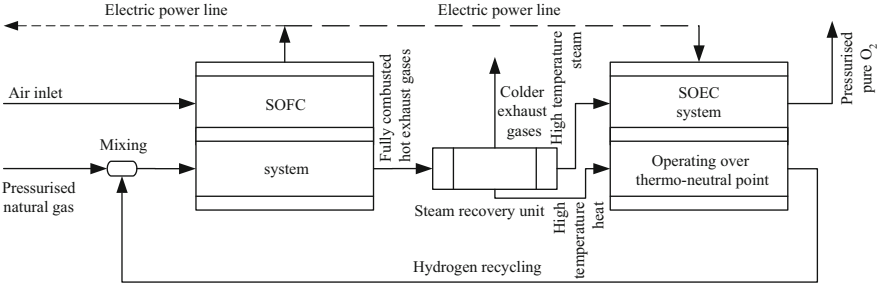


**Fig. 13.55** Integrated system with SOFC and SOEC for pure pressurized oxygen production

**Illustrative Example: An SOEC System**

Let's assume that for the oxygen-producing system above, the energy efficiency of the SOFC is 90% and that of the electrolyzer subsystem, operating above its thermal neutral point, is 95%. We need to calculate the natural gas energy (with respect to LHV) to generate 1 mol of oxygen assuming that the system operates at 1 bar pressure.

The calculation can be made backward from the output to the input. To generate 1 mol of oxygen, we need 2 mol of water and we generate 2 mol of hydrogen. The total energy needed to operate the SOFC at, say, 800°C is simply calculated with EES software assuming that 2 mol of steam is fed at 950°C: $\Delta H = 2h_{H_2O}|_{950°C} - (2h_{H_2} + h_{O_2})|_{800°C} = -483.6\,\text{kJ/mol}$ of oxygen. The associated entropy change is calculated similarly, but, in addition, we assume complete conversion, that is in the inlet stream the steam concentration is 1 as well as in the outlet streams—since the products are not mixed, the hydrogen as well as the oxygen concentration is also 1; thus, we obtain $\Delta S = -100.1\,\text{J}$ and $\Delta G = \Delta H + (800 + 273.15)\Delta S = 591\,\text{kJ}$, both per mol of oxygen produced. Accounting for the SOEC efficiency, the electrical energy needed to drive the electrolysis is $E = -\Delta G/0.95 = 591/0.95 = 622.1\,\text{kJ/mol}\,O_2$. The thermal energy is $Q = -(800 + 273.15)\Delta S/0.95 = 113\,\text{kJ/mol}\,O_2$. The 2 mol of steam deliver to the electrochemical reaction a quantity of heat $Q_1 = 2c_p(950 - 800) = 4.4\,\text{kJ}$ while the rest of $Q_2 = Q - Q_1 = 108.6\,\text{kJ}$ is provided by the heat recovery unit driven by the exhaust gases produced by the SOFC subsystem. It is fair to assume 10% losses in the heat recovery unit; therefore, the heat generated by the SOFC is $Q_g = Q/0.9 = 125.6\,\text{kJ}$. In order to generate the needed electricity, the SOFC must be supplied with 2.29 mol of hydrogen at 800°C and additionally 53.4 kJ of heat is generated per mol of hydrogen consumed. In order to generate 125.6 kJ of heat, the number of mols of supplied hydrogen becomes 4.7; the generated electricity is 1,150 kJ, from which only 622.1 kJ are used to generate 1 mol of oxygen while the rest, 527 kJ, is available as electricity. This calculation suggests that the oxygen-generation system may be used for cogeneration of electricity and oxygen. Note that 2 mol of hydrogen from the total of 4.7 are recycled internally; thus, the consumption of hydrogen is 2.7 mol, which comes from reforming 1.35 mol of methane.

Another integrated fuel cell system, this time operating at intermediate temperature with a SOFC+ device and gas turbine, is presented in Fig. 13.56. This system operates with ammonia and cogenerates refrigeration and electric power. The cooling effect is produced in the ammonia storage tank, which features a cooling coil (point 10) and is thermally insulated. When ammonia vapor is drawn out of the tank (point 1), it removes enthalpy. Some liquid thus evaporates and generates refrigeration.

At start-up, ammonia can be heated electrically through the heating element (point 2). At steady operation, heating is applied in steps (2–3) and (3–4) up to about 700°C, the temperature at which ammonia is fed into the fuel cell. There, ammonia is decomposed catalytically at the anode and hydrogen is consumed.

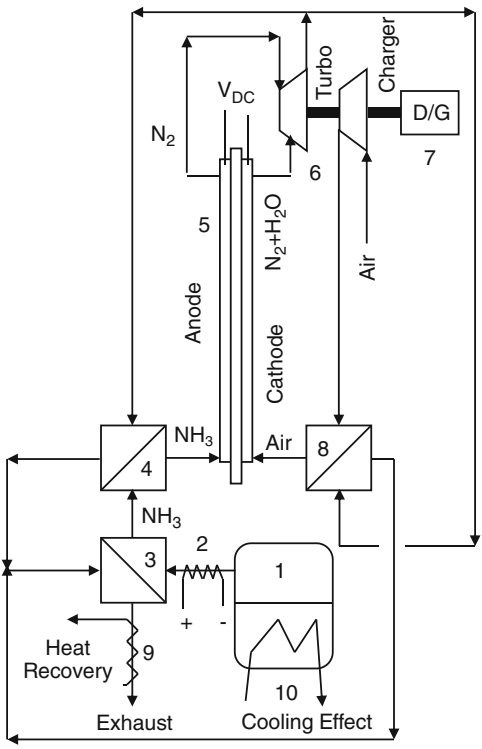


**Fig. 13.56** Integrated fuel cell system with SOFC+ and gas turbine for power and cooling. *D*/*G* drive generator; *VDC* direct current voltage

Steam is formed at the cathode and expanded at point 6 together with the resulting nitrogen to generate power for air compression. The element (point 7) is an electric drive-generator that during the start-up drives the air compressor, while during the steady operation of the system it generates some electricity. Heat recovery can be applied to the exhaust gases. The system emits only benign gases such as steam and nitrogen.

Alkaline fuel cells also need improved fuel utilization, which can be done in principle by recirculation of the exhaust gases. However, their operating temperature is ~200°C, which means a low enthalpy of the reaction products. Moreover, the electrodes of the alkaline fuel cells are sensitive to poisoning, especially if the pressure is increased. Consequently, it is not appropriate to recycle the products or to expand them in a gas turbine. An alternative is to couple alkaline fuel cell systems with an organic Rankine cycle operating at the bottoming side. Figure 13.57 illustrates the concept: the exhaust gases from the alkaline fuel cell are combusted externally at constant pressure, and the combustion heat from the exhaust gases is recovered through a heat exchanger. The heat is further transferred to a Rankine cycle, which generates additional power. Preferably, for low- to medium-capacity application, the Rankine cycle should run with an organic fluid.

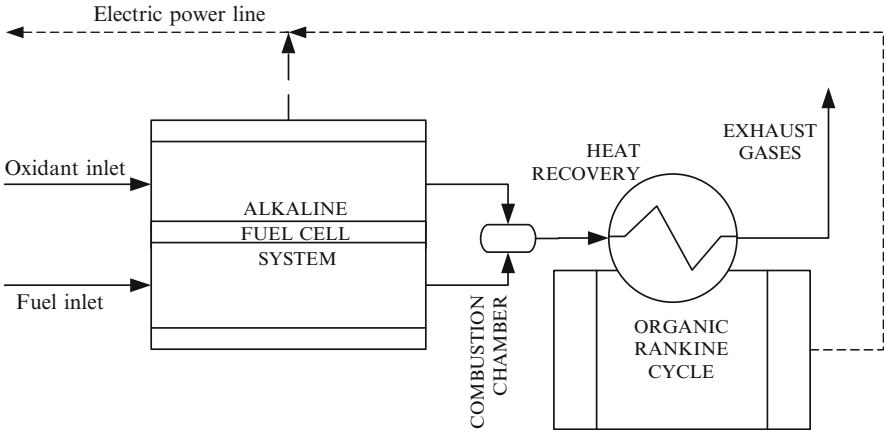


**Fig. 13.57** Alkaline fuel cell system with a bottoming Rankine cycle for better fuel utilization

## 13.12 Fuel Cells: Analysis and Modeling

There are a number of fundamental equations from electrochemistry that must be applied for any fuel cell modeling attempt. In addition, first law and second law analyses together with molar balances can be written for the fuel cell itself and for each subsystem. Reaction kinetics and chemical equilibrium are important factors in fuel cell modeling and analysis. Fluid mechanics and heat transfer problems occur when analyzing and designing fuel cell stacks. Optimization of geometry and of the operating parameters is required for the fuel cell stack and the overall system. In brief, the analysis and modeling of fuel cells and fuel cell systems are complex problems, but they are very important for the optimized design of such systems. In this section, we discuss various factors in fuel cell analysis and modeling.

### *13.12.1 Classification of Fuel Cell Models*

A classification of fuel cell models is presented in Fig. 13.58. It is difficult to classify models of fuel cells. In principle, one can categorize the model based on the modeling level, the number of spatial dimensions taken into consideration, the process time consideration, and the modeled processes taken into account. Modeling can be done at the cell level (which is the deepest analysis) and at the stack level (which accounts for flow distribution, channeling, flow collection, temperature distribution, spatial component concentration, etc.). Also, modeling can be done at the system level, where the fuel cell stack is integrated into a larger system. General thermodynamic analysis through conservation laws and specific equations must be applied at the system level.

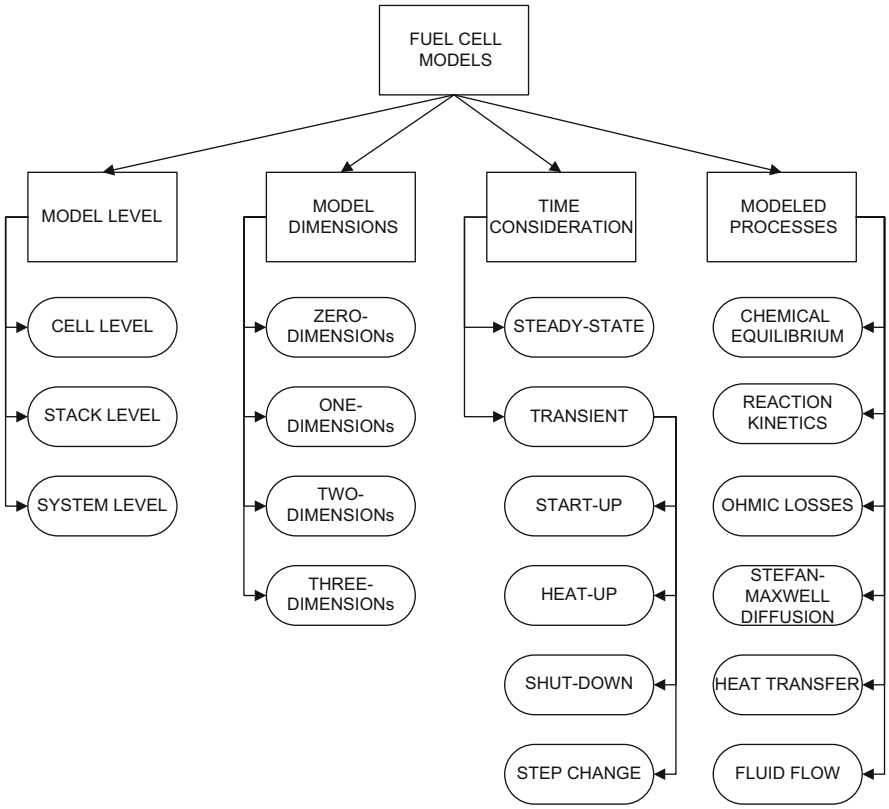


**Fig. 13.58** Classification of fuel cell models

The zero-dimension models consider the fuel cell as a black box, characterized by unique parameters such as temperature, generated voltage, current density, inlet and outlet flow rates, and concentrations. A one-dimensional approach can be applied to planar fuel cell or to tubular configurations with axial symmetry. Parameter variation is considered only in one relevant direction (that is across electrolyte) while the other directions are neglected. In two-dimensional modeling, one of the considered directions is across the electrolyte, and the other direction is parallel with the stream flow directions in the channel (which in general is the direction along which one observes relevant gradients of important quantities).

Models can be either steady state or transient. Most of the published models in the literature refer to steady-state operation because it affects the design. However, operation at start-up, heat-up, shut-down, and step-change events must be analyzed, too. Thus, transient models are applied for these situations.

Models can also be categorized by the function of the physical–chemical processes. In general, reaction heat must be taken into the account in modeling, as well as the Gibbs free energy and the entropy of the overall reaction. Moreover, chemical equilibrium should be included in the models. Other aspects to be studied

are reaction kinetics, electric charge distribution, ohmic losses of various kinds, diffusion of chemical species and of ionic species (Stefan-Maxwell-Knudsen), heat transfer, and fluid flow in channels.

Fuel cell models can also be classified as macro- and micromodels. In macromodels, porous media models are applied to electrodes, which are assumed to be electron-conducting media. The electrode/electrolyte interface is the place where electrochemical reactions occur. In micromodels, electrodes are considered porous structures made of electron-conducting and ion-conducting particles. The micromodels predict the electrochemical characteristics at the electrodes.

### *13.12.2 Fundamental Equations and Definitions*

A number of parameters and fundamental equations are very important for fuel cell modeling. These are reviewed in this section. The first equation introduced here is the Nernst equation. This equation was proposed by the German scientist Walther Nernst and can be understood if one reconsiders the Gibbs energy of water formation based on Eq. (13.4). The water formation reaction is $H_2 + 0.5O_2 \rightarrow H_2O$; we assume here all the reactants and the product in the gas phase. The total electric potential generated at the electrodes of the fuel cell comes from the Gibbs free energy of the reaction, and it is given by $\Delta H - T\Delta S = -nF\Delta E_{EL}$, where $n = 2$. Treating all chemicals as ideal gases, we find that the enthalpies do not depend on pressure $H(T,P) = H(T)$. Therefore, the reaction enthalpy can be calculated as if the reaction occurs at the reference pressure $P_0 = 1.01325$ bar. Note that $\Delta H = \Delta H^0(T)$. The reaction entropy is given as the difference between the molar entropy of the products and of the reactants $\Delta S = S_{\text{Products}} - S_{\text{Reactants}}$; thus, $\Delta S(T,P) = S_{H_2O}(T,P_{H_2O}) - S_{H_2}(T,P_{H_2}) - 0.5S_{O_2}(T,P_{O_2})$, where $P_{H_2O}$, $P_{H_2}$, and $P_{O_2}$ are the partial pressure of the species. Recall that the entropy variation of ideal gases in isothermal transformation is $S(P) - S(P_0) = -R\ln(P/P_0)$. Thus, $\Delta S(T,P) = S_{H_2O}(T,P) - S_{H_2}(T,P) - 0.5S_{O_2}(T,P) - R\left[\ln\left(\frac{P_{H_2O}}{P_0}\right) - \ln\left(\frac{P_{H_2}}{P_0}\right) - \ln\left(\frac{P_{O_2}}{P_0}\right)^{0.5}\right]$. Finally,

$$\Delta S = \Delta S^0(T) - R\ln\left(\frac{P_{H_2O}}{P_{H_2}P_{O_2}^{0.5}}P_0^{0.5}\right). \tag{13.54}$$

Thus, the maximum electric potential retrieved at the electrodes is

$$-nF\Delta E_{EL} = \Delta H^0(T) - T\Delta S^0(T) - RT\ln\left(\frac{P_{H_2O}}{P_{H_2}P_{O_2}^{0.5}}P_0^{0.5}\right). \tag{13.55}$$

Expression (13.55) can be rearranged as

$$\Delta E_{\mathrm{EL}} = -\frac{\Delta H^{\,0}(T) - T\Delta S^{\,0}(T)}{nF} - \left(\frac{RT}{nF}\right)\ln\left(\frac{P_{\mathrm{H_2O}}}{P_{\mathrm{H_2}} P_{\mathrm{O_2}}^{\,0.5}} P_{\,0}^{\,0.5}\right), \tag{13.56}$$

where the quantity $-[\Delta H^{\,0}(T) - T\Delta S^{\,0}(T)]/nF = \Delta E_{\mathrm{EL}}^{\,0}$ is the standard cell potential (also called reversible cell voltage) at the given temperature (and standard pressure).

This quantity is fixed. We observe that the maximum cell potential is obtained if the second term in Eq. (13.56) is nil. This is possible if the argument of the logarithm is 1; if $P_{\mathrm{H_2O}} = P_{\mathrm{H_2}}$ and $P_{\mathrm{O_2}} = P_0$, this fact is accomplished; however, this is not possible in practical implementations because of various losses. Therefore, always $\Delta E_{\mathrm{EL}} < \Delta E_{\mathrm{EL}}^{0}$. Several definitions follow:

- *Air utilization ratio*: the number of mols of oxygen utilization with respect to the quantity fed at the fuel cell inlet $U_{\mathrm{a}} = n_{\mathrm{O_2,utilized}}/n_{\mathrm{O_2,inlet}}$.
- *Fuel utilization ratio*: similar to air utilization, it is $U_{\mathrm{f}} = n_{\mathrm{H_2,utilized}}/n_{\mathrm{H_2inlet}}$.
- *Excess air coefficient*: amount of oxygen at the inlet vs. stoichiometric oxygen: $\lambda_{\mathrm{a}} = U_{\mathrm{f}}/U_{\mathrm{a}}$.
- *Electric current through fuel cell*: $I = n \times n_{\mathrm{H_2}} \times F$, where $n$ is the number of mols of electrons per reaction and $F = 96{,}485.3$ A/mol is the constant of Faraday.
- *Open circuit cell voltage*: $V_{\mathrm{oc}} = \Delta E_{\mathrm{EL}}^{\,0} - V_{\mathrm{ohm}} - V_{\mathrm{act}} - V_{\mathrm{conc}}$, where $V$ means voltage and the indices ohm, act, and conc represent ohmic, activation, and concentration losses. This voltage exists between electrodes if there is no load connected. The actual load voltage is $V < V_{\mathrm{oc}}$.
- *Electric power output of the cell*: $W = VI$, where $V$ is the actual voltage on the load.
- *Cell energy efficiency*: $\eta_{\mathrm{cell}} = W/(n_{\mathrm{H_2,inlet}} \times \mathrm{LHV})$.
- *Cell exergy efficiency*: $\psi_{\mathrm{cell}} = W/(n_{\mathrm{H_2,inlet}} \times ex^{\mathrm{ch}})$.
- *Current density:* the current per unit area of the electrolyte in the direction normal to ionic flow $i = I/A$.
- *Area-specific ohmic resistance*: the ohmic resistance of the electrolyte, and it has two different components: $\mathrm{ASR} = \mathrm{ASR_{contact}} + \mathrm{ASR_{bulk}}$, where $\mathrm{ASR_{contact}}$ represents the contact resistance per unit of area and $\mathrm{ASR_{bulk}}$ represents the summation of the resistivities of the materials traversed by ions and electrons (copper wires/leads, electrolyte, etc.), given as per unit of area of electrolyte.
- *Ohmic polarization*: $V_{\mathrm{ohm}} = \mathrm{ASR} \times i$, the total ohmic voltage losses.
- *Concentration polarization*: the partial pressure of the reactants decreases while they diffuse through the porous layers of the electrodes; this creates an additional voltage loss called the concentration polarization. The $V_{\mathrm{conc}}$ can be estimated with complicated empirical equations as reviewed in Colpan et al. (2008).
- *Activation polarization*: any reaction needs some energy to be activated; in the fuel cell case, the activation energy is transmitted to the ions electrically;

this is sensed as a loss of electric potential, according to the comments in Colpan et al. (2008):

$$V_{\text{act}} = \frac{RT}{F}\left[\sinh^{-1}\left(\frac{i}{2i_{\text{o,a}}}\right) + \sinh^{-1}\left(\frac{i}{2i_{\text{o,c}}}\right)\right], \tag{13.57}$$

where $i_{\text{o,a}}$ and $i_{\text{o,c}}$ are exchange current densities at the anode and cathode, respectively; these are the currents that exist at the electrode level even when the load is not connected; the cathode and anode exchange currents balance each other so that the total effect is nil, when the load is not connected.

In a detailed modeling of the fuel cell, the conservation laws take the form of partial differential equations. Since in fuel cells one works with several chemical species, the conservation equation of species becomes important; this equation is

$$\left[\frac{\partial C}{\partial t} + \nabla \cdot (\boldsymbol{u} \cdot C) = \nabla \cdot (D \nabla C) + \dot{S}\right]_k, \tag{13.58}$$

where $t$ is time, $C$ is the concentration, $\boldsymbol{u}$ is the velocity vector of the species $k$, and $\dot{S}$ is the source term that takes into account the rate of apparition or disparition of chemicals.

One important characteristic for the design and analysis of fuel cells is the voltage– current density curve, which Fig. 13.59 illustrates for a typical fuel cell. This kind of curve is determined from experimental measurements. Advanced modeling can roughly predict the curve. Once the curve is available, it is possible to use it for fuel cell optimization purpose. On the abscissa is the current density. If the current density is nil, that is, the circuit is open, then the voltage read at the fuel cell electrodes is the open circuit voltage $V_{\text{oc}}$. The diagram illustrates also the standard cell potential $\Delta E^{0}_{\text{EL}}$ and the $\Delta E_{\text{EL}}$.

At low current density, in the region indicated with "A," the voltage losses are dominated by the activation polarization effects. In the region where the cell voltage decreases quasi-linearly, indicated with "Ω," the ohmic polarization is the dominant effect. In the region "C," the concentration losses become dominant. The actual power density delivered by the fuel cell is obtained by $W = Vi$; therefore, it can be calculated from the $V - i$ diagram. It can be observed that at low current density (no load) the power tends to zero (because $i \to 0$); similarly, at high current density there is a limiting value over which the power tends to zero (because $V \to 0$). The polarization losses become very high in region C. For a current density higher than $i_{\text{Limiting}}$, the fuel cell cannot generate power anymore because of the dissipative effects that can be observed in the form of heat, $Q = -T\Delta S$, and increase dramatically at high current density (see the thermal power density curve in Fig. 13.59). At a certain current density, the power delivered by the fuel cell represents a maximum.

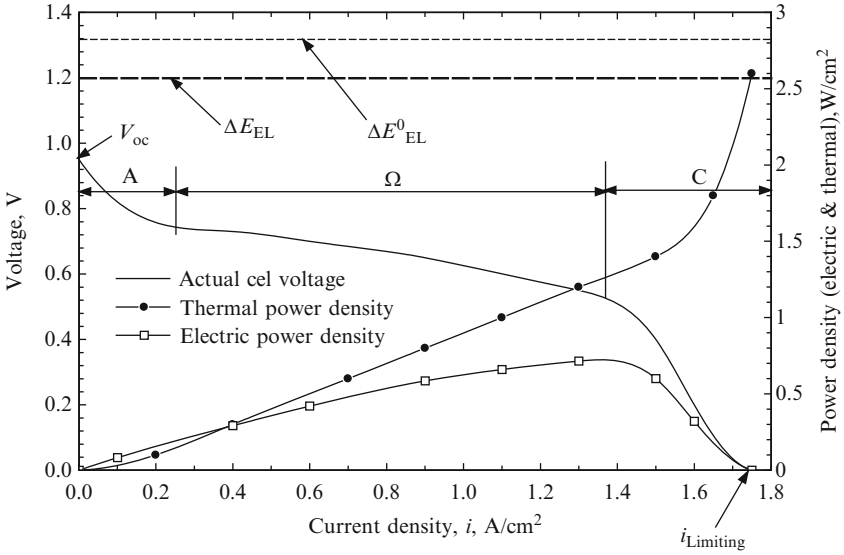


**Fig. 13.59** Voltage-current density curve of a typical fuel cell

**Table 13.18** Equations for fuel cell modeling

| Parameter | Equation |
|---|---|
| Stoichiometric oxygen consumption | $\dot{m}_{O_2 s} = 0.0000000829 i_{opt}$, kg/s |
| Number of moles of stoichiometric oxygen | $\dot{n}_{O_2 s} = \dot{m}_{O_2 s}/\mu_{O_2 s}$, kmol/s |
| Number of moles of stoichiometric air | $\dot{n}_{Air,s} = \dot{n}_{O_2 s}/c_{O_2}$, kmol/s |
| Mass flow rate of stoichiometric air | $\dot{m}_{Air,s} = \dot{n}_{Air,s}\mu_{Air}$, kg/s |
| Mass flow rate of air | $\dot{m}_{Air} = \dot{m}_{Air,s}\lambda$, kg/s |
| Water consumption | $\dot{m}_{H_2O} = 0.0000000934\, i_{opt}$, kg/s |
| Hydrogen consumption | $\dot{m}_{H_2} = 0.0000000105 \cdot i_{opt}$, kg/s |
| Molar flow rate of hydrogen | $\dot{n}_{H_2} = \dot{m}_{H_2}/2$, kmol/s |

Data from Zamfirescu and Dincer (2009c)

### *13.12.3 Case Study: Design Optimization of a Fuel Cell System*

We consider here the SOFC+ system introduced above in Fig. 13.51. The aim of this case study is to develop an optimal design of the system for maximum power generation per unit of cell volume and maximum efficiency. The study is based on the work of Zamfirescu and Dincer (2009c). Since the fuel cell considered here is of the proton exchange type, some basic modeling equations relating the current density to hydrogen and oxygen consumption and water formation can be employed as summarized in Table 13.18. The stack is assumed to operate at the optimal current density $i_{opt}$ and its corresponding maximum power density, $W_{max}$.

All of the supplied hydrogen is assumed to be consumed by the reaction. The current generated is proportional to the mass exchange surface of the stack

**Table 13.19** Summary of the parameters used in the modeling

| Parameter | Value |
|---|---|
| $T_1$ | 25°C |
| $P_1$ | 1.01325 bar |
| $v_{N_2}$ | 0.775 kmol/kmol |
| $e_{ch,N_2}$ | 631.51 kJ/kmol |
| $v_{O_2}$ | 0.206 kmol/kmol |
| $e_{ch,O_2}$ | 3,914.26 kJ/kmol |
| $v_{H_2O}$ | 0.018 kmol/kmol |
| $e_{ch,H_2O}$ | 9,953.35 kJ/kmol |
| $v_{CO_2}$ | 0.0003 kmol/kmol |
| $e_{ch,CO_2}$ | 20,108.5 kJ/kmol |
| $v_{Ar}$ | 0.0007 kmol/kmol |
| $e_{ch,Ar}$ | 17,998.14 kJ/kmol |
| $e_{ch,H_2}$ | 236,100 kJ/kmol |
| $P_2$ | 5 bar |
| $\eta_{cmp}$ | 0.75 |
| $\eta_T$ | 0.85 |
| $P_{11}$ | 14 bar |
| $P_{12}$ | 5.3 bar |
| $US_{Loss}$ | 0.05 W/K |

(total membrane surface). The cell voltage is calculated with $V_C = W/i_{opt}$, the cell efficiency with $\eta_C = V_C/1.25$, where the reversible cell voltage is 1.25 V, the heat generated with $Q_C = W_m(1/\eta_C - 1)$, and lastly the heat loss through the stack's insulation (see Fig. 13.51) with $Q_L = US_L(\bar{T}_e - T_1)$.

In order to perform the calculations, a series of modeling parameters are assumed to have constant values, as summarized in Table 13.19. These parameters and their values are set based on some relevant engineering data for fuel cell systems. They refer to the ambient temperature and pressure, intake air composition, turbocharger efficiency and its operating pressure, hydrogen storage pressure, characteristics of the stack's thermal insulation, and chemical exergies.

The heat balance at the level of the fuel cell states that the heat generated by the electrochemical reaction $Q_C$ upgrades the enthalpy of the input streams of hydrogen (point 14) and of air (point 3) (referring to Fig. 13.51), and the energy balance for the stack can be written as

$$\dot{m}_{14}h_{14} + \dot{m}_3h_3 + \dot{Q}_C = \dot{m}_4h_4 + \dot{Q}_L. \tag{13.59}$$

Two streams at equal temperature enter the stack, (points 3 and 14), and one stream of oxygen depleted air exits at point 4. Taking into account the above-mentioned design criterion as $T_{14} = T_3$, one may assume an average electrolyte temperature as

$$\bar{T}_e = \frac{2T_3 + T_4}{3}. \tag{13.60}$$

The pressure is evaluated starting from the assumed compressor discharge pressure $P_2$ and by approximating the pressure losses in the heat exchangers so that the exhaust discharges at the atmospheric pressure. It is also assumed that the flow is turbulent and fully developed. Here, compact plate heat exchangers are used. The pressure drop calculations entail a rough estimation of the friction coefficient; their corresponding values range between 0.1 and 0.5 bar.

The air composition at state 4 is calculated based on the air composition in the surroundings (through states 1, 2, and 3) and the amount of oxygen consumed and water generated, which are

$$\left.\begin{aligned} \dot{m}_{4,\mathrm{O_2}} &= \dot{m}_{3,\mathrm{O_2}} - \dot{m}_{\mathrm{O_2 s}} \\ \dot{m}_{4,\mathrm{H_2O}} &= \dot{m}_{3,\mathrm{H_2O}} + \dot{m}_{\mathrm{H_2O}} \end{aligned}\right\}. \tag{13.61}$$

Based on Eq. (13.61), the mass concentration of each air component at state 4 can be calculated:

$$c_i = \frac{\dot{m}_i}{\dot{m}_4}, \quad i = \mathrm{N_2,O_2,H_2O,CO_2,Ar}. \tag{13.62}$$

The enthalpy, entropy, and exergy values of each state point are calculated by assuming the turbine and compressor isentropic efficiencies as listed in Table 13.19, and hence, assuming that the heat losses from the heat exchangers are negligible as compared to the heat losses at the level of the fuel cell stack (which is in fact the component where the heat is generated and, therefore, the maximum temperature on the system occurs). The system performance is quantified here by two parameters, namely, the energy efficiency as

$$\eta = \frac{\dot{W}_\mathrm{C} + \dot{W}_\mathrm{T} - \dot{W}_\mathrm{Cmp}}{\dot{m}_{11}\mathrm{HHV}} \tag{13.63}$$

and the volumetric power density as

$$\dot{W}''' = \frac{\dot{W}_\mathrm{C} + \dot{W}_\mathrm{T} - \dot{W}_\mathrm{Cmp}}{\vartheta_\mathrm{C} + \vartheta_\mathrm{hx}}, \tag{13.64}$$

where $\vartheta_\mathrm{C}$ is the stack volume and $\vartheta_\mathrm{hx}$ represents the volume of the heat exchangers used to preheat the reactants between states 2 and 3 for air and 12–13–14 for hydrogen (see Fig. 13.50).

The volume of the fuel cell stack $\vartheta_\mathrm{C}$ can be estimated based on the electrolyte membrane thickness, the number of cells, and the thickness of the thermal insulation. Here, we first consider a fixed fuel cell stack volume $\vartheta_\mathrm{C}$ in the subsequent analysis and vary the volume occupied by the heat exchangers $\vartheta_\mathrm{hx}$. The total volume of the heat exchangers can be simply estimated based on their total energy (heat) capacities:

$$\dot{Q}_\mathrm{hx} = \dot{Q}_{2-3} + \dot{Q}_{12-13} + \dot{Q}_{13-14} \tag{13.65}$$

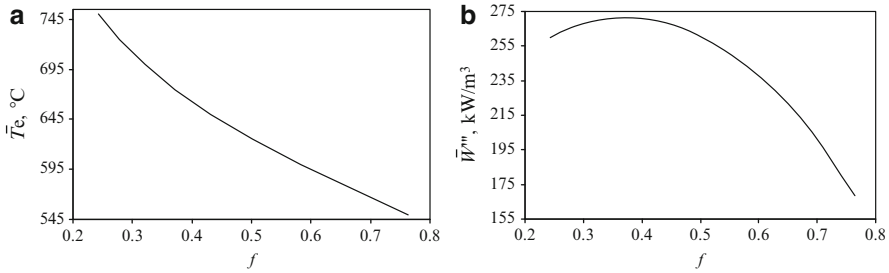


**Fig. 13.60** The effect of the system's configuration $f$ on the operating parameters and performance; (**a**) variation of the electrolyte temperature; (**b**) variation of the power density [data from Zamfirescu and Dincer (2009c)]

and a compactness factor $\varphi$ is introduced to represent the power density of the heat exchanger as

$$\vartheta_{hx} = \frac{\dot{Q}_{hx}}{\phi}. \tag{13.66}$$

Here, the typical values of $\varphi$ for compact plate-type heat exchangers are expected to range from 100 to 400 kW/m$^3$, respectively. In the present analysis, we consider 300 kW/m$^3$ as a common figure and an air stoichiometry of 3, and perform the calculations according to the scheme presented above. As already mentioned, the results regarding the system power density and system efficiency are correlated to the volumetric fraction $f$, occupied by the fuel cell stack with respect to the overall system volume as follows:

$$f = \frac{\vartheta_C}{\vartheta_C + \vartheta_{hx}}. \tag{13.67}$$

This helps determine the amount of heat exchanger capacity and volume required for better design, analysis, and optimization. In this regard, the results of our calculations are presented in Fig. 13.60, in terms of variation of the average electrolyte temperature (a) and the power density (b) with $f$. As the volumetric fraction $f$ increases, both the volume and capacity of the heat exchangers for reactant streams heating decrease. Therefore, the hydrogen and air streams need to be less heated and this reduces the electrolyte temperature as clearly seen in Fig. 13.60a. As shown in Fig. 13.60b, one can observe that there is a maximum value of the power density between these two extreme cases. The first extreme occurs when $f$ is low. Then, the fuel cell operates at high temperature and generates high power; however, the overall system volume is large, due to the large heat exchanger volumes that occupy the fraction $1 - f$ from the overall system.

The combination high-power/high-system volume leads to a low power density. In the second case, one ends up with a large $f$, and thus the heat exchangers having

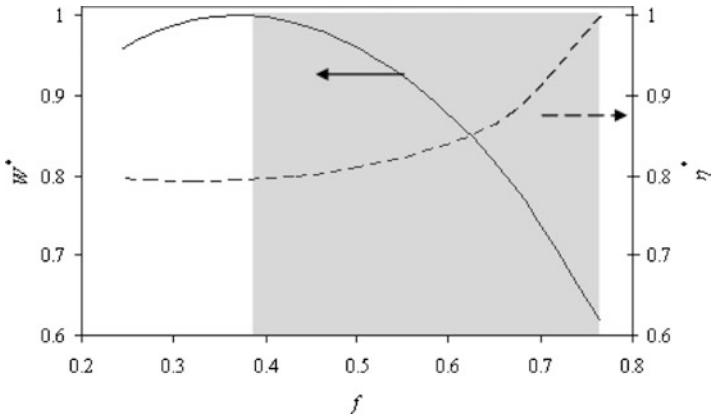


**Fig. 13.61** Variation of the system's power density and energy efficiency with the volumetric fraction occupied by the stack. The quantities are normalized with respect to their maxima [data from Zamfirescu and Dincer (2009c)]

smaller size (capacity) makes the fuel cell operate at low temperature and hence to generate low power. The combination low-power/low-system volume leads to a low power density. As demonstrated by the results obtained in Fig. 13.60b, in between the two extreme situations is found an optimum $f$ that maximizes the power density.

The design problem as illustrated in Fig. 13.60b can be reformulated as an optimization problem under constraints as follows: find the optimum system configuration that maximizes the power generated per unit of system volume; the system configuration is defined by the parameter $f$, and the volume of the system, consisting of the stack and heat exchangers, is fixed:

$$\max\{\dot{W}'''(f), \vartheta = \vartheta_C + \vartheta_{hx}, \text{fixed}\}. \tag{13.68}$$

The result of the optimization can be better contemplated in Fig. 13.61, where both the power density and energy efficiency are plotted on the same graph against the volume fraction $f$. In order to plot the two curves on the same graph, they were normalized with their maximal values. Therefore, one plots the quantities $W^* = \dot{W}'''/\dot{W}'''_{max}$ and $\eta^* = \eta/\eta_{max}$ against $f$. As can be seen in Fig. 13.62, the system's geometrical configuration, as defined by $f$, affects the performance of the system in terms of both energy efficiency and power density. As mentioned before, these two parameters are important especially in hydrogen-fueled vehicles; the designers have struggled with the problem of fitting a large hydrogen storage tank onboard and with the problem of maximizing the driving range (Fig. 13.61).

The results shown in Fig. 13.62 suggest that there are two design options for such fuel cell systems. The first option is to design the system for maximum efficiency. In this case, the system configuration is such that $f$ is large, that is, the fuel cell stack is large with respect to the other system components (the heat exchangers).

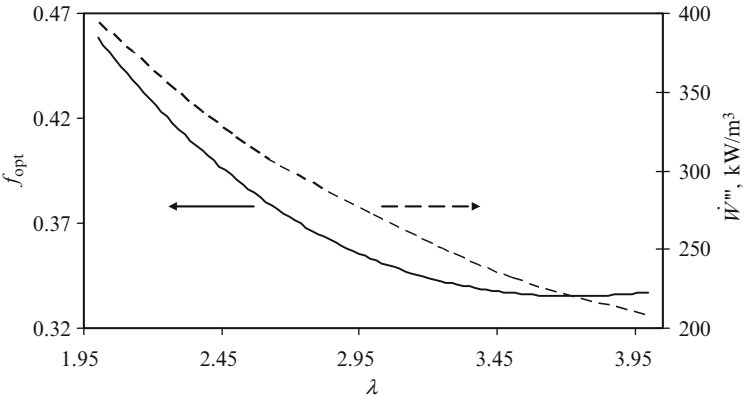


**Fig. 13.62** Optimal volume fraction occupied by the stack and the maximum power density as a function of the air stoichiometry [data from Zamfirescu and Dincer (2009c)]

For obtaining the maximum efficiency, the stack occupies about 75% from the system volume ($f$ is 0.75), as can be seen in Fig. 13.62. The second option is to design the system for maximum power per unit of volume, that is, for more compactness. In this case, the system configuration is such that the stack occupies about 40% of the system's volume while the rest of the system is occupied by the heat exchangers. It can also be said that if a system is designed for maximum power generation, it loses efficiency by about 20% of its maximum efficiency. This is expected to reduce the driving range by the same percent.

In addition, if the system is designed for a maximum energy efficiency to get a maximum driving range with a vehicle, the power density of the system is reduced by about 40% with regard to the system for a maximum power density. Therefore, if this option is chosen, one may end up with less useful space onboard for the system. This is even clearer in Fig. 13.62 as the gray-shaded area for the range of the design parameter $f$. It apparently ranges in between the two extreme points, that is, 0.35 and 0.75. It is not feasible to go beyond this range. So, one can consider this as the optimum configuration domain for design.

Furthermore, the minimum threshold of $f$ depends on the adjustment of air stoichiometry. Small air stoichiometry means large $f$ and high power density, while large $\lambda$ means small $f$ and low power density. These aspects can be contemplated from the results presented in Fig. 13.62. As shown here, the system power density reaches about 400 kW/m$^3$ for an air stoichiometry of 2.

The exergy efficiency is generally defined as the useful exergy output divided by the exergy input:

$$\psi = \frac{\dot{W}_c + \dot{W}_T - \dot{W}_{cmp}}{\dot{m}_{11}\mathrm{ex}_{11} + \dot{m}_1\mathrm{ex}_1}. \tag{13.69}$$

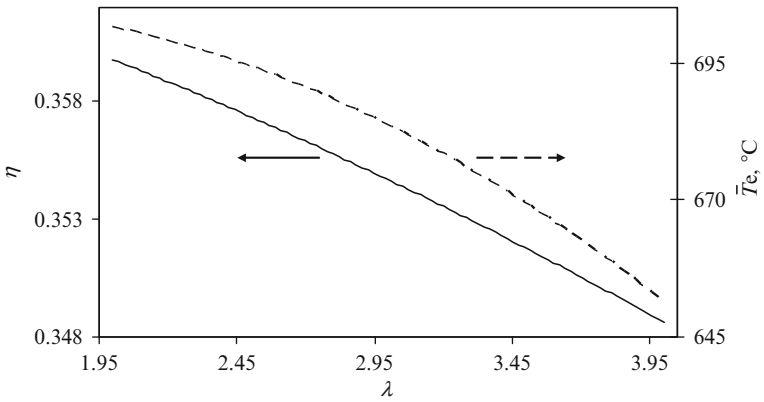


**Fig. 13.63** The energy efficiency and the cell's average temperature of the optimized system as a function of the air stoichiometry [data from Zamfirescu and Dincer (2009c)]

Moreover, if the exhaust heat is recovered, the corresponding heat exergy results in

$$\dot{E}_{9-10} = \dot{Q}_{9-10}\left(1 - \frac{T_1}{\bar{T}_{9-10}}\right) \tag{13.70}$$

and therefore, the system effectiveness, including heat recovery, then becomes

$$\psi_{\text{hr}} = \frac{\dot{W}_{\text{c}} + \dot{W}_{\text{T}} - \dot{W}_{\text{cmp}} + \dot{E}_{9-10}}{\dot{m}_{11}\text{ex}_{11} + \dot{m}_1\text{ex}_1}. \tag{13.71}$$

The energy and exergy efficiencies of the system optimized for a maximum power density are studied for a range of air stoichiometry values. The results are presented in Fig. 13.63, which correlates both energy efficiency and electrolyte temperature with $\lambda$. As can be seen, the efficiency of the optimized system is less affected by varying the air stoichiometry while the stack temperature is affected more drastically. This remains the same if the exergy efficiency is considered instead of energy efficiency. The energy efficiency is thus about 35%; also, the exergy efficiency has been calculated; this is according to Eq. (13.69) around 40% while the exergy efficiency of the system with heat recovery, calculated according to Eq. (13.71), is 61% to 74%, depending upon the chosen excess air ratio.

In brief, it is shown that there is an optimal allocation of volumes for the various components of the fuel cell system that leads to power maximization per unit of system volume. If more volume is allocated to the heat exchangers, the temperature of the preheated gases increases and so does the average cell temperature. Therefore, the cell power density increases. However, the overall volume of the system is large because of the volume occupied by the heat exchangers; thus, a decrease in the system power density is induced. If the volume allocated to the heat exchangers

is small, the average cell temperature decreases, and so does the power density of the stack; the combination of low power and small system volume means low power density. The optimal design configuration, as defined by the volumetric fraction occupied by the stack from the whole system volume, is found in between the two above-stated extreme situations.

## 13.13 Case Study: Environmental Impact, Efficiency, and Sustainability Assessment

Here, we investigate three important parameters to compare the renewable energy-based hydrogen production options and other conventional methods.

As discussed earlier, electricity is one of the energy inputs for hydrogen production; therefore, its generation cost, efficiency, and environmental impact become important parameters for environmentally benign and cost-effective hydrogen production. Table 13.20 shows these parameters along with the efficiency of the hydrogen production system using the electrolyzer unit and the environmental impact reduction factor.

The efficiency of hydrogen production is calculated by multiplying the efficiencies of electricity production and the electrolyzer unit, whereas environmental impact reduction factor can be given as

$$\mathrm{EIRF} = \frac{\mathrm{gCO_{2\,coal}} - \mathrm{gCO_2}}{\mathrm{gCO_{2\,coal}}}, \tag{13.72}$$

where the numerator denotes the difference in carbon dioxide ejection into the environment by conventional (coal-based) and nonconventional methods and the denominator denotes the carbon dioxide ejection into the environment by coal-based electricity generation. There is no carbon dioxide produced during the electrolysis of water, but it is produced during electricity production. Hence, the environmental impact reduction factor (EIRF) is calculated by using the carbon dioxide emission from different sources for electricity production only.

The value of EIRF is between 0 and 1: where 1 is the best technology and 0 is the worst for which the environmental impact is lowest and highest, respectively. Table 13.20 shows that the conventional technologies like coal and gas are more economical for per kWh of electricity generation, but they pollute the environment more. However, the price of per kWh of electricity generation for coal and gas is lower than that for the renewable energy sources. Therefore, one can say that renewable energy sources are either cost-effective (for example, wind, biomass, and geothermal) or are less polluting of the environment.

Further, the electricity generation efficiency of the different technologies is given in the same table, and it is clear that some renewable sources (e.g., wind and hydro), if not more efficient, are competitive with the conventional

**Table 13.20** Mean price of electricity generation, efficiencies of electricity and hydrogen generation, average greenhouse gas emissions expressed as $CO_2$ equivalent and environmental impact reduction factor for individual energy generation technologies

| | | Efficiency | | | |
|---|---|---|---|---|---|
| Energy sources | US$/kWh | Electricity (%) | Hydrogen production[a] (%) | $gCO_2$/kW h | EIRF |
| Photovoltaic | 0.24 | 4–22 | 2–12 | 90 | 0.91 |
| Wind | 0.07 | 24–54% | 13–28 | 25 | 0.98 |
| Hydro | 0.05 | >90 | 47 | 41 | 0.96 |
| Geothermal | 0.07 | 10–20 | 5–11 | 170 | 0.83 |
| Coal | 0.042 | 32–45 | 17–23 | 1,004 | 0.00 |
| Gas | 0.048 | 45–53% | 23–28 | 543 | 0.46 |

[a]Hydrogen production considered here is by using electrolyzer unit only
Data from Evans et al. (2009)

technologies (coal, gas, etc.) The efficiency of hydrogen production is greatly affected by the efficiency of electricity production. One can see from the above table that by using photovoltaic, wind, and geothermal, the hydrogen production efficiency can be 2–12%, 13–28%, and 5–11%, whereas for hydro it is the highest, that is, 47% and for coal and gas it remains between 17–23% and 23–28%, respectively. However, for the EIRF coal is the most polluting (0.00 for coal is taken as base case) and gas is the second highest (0.46). Wind, hydro, photovoltaic, and geothermal energies are said to be more environmentally benign and sustainable sources, as the EIRF is quite high, that is 0.98, 0.96, 0.91, and 0.83, respectively.

Evans et al. (2009) present sustainability indicators for some renewable technologies; wind, hydro, photovoltaic, and geothermal are ranked 1 to 4 based on the indicators as shown in Table 13.21, with 1 being the best technology for that indicator. The average and range were considered together, where values were quantifiable, as there was often significant overlap between the values. Some impact categories, such as availability and limitations as well as social impacts, that are unable to be quantified were assessed qualitatively. In the case of limitations, hydro was chosen as the least limited, due to its ability to provide base load power, a number of suitable sites worldwide, and the flexibility of operation. Wind was considered the second best for similar reasons. Geothermal is slightly more limited worldwide, with fewer suitable locations. Solar is considered the most limited, since excess power during the daylight hours is not yet able to be stored sufficiently to provide adequate power during periods with no sunshine(nights and on cloudy days). As far as social impact was concerned, wind was allocated the least negative social impact, due to its benign nature. Solar was second, as careful management during manufacturing and proper site selection mitigate its potential negative impacts, and geothermal was third due to increased seismic activity and pollution potential. Hydro had the largest impact, primarily due to the large number of people and animals displaced during dam inundation. The ranking in Table 13.21 suggests that electricity production from wind is the most sustainable followed by hydropower, and solar and geothermal were found to rank the lowest of the four noncombustion renewable energy technologies. This ranking was provided for

**Table 13.21** Sustainability indicators for some renewable energy sources

| | Photovoltaic | Wind | Hydro | Geothermal |
|---|---|---|---|---|
| Price | 4 | 3 | 1 | 2 |
| $CO_2$ emission | 3 | 1 | 2 | 4 |
| Availability and limitations | 4 | 2 | 1 | 3 |
| Efficiency | 4 | 2 | 1 | 3 |
| Land use | 1 | 3 | 4 | 2 |
| Water consumption | 2 | 1 | 3 | 4 |
| Social impact | 2 | 1 | 4 | 3 |
| Total | 20 | 13 | 16 | 21 |

Data from Evans et al. (2009)

global international conditions, while each technology can be significantly geographically affected. For a specific geographical location, some of the listed sustainability indicators may become more important than others.

Sustainable development requires not only that the sustainable energy resources be used, but also that they should be used efficiently. Exergy analysis is essential to improve efficiency, which allows society to maximize the benefits it derives from its resources while minimizing the negative impact (such as environmental damage). Exergy efficiency gives an idea not only of the amount (quantity) of useful energy that can be completely utilized in useful work, but also of the quality of the energy. The part of energy that is not going to be utilized for useful work is called exergy destruction. Exergy analysis gives a realistic analysis of a system for its possible feasibility, and the exergy destruction gives the scope for improvement in the existing system. Another way to understand the scope for improvement or the performance of a system is through the sustainability index, which indicates how sustainable a system is in actual practice.

The exergy efficiency of a system can be defined in terms of exergy efficiency of the different units involved in that particular system, for example, a photovoltaic-based solar hydrogen system involves PV panels, a charge regulator, an inverter, and an electrolyzer. Recall that the relation between exergy efficiency ($\psi$) and the sustainability index (SI) can be given as (Dincer and Rosen 2007)

$$\psi = 1 - \frac{1}{\mathrm{SI}}, \quad \text{where SI} = \frac{1}{D_\mathrm{P}} \tag{13.73}$$

and $D_\mathrm{P}$ is the depletion factor/number defined as the ratio of the exergy destruction rate to the input exergy rate to the system and can be given as

$$D_\mathrm{P} = \frac{\dot{E}x_\mathrm{D}}{\dot{E}x_\mathrm{in}}. \tag{13.74}$$

The exergy efficiency of the system is calculated as a minimum of 3.68% to a maximum of 4.84%. Similarly, the energy efficiency of the system is also calculated as a minimum of 4.53% to a maximum of 5.62% for comparison purposes.

**Table 13.22** Exergy efficiency and sustainability index for some $H_2$ production methods

| Hydrogen production methods | Exergy efficiency (%) | Sustainability index |
|---|---|---|
| • Electrolysis | | |
| Low-temperature (353 K) | 58–64 | 2.38–2.78 |
| Medium-temperature (473 K) | 79 | 4.76 |
| High-temperature (1,173 K) | 86 | 7.14 |
| • Photoelectrolysis | 35[a] | 1.54 |
| • Steam gasification of petroleum coke | 17 | 1.20 |
| • Steam gasification of coal | 46 | 1.85 |
| • Decomposition of natural gas | 32 | 1.47 |
| • Steam reforming of natural gas | 46 | 1.85 |
| • Thermolysis | 3.39 | 1.04 |
| • Hybrid thermolysis + electrolysis | 4.44 | 1.05 |
| • Thermochemical cycle (e.g., Cu–Cl cycle) | 33–65 | 1.49–2.86 |

[a]Maximum theoretical efficiency according to Dincer (2002)

Slightly higher values for energy efficiency can be seen, as the first law analysis does not incorporate losses due to irreversibility.

The sustainability index for the PV array varies between 1.11 and 1.13, for both charge regulator and inverter, between 6.67 and 10 for the electrolyzer unit is 2.08, whereas the sustainability index of the entire system is between 1.04 and 1.05. A higher sustainability index shows better sustainability of the process/unit. It should be noted here that despite the higher exergy efficiency of the electrolyzer, charge regulator, and inverter units, the system exergy efficiency remains low, mainly because of the low PV exergy efficiency. There is a need to improve the PV array efficiency in order to have a better sustainability index and hence better sustainability.

The exergy efficiency and sustainability index of the different hydrogen production methods discussed earlier are listed in Table 13.22. It is evident that the electrolysis process has better exergy efficiency, and subsequently the sustainability index is also high. For a temperature range of 353 to 1,173 K, the exergy efficiency range of the electrolysis process is 58% to 86% and the sustainability index range is (MS PAGE NO 620) 2.38 to 7.14. The biophotolysis range is the lowest of all, as the conversion efficiency of plants is very low. The sustainability index for photoelectrolysis is 1.54 for the maximum theoretical efficiency of 35%.

Exergy efficiency of steam gasification of petroleum coke and coal is 17% and 46% and the sustainability index is 1.2 and 1.85, respectively. Exergy efficiency of decomposition (also known as cracking) and steam reforming of natural gas is 46% and 32% and their sustainability index is 1.47 and 1.85. High-temperature thermolysis has a relatively low exergy efficiency (3.39%) and sustainability index (1.04). However, its performance can be improved by coupling thermolysis with electrolysis (also known as the hybrid thermolysis and electrolysis process). In this case, exergy efficiency is 4.44% and the sustainability index is 1.05. Thermochemical cycles, such as the Cu–Cl cycle, have a reasonably good exergy efficiency range (33–65%), and its sustainability range is 1.49–2.86.

## 13.14 Concluding Remarks

In this chapter, potential technologies for hydrogen production were thoroughly reviewed. It was explained why hydrogen is important for sustainable energy development: it is the cleanest energy carrier that can be produced from any kind of energy source such as water or other abundant materials. There are many hydrogen production methods. They were categorized here based on the energy source they use, such as electric, thermal, biochemical, and photonic-based methods. Each of these kinds of energy can be obtained from primary energy such as nuclear, fossil fuel, renewable sources, or recovered energy.

Various solar hydrogen production methods have been studied. Water electrolysis using photovoltaic cells is the most mature method for producing hydrogen. Photoelectrolysis is still at an early stage of development, and material cost and practical issues have yet to be solved. The photobiological processes are also still at a very early stage of development and thus far only low conversion efficiencies have been attained. High-temperature processes need further material development that focuses on high-temperature membranes and heat exchangers for solar–thermal processes. Therefore, the world's solar hydrogen utilization systems consist mainly of photovoltaic-hydrogen systems for transportation and stationary applications. Eco-friendly hydrogen production via solar energy is very important to save the environment as it does not emit any greenhouse gases during operation. At present, it is a challenging task for researchers and scientists, as the exergy efficiency of the PV array is low, and hence the overall exergy efficiency of a solar hydrogen system is low. The geothermal-based hydrogen production is another suitable alternative that uses the renewable energy of the geothermal water/steam to produce hydrogen using a high-temperature electrolyzer. Environmentally benign and sustainable hydrogen production via artificial photosynthesis is also discussed. The EIRF and SI have been evaluated and studied for different energy sources, and it can be concluded that renewable energy sources are environmentally benign as they have a higher value for the EIRF. In the end, a case study showing energy and exergy efficiencies of a hydrogen production system are discussed in brief, as is the sustainability index of some processes. The variation ranges of exergy efficiency and sustainability index for various hydrogen production methods are summarized in the form of a table. It can be concluded that the hydrogen systems with high sustainability index are desirable to ensure high exergy efficiency, which in turn ensures high exergy output for the maximum benefit for society.

Hydrogen is difficult to store and distribute, but technologies evolve and in the future they will become commercially available. The utilization of hydrogen is predicted to grow, with a large share of the petrochemical industry and of agriculture, where it is used as fertilizer. The use of hydrogen as fuel is expanding constantly. Fuel cells are the main systems that utilize hydrogen fuel for power production. They have high efficiency, a fact that justifies efforts for their improvement and commercialization. Here, fuel cells were classified and their basic modeling and optimization issue were presented with some examples.

## Nomenclature

| | |
|---|---|
| $C$ | Cost, $ or concentration |
| $CI$ | Cost index |
| $e$ | Elementary charge, C |
| $E$ | Energy, kJ |
| EIRF | Environmental impact reduction factor |
| $ex$ | Specific exergy, kJ/kg |
| $Ex$ | Exergy, kJ |
| $D_p$ | Depletion factor |
| $f$ | Volume fraction |
| $F$ | Faraday constant, As/mol |
| $G$ | Gibbs free energy, kJ/mol |
| $h$ | Specific enthalpy, kJ/kg or heat transfer coefficient, W/m$^2$K |
| $H$ | Enthalpy, kJ/kg |
| HHV | Higher heating value, MJ/kg |
| $I$ | Solar irradiance, W, or current intensity, A |
| $k$ | Thermal conductivity, W/mK |
| LHV | Lower heating value, MJ/kg |
| $m$ | Mass, kg |
| $MR$ | Mols ratio |
| $n$ | Number of mols |
| $N_A$ | Number of Avogadro |
| $P$ | Pressure, bar |
| $Q$ | Heat, kJ |
| $R$ | Universal gas constant, J/molK |
| $s$ | Specific entropy, kJ/kgK |
| $S$ | Entropy, kJ/K |
| SI | Sustainability index |
| $T$ | Temperature, K |
| $U$ | Overall heat transfer coefficient, W/m$^2$K |
| $V$ | Voltage, V |
| $W$ | Work, kJ |

## Greek Letters

| | |
|---|---|
| $\delta$ | Thickness, m |
| $\gamma$ | Specific heat ratio |
| $\Delta$ | Difference |

$\lambda$ Excess ratio
$\phi$ Compactness factor, kW/m$^3$
$\eta$ Utilization efficiency
$\psi$ Exergy efficiency
$\upsilon$ System volume, m$^3$

## Subscripts

0 Reference state
C Condenser
Cmp Compresser
E Electrical
EL Electrolysis
FC Fuel cell
gen Generator
geo Geothermal
H Heating
hx Heat exchanger
hr Heat recovery
in Inlet
ins Insulation
m Material or mean
N Nernst
o Output
oc Open circuit
ohm Ohmic
ox Oxidation
OP Other product
PF Primary fuel
pmp Pump
red Reduction
S Salt
sc Short circuit
SF Synthetic fuel
SH Space heating
TH Thermal
TOT Total
W Wall
WF Working fluid

## Superscripts

| | |
|---|---|
| ch | Chemical |
| thrm | Thermomechanical |
| $\dot{(\ )}$ | Rate (per unit of time) |
| $\bar{(\ )}$ | Average value |

## References


Abanades S., Charvin P., Flamant G., Neveu P. 2006. Screening of water-splitting thermochemical cycles potentially attractive for hydrogen production by concentrated solar energy. *Energy* 31:2805–2822.

Abuadala A., Dincer I., Naterer G.F. 2010. Exergy analysis of hydrogen production from biomass gasification. *International Journal of Hydrogen Energy* 35:4981–4990.

Ay M., Midilli A., Dincer I. 2006. Investigation of hydrogen production from boron compounds for PEM fuel cells. *Journal of Power Sources* 157:104–113.

Balta M.T., Dincer I., Hepbasli A. 2009. Thermodynamic assessment of geothermal energy use in hydrogen production. *International Journal of Hydrogen Energy* 34:2925–2939.

Brewer K.J., Elvington M. 2006. Supramolecular complexes as photocatalysts for the production of hydrogen from water. US Patent 7,122,172 B2.

CHA 2010. Hydrogen systems. The Canadian opportunity for greenhouse gas reduction and economic growth through the deployment of hydrogen technologies and infrastructures. Canadian Hydrogen Association. Internet source http://www.h2.ca (accessed on September 1, 2010).

Christensen P.A., Erbs W., Harriman A. 1985. Photo-oxydation of water in non-sacrificial systems. *Journal of Chemical Society, Faraday Transactions* 81:575–580.

Cohce M.K., Dincer I., Rosen M.A. 2010. Thermodynamic analysis of hydrogen production from biomass gasification. *International Journal of Hydrogen Energy* 35:4970–4980.

Collings A.F., Critchley C. 2005. Artificial Photosynthesis from Basic Biology to Industrial Application. Wiley-VCH Verlag GmbH & Co, Weinheim, Germany.

Colpan C.O., Dincer I., Hamdullahpur F. 2008. A review on macro-level modeling of planar solid oxide fuel cells. *International Journal of Energy Rresearch* 32:336–355.

Das D., Veziroglu T.N. 2008. Advances in biological hydrogen production processes. *International Journal of Hydrogen Energy* 33:6046–6057.

Dincer I. 2002. Technical, environmental and exergetic aspects of hydrogen energy systems. *International Journal of Hydrogen Energy* 27:265–285.

Dincer I., Rosen M.A. 2007. Exergy: Energy, Environment and Sustainable Development. Elsevier, Oxford, UK.

Evans A., Strezov V., Evans T.J. 2009. Assessment of sustainability indicators for renewable energy technologies. *Renewable and Sustainable Energy Reviews* 13:1082–1088.

Fujishima A., Honda K. 1972. Electrochemical photolysis of water at a semiconductor electrode. *Nature* 238: 37–38.

Granovskii M., Dincer I., Rosen M.A., Pioro I. 2008a. Performance assessment of a combined system to link a supercritical water-cooled nuclear reactor and a thermochemical water splitting cycle for hydrogen production. *Energy Conversion and Management* 49:1873–1881.

Granovskii M., Dincer I., Rosen M.A. 2008b. Exergy analysis of a gas turbine cycle with steam generation for methane conversion within solid oxide fuel cells. *Journal of Fuel Cell Science and Technology* 5/031005:1–9.

Gutsol A.F., Fridman A. 2008. Hydrogen production from hydrogen sulfide. Patent #WO 137936.

Haseli Y., Naterer G.F., Dincer I. 2009. Fluid-particle mass transport of cupric chloride hydrolysis in a fluidized bed. *International Journal of Heat and Mass Transfer* 52:2507–2515.

Isachenko V.P., Osipova V.A., Sukomel A.S. 2004. Heat transfer. In: Solid Fuels Combustion and Gasification Modeling, Simulation, and Equipment Operation, de Souza-Santos M.L., eds., Marcel Dekker, New York.

Kalinci Y., Hepbasli A. Dincer I. 2009. Biomass-based hydrogen production: A review and analysis. *International Journal of Hydrogen Energy* 34:8799–8817.

Kanoglu M. Dincer I., Rosen M.A. 2007. Geothermal energy use in hydrogen liquefaction. *International Journal of Hydrogen Energy* 32:4250–4257.

Karkamkar A., Ardahl C., Autrey T. 2007. Recent developments on hydrogen release from ammonia borane. *Mater Matters* 2:6–9.

Kogan A. 1998. Direct solar thermal splitting of water and onsite separation of the products. II. Experimental feasibility study. *International Journal of Hydrogen Energy* 23:89–98.

Kotay S.M., Das D. 2008. Biohydrogen as a renewable energy resource—prospects and potentials. *International Journal of Hydrogen Energy* 33:258–63.

Koutrouli E.K., Kalfas H., Gavala H.N., Skiadas I.V., Stamatelatou K., Lyberatos G. 2009. Hydrogen and methane production through two-stage mesophilic anaerobic digestion of olive pulp. *Bioresource Technology* 100:3718–3723.

Licht S., Wang B., Mukerji S., Soga T., Umeno M., Tributsch H. 2001. Over 18% solar energy conversion to generation of hydrogen fuel; theory and experiment for efficient solar water splitting. *International Journal of Hydrogen Energy* 26:653–659.

Marmier A., Füterer M.A. 2008. Nuclear powered heat pumps for near-term process heat applications. *Nuclear Engineering and Design* 238:2272–2284.

Midilli A., Murat Ay, Kale A., Veziroglu T.N. 2007. A parametric investigation on hydrogen energy potential based on $H_2S$ Black Sea deep waters. *International Journal of Hydrogen Energy* 32:117–124.

Muradov N.Z., Veziroglu T.N. 2008. "Green" path from fossil-based to hydrogen economy: An overview of carbon neutral technologies. *International Journal of Hydrogen Energy* 33:6804–6839.

Naterer G.F., Suppiah S., Lewis M., Gabriel K., Dincer I., Rosen M.A., Fowler M., Rizvi G., Easton E.B., Ikeda B.M., Kaye M.H., Lu L., Pioro I., Spekkens P., Tremaine P., Mostaghimi J., Avsec J., Jiang J. 2009. Recent Canadian advances in nuclear-based hydrogen production and the thermochemical Cu–Cl cycle. *International Journal of Hydrogen Energy* 34:2901–2917.

Orhan M.F., Dincer I., Naterer G.F. 2008a. Cost analysis of a thermo-chemical Cu–Cl pilot plant for nuclear-based hydrogen production. *International Journal of Hydrogen Energy* 33:6006–6020.

Orhan M.F., Dincer I., Rosen M.A. 2008b. Thermodynamic analysis of the copper production step in a copper–chlorine cycle for hydrogen production. *Thermochimica Acta* 480:22–29.

Orhan M.F., Dincer I., Rosen M.A. 2009a. Efficiency analysis of a hybrid copper–chlorine (Cu–Cl) cycle for nuclear-based hydrogen production. *Chemical Engineering Journal* 155:132–137.

Orhan M.F., Dincer I., Rosen M.A. 2009b. Energy and exergy analyses of the fluidized bed of a copper–chlorine cycle for nuclear-based hydrogen production via thermo-chemical water decomposition. *Chemical Engineering Research and Design* 87:684–694.

Orhan M.F., Dincer I., Rosen M.A. 2009c. The oxygen production step of a copper–chlorine thermo-chemical water decomposition cycle for hydrogen production: Energy and exergy analyses. *Chemical Engineering Science* 64:860–869.

Rashidi R., Berg P., Dincer I. 2009. Performance investigation of a combined MCFC system. *International Journal of Hydrogen Energy* 34:4395–4405.

Sørensen R.Z., Hummelshøj J.S., Klerke A., Reves J.B., Vegge T., Nørskov J.K., Christensen C.H. 2008. Indirect, reversible high density hydrogen storage in compact metal ammines. *Journal of American Chemical Society* 130:8660–8668.

Taylor J.B. 1983. Hydrogen energy prospects in Canada. *International Journal of Hydrogen Energy* 1/2:1–7.

Yilanci A., Dincer I., Ozturk H.K. 2009. A review on solar-hydrogen/fuel cell hybrid energy systems for stationary applications. *Progress in Energy and Combustion Science* 35:231–244.

Zaman J., Chakma A. 1995. Production of hydrogen and sulphur from hydrogen sulfide. *Fuel Processing Technology* 41:159–198.

Zamfirescu C., Dincer I. 2009a. Performance investigation of high-temperature heat pumps with various BZT working fluids. *Thermochimica Acta* 488:66–77.

Zamfirescu C., Dincer I. 2009b. Ammonia as a green fuel and hydrogen source for vehicular applications. *Fuel Processing Technology* 90:729–737.

Zamfirescu C., Dincer I. 2009c. Thermodynamic performance analysis and optimization of a SOFC-$H^+$ system. *Thermochimica Acta* 486:32–40.

Zamfirescu C., Dincer I., Naterer G.F. 2009a. Performance evaluation of organic and titanium based working fluids for high temperature heat pumps. *Thermochimica Acta* 496:18–25.

Zamfirescu C., Dincer I., Naterer G.F. 2010a. Thermophysical properties of copper compounds in copper–chlorine thermochemical water splitting cycles. *International Journal of Hydrogen Energy* 35:4839–4852.

Zamfirescu C., Dincer I., Naterer G.F. 2010b. Upgrading of waste heat for combined power and hydrogen production with nuclear reactors. *Journal of Engineering for Gas Turbines and Power* 132/102911:1–9.

Zamfirescu C., Dincer I., Naterer G.F. 2010c. Design and analysis of a photocatalytic hydrogen production system with mixed-metal photoinitiated electron collection. International Conference on Hydrogen Production ($ICH_2P$), Istanbul, June 16-18.

Zamfirescu C., Dincer I., Naterer G.F. 2010d. Biomass-based heat driven water splitting using copper-chlorine cycle. Eightieth World Hydrogen Energy Conference (WHEC 2010) Essen, Germany, May 16-20.

Zamfirescu C., Naterer G.F., Dincer I. 2010e. Kinetics study of the copper/hydrochloric acid reaction for thermochemical hydrogen production. *International Journal of Hydrogen Energy* 35:4853–4860.

Zamfirescu C., Naterer G.F., Dincer I. 2010f. Novel CuCl vapor compression heat pump integrated with a water splitting plant. *Thermochimica Acta* 512:40–48.

## Study Questions/Problems

13.1 What characteristics of hydrogen make it attractive for energy economy?
13.2 Describe the idea of hydrogen economy.
13.3 Categorize the methods for hydrogen production.
13.4 Calculate the reaction enthalpy and the Gibbs energy of water decomposition reaction at 25°, 1,000°, and 2,500°C and compare the results.
13.5 Calculate the energy efficiency of the system in Fig. 13.5 using the data from Table 13.3.
13.6 Explain the concept of thermochemical water splitting.
13.7 Calculate the reaction heat for Eq. (13.15).
13.8 Describe the S–I cycle.
13.9 What is the difference between fuel reforming and gasification?

13.10 Calculate the reaction heats for Eq. (13.27) at 1,000°C.
13.11 Describe the nuclear–thermal routes for hydrogen production.
13.12 What are the envisaged hydrogen production methods coupled with nuclear reactors?
13.13 Calculate the reaction heats for Eq. (13.37) at 1,100°C.
13.14 Making reasonable assumptions, calculate the copper chlorine hydrogen production cycle in Fig. 13.21.
13.15 Making reasonable assumptions, calculate the biomass-driven high-temperature electrolysis cycle in Fig. 13.29.
13.16 Explain the principle of photocatalytic water splitting.
13.17 Calculate the reaction enthalpy for Eq. (13.43) at standard temperature.
13.18 Calculate the work needed to compress 1 kg of hydrogen from 1 bar pressure to 800 bar according to the process described by Eq. (13.46).
13.19 Calculate the simplified Claude cycle in Fig. 13.44 under reasonable assumptions.
13.20 Comment on the storage density of various hydrogen storage methods according to Fig. 13.45.
13.21 Comment on the potential of ammonia borane for hydrogen storage. Investigate the sufficiency of natural reserves of boron.
13.22 Compare the hydrogen utilization in Canada in 1983 with respect to 2010.
13.23 Describe the fuel cell principle.
13.24 Is the fuel cell operation benefited by high pressure and low temperature or by low pressure and high temperature?
13.25 Present a classification of fuel cell types.
13.26 Present a classification of fuel cell applications.
13.27 Calculate the system in Fig. 13.50 under reasonable assumptions.
13.28 Calculate the system in Fig. 13.51 under reasonable assumptions.
13.29 Calculate the system in Fig. 13.52 under reasonable assumptions.
13.30 Calculate the system in Fig. 13.54 under reasonable assumptions.
13.31 Calculate the system in Fig. 13.56 under reasonable assumptions.
13.32 Present a classification of fuel cell modeling techniques.
13.33 Explain the equation of Nernst.
13.34 Describe the type of energy losses in fuel cells.